

Detection and Characterisation of Low-Concentration Components in Drugs and Drug Formulations; Exploring the Value of Soft X-ray Synchrotron Radiation Techniques for the Pharmaceutical Industry

Alastair Murray Booth

2008

A thesis submitted to the University of Manchester for the
degree of Doctor of Philosophy in the Faculty of Science and Engineering

Department of Chemical Engineering and Analytical Science

Contents

Abstract	15
Declaration	16
Acknowledgements	17
Abbreviations	19
1 Introduction	20
1.1 Objectives	20
1.2 Outline	22
1.3 Surfaces	25
1.4 Drug Discovery, Development and Testing	31
1.4.1 Drug Discovery	31
1.4.2 Drug Testing	32
1.5 Soft X-ray Spectroscopy in the Pharmaceutical Sciences	36
1.5.1 Introduction	36
1.5.2 X-ray Photoelectron Spectroscopy (XPS)	39
1.5.3 X-ray Absorption Spectroscopy (XAS)	44

CONTENTS

1.5.4	X-ray PhotoElectron Emission Microscopy (XPEEM)	49
1.5.5	Conclusions	50
2	Experimental: Theory, Methods and Techniques	52
2.1	Introduction	52
2.1.1	X-ray Tubes	53
2.1.2	Synchrotron Radiation Sources	55
2.1.3	Vacuum Conditions	62
2.1.4	Focusing and Monochromatisation	63
2.2	X-ray Spectroscopy	65
2.2.1	Spectroscopic Notation	65
2.2.2	X-ray Absorption Spectroscopy (XAS)	66
2.2.3	X-ray Photoelectron Spectroscopy (XPS)	77
2.3	Microscopy	87
2.3.1	Introduction	87
2.3.2	Electron Microscopy	88
2.3.3	Scanning Electron Microscopy (SEM)	89
2.3.4	Transmission Electron Microscopy (TEM)	92
2.3.5	X-ray PhotoElectron Emission Microscopy (XPEEM)	92
2.3.6	Imaging XPS	95
2.3.7	Atomic Force Microscopy (AFM)	95
3	Soft X-ray Cell Development	97
3.1	Introduction	97
3.2	Requirements	98

CONTENTS

3.3	Initial Design	99
3.4	Cell Versions	104
3.4.1	Mark I	104
3.4.2	Mark II	105
3.4.3	Mark III	108
4	Polymer Coatings for Improving Bioavailability	111
4.1	Introduction	111
4.2	SR 142801, Osanetant	115
4.3	Near Edge X-ray Absorption Fine Structure (NEXAFS)	117
4.3.1	Nitrogen K-edge	118
4.3.2	Carbon K-edge	121
4.3.3	Oxygen K-edge	123
4.4	Discussion	127
4.5	SSR 180575	130
4.6	X-ray Photoelectron Spectroscopy (XPS)	131
4.6.1	Valence Bands	132
4.6.2	Survey Spectra	133
4.6.3	Chlorine 2p	136
4.6.4	Nitrogen 1s	137
4.6.5	Carbon 1s	138
4.6.6	Oxygen 1s	140
4.7	Near Edge X-ray Absorption Fine Structure (NEXAFS)	143
4.7.1	Carbon K-edge	143
4.7.2	Oxygen K-edge	146

CONTENTS

4.8	Environmental Scanning Electron Microscope (ESEM)	147
4.9	Discussion	151
4.10	Conclusions	154
5	Crystalline and Amorphous Drug Surfaces	156
5.1	Introduction	156
5.2	SR 49059	160
5.3	X-ray Photoelectron Spectroscopy (XPS)	162
5.3.1	Oxygen 1s	162
5.3.2	Carbon 1s	164
5.4	Near Edge X-ray Absorption Fine Structure (NEXAFS)	166
5.4.1	Carbon K-edge	166
5.4.2	Oxygen K-edge	169
5.5	Transmission Electron Microscopy (TEM)	171
5.6	Discussion	173
5.7	Indomethacin	175
5.8	Near Edge X-ray Absorption Fine Structure (NEXAFS)	177
5.8.1	Carbon K-edge	177
5.9	Discussion	180
5.10	Conclusions	181
6	Suspension Stability	182
6.1	Introduction	182
6.2	Ibuprofen	183
6.3	Stability Tests	184
6.4	X-ray Photoelectron Spectroscopy (XPS)	187

CONTENTS

6.4.1	Carbon 1s	187
6.4.2	Oxygen 1s	189
6.5	2-D correlation spectroscopy	192
6.6	Discussion	197
6.7	Conclusions	198
7	Additional Work	199
7.1	Introduction	199
7.2	Ink Films	201
7.2.1	X-ray Photoelectron Spectroscopy (XPS)	202
7.2.2	Atomic Force Microscopy (AFM)	205
7.2.3	X-ray PhotoElectron Emission Microscopy (XPEEM)	207
7.2.4	Conclusion	210
7.3	SSR 180575 - X-ray PhotoElectron Emission Microscopy (XPEEM)	212
7.4	Drug Nanoparticle Formulations - XPEEM	215
7.5	Further NEXAFS	218
7.6	Hemispherical Ambient Pressure Photoelectron Yield (HAPPY) Analyser	221
7.7	X-ray Excited Optical Luminescence (XEOL) detection	224
8	Conclusions	226
8.1	Importance	226
8.2	Practicality	229
8.3	Future Developments	231

List of Figures

1.1	Contrasting surface vs. bulk analysis	26
1.2	Typical surface catalytic reaction (CO oxidation)	28
1.3	Corona discharge treatment of polymer films	29
1.4	Rational drug discovery	32
1.5	The drug testing process	34
1.6	Surface effects of enzymes	41
1.7	Diagram of core-shell and homogeneous particles	42
1.8	Variations in cross-sectional drug concentration	43
1.9	Physical principle of EXAFS	46
1.10	Linear combination analysis of XANES	47
1.11	Surface sensitive techniques, spatial vs. chemical resolution . .	51
2.1	X-ray anode operation	54
2.2	X-ray emission diagram	54
2.3	X-ray tube emission spectra	54
2.4	Comparative Flux in X-ray sources over time	56
2.5	Typical synchrotron schematic (Daresbury)	58
2.6	A relativistic electron accelerated in a magnetic field	59

LIST OF FIGURES

2.7	Typical bending magnet spectrum for a synchrotron	60
2.8	Comparison of Flux from a bending magnet, a wiggler and an undulator	61
2.9	An array of magnets functioning as an undulator	62
2.10	Rowland sphere monochromator	64
2.11	A typical beamline setup	65
2.12	Absorption of X-rays	67
2.13	Variation of X-ray absorption coefficient, $\mu(E)$	67
2.14	X-ray absorption edges	68
2.15	Scattering effects leading to EXAFS.	69
2.16	Extracting the fine structure from μ	70
2.17	A Fourier transform of X-ray absorption fine structure, χ showing a radial distribution of scattering neighbours	70
2.18	NEXAFS spectra in relation to transitions to unoccupied molecular orbitals	72
2.19	Angular dependence of NEXAFS spectra	73
2.20	Electronic processes for electron and fluorescence yield	74
2.21	Schematic for transmission yield	75
2.22	A typical commercial XPS instrument (Kratos Axis Ultra)	77
2.23	Schematic of a typical XP spectrometer	78
2.24	Electron analyser	79
2.25	Universal curves for electron inelastic mean free paths.	80
2.26	Fraction of electrons escaping the surface in terms of inelastic mean free path.	81
2.27	The features of an XP spectrum	83

LIST OF FIGURES

2.28	Origin of binding energy shifts in XPS	84
2.29	Schematic of the principal of depth profiling by angle resolved XPS	86
2.30	Interactions of electrons with matter	89
2.31	A schematic of a scanning electron microscope	90
2.32	Differential pressures in an environmental scanning electron microscope	91
2.33	A schematic of a transmission electron microscope	93
2.34	schematic of an XPEEM instrument	94
2.35	Schematic of an atomic force microscope	96
3.1	Conflat (CF) style flange and gasket	99
3.2	Schematic of the vacuum system	101
3.3	Schematic of data collection	103
3.4	Mechanism of operation for the gas microstrip detector	103
3.5	Mark I cell design	104
3.6	Mark II cell design	106
3.7	NEXAFS spectra of CO gas over gold	106
3.8	Sample mounting system	107
3.9	NEXAFS spectra of CO gas over gold at different temperatures	107
3.10	Window section basis	109
3.11	Mark III cell design	110
4.1	Bioavailability, absorption, excretion and metabolism	112
4.2	SR 142801 Molecular Structure	115
4.3	Poloxamer Molecular Structure	116

LIST OF FIGURES

4.4	SR 142801 nitrogen K edge total electron yield NEXAFS, top: normal spectra, bottom: difference spectra relative to the pure drug	119
4.5	SR 142801 carbon K-edge total electron yield NEXAFS. . . .	122
4.6	SR 142801 carbon K-edge fluorescence yield NEXAFS	123
4.7	SR 142801 oxygen K-edge fluorescence yield NEXAFS. . . .	124
4.8	SR 142801 oxygen K-edge total electron yield NEXAFS. . . .	125
4.9	Poloxamer 388 oxygen K-edge total electron yield NEXAFS. .	126
4.10	SR 142801 oxygen K edge difference spectra, surface - bulk NEXAFS	127
4.11	Possible orientation effect	128
4.12	SSR 180575 Molecular Structure	131
4.13	Coating Polymers Molecular Structure	131
4.14	Valence Band X-ray Photoelectron Spectra, Top: Pure Drug, Middle: Polymer (PEG), Bottom: Polymer Coated Drug . . .	133
4.15	SSR 180575 Survey spectra	134
4.16	SSR 180575 chlorine 2p spectra	136
4.17	SSR 180575 nitrogen 1s spectra	137
4.18	SSR 180575 carbon 1s spectra of top: Pure drug, bottom: Poloxamer 388 coated drug	139
4.19	SSR 180575 oxygen 1s spectra of PEG coated drug substance, inset: pure drug spectra	141
4.20	SSR 180575 carbon K-edge total electron yield NEXAFS (PEG Coated)	144

LIST OF FIGURES

4.21	SSR 180575 carbon K-edge total electron yield NEXAFS (Poloxamer 388 Coated)	145
4.22	SSR 180575 (humidity treatment, PEG) carbon K-edge total electron yield NEXAFS	146
4.23	SSR 180575 (Poloxamer 388) oxygen K-edge total electron yield NEXAFS	147
4.24	ESEM images of PEG over one cycle of rising and lowering humidity	149
4.25	ESEM images of PEG coated drug over one cycle of rising and lowering humidity	150
4.26	Possible models for surface polymer present on drug	152
4.27	Effects of high relative humidity on polymer coating	152
5.1	Defects at a newly formed surface	158
5.2	SR 49059 molecular structure	160
5.3	Oxygen 1s XP Spectra for SR 49059	163
5.4	Carbon 1s XP Spectra for SR 49059	165
5.5	Carbon K-edge NEXAFS spectra SR 49059 before and after exposure to 100% relative humidity	167
5.6	Oxygen K-edge NEXAFS spectra SR 49059	169
5.7	Transmission electron micrograph of micronised drug at 20000x and an edge section at 220000x magnification.	172
5.8	A thin section of the micronised drug and the diffraction pat- tern from that area	172
5.9	Suggestion for surface orientation effects	173

LIST OF FIGURES

5.10	Model for surface profile of micronised drug.	174
5.11	Indomethacin molecular structure	175
5.12	Carbon K-edge NEXAFS spectra of indomethacin samples . .	178
5.13	Carbon K-edge NEXAFS spectra of indomethacin samples . .	179
6.1	Ibuprofen Molecular Structure	183
6.2	Schematic of transmission based suspension stability tests. . .	185
6.3	Transmission suspension stability data.	185
6.4	Carbon 1s XP spectra for 15%(wt) poloxamer 388, 188 and PEG respectively.	188
6.5	Oxygen 1s XP spectra for 15%(wt) poloxamer 388, 188 and PEG respectively.	190
6.6	2-D correlation Spectra of poloxamer 188 formulations at (5%, 10%, 15% and 20%)	195
6.7	2-D correlation Spectra of poloxamer 388 formulations at (5%, 10%, 15% and 20%)	196
7.1	XPS spectra of Ar ⁺ sputtered ink coating.	204
7.2	ARXPS ink coating.	204
7.3	AFM image showing partially removed ink layer on polymer substrate.	206
7.4	AFM image showing wax particle protruding through polymer melt.	206
7.5	XPEEM image of a ink coating showing wear tracks and wax particles.	208
7.6	Close up XPEEM image of a wax particle on the ink surface. .	209

LIST OF FIGURES

7.7	Tentative model for ink layer on (polymer) substrate.	211
7.8	XPEEM images of pure SSR 180575 crystals.	213
7.9	XPEEM images of PVP coated SSR 180575.	214
7.10	Carbon K-edge XPEEM of drug nanoparticles.	216
7.11	Carbon K-edge XPEEM of ground tablet containing drug nanoparticles.	217
7.12	Carbon K-edge NEXAFS comparing intact and ground sam- ples of the same melt extruded tablet.	219
7.13	Schematic of the 'HAPPY' <i>in situ</i> XPS analyser.	222
7.14	Preliminary data with HAPPY on a test system, Oxygen Ad- sorption on TiO_2	223
7.15	Preliminary Test data for X-ray Excited Optical Luminescence (XEOL).	225

List of Tables

1.1	Surface to volume ratios of common objects	28
3.1	Classification of different levels of vacuum	98
3.2	Cell Comparisons	110
4.1	Relative elemental abundances for drug substance and coating polymers (XPS)	134
4.2	Relative percentage elemental abundances for 5% solution coated samples	135
4.3	Carbon peak assignments for 5% solution coated samples . . .	140
4.4	Oxygen component assignments for 5% solution coated samples	142
5.1	Carbon peak assignments for SR 49059 samples	164
6.1	Carbon peak assignments for polymer coated ibuprofen	189
6.2	Oxygen peak assignments for polymer coated ibuprofen	191
7.1	Ink samples	202

Abstract

Surface properties affect pharmaceuticals by influencing physical behaviour, which can cause problems for both formulation and medication. Poorly water soluble compounds are often modified with polymer surfactants. The presence of amorphous material, due to its effect on dissolution rate, can modify the bioavailability of a compound. This thesis reports the novel application of X-ray Absorption Spectroscopy (XAS) and X-ray Photoelectron Spectroscopy (XPS) to surface related pharmaceutical problems. XAS is sensitive to bond angles, local symmetry and oxidation states and XPS provides information on local chemical environment. Both have a probing depth <10 nm in the soft X-ray range.

It is shown that XAS and XPS are capable of determining the physical coverage of ultra-thin polymer coatings. *In situ* XAS confirmed they form raft-like structures on the drug surface. Adsorbed water could also be detected on the surface and this corresponds to improvement in dissolution rate, which implies an improvement in bioavailability. XAS was capable of distinguishing between amorphous and crystalline batches of two drugs at the surface. It was also able to detect a nanoscale amorphous overlayer in predominantly crystalline micronised batches of the drug. High relative humidity was shown to recrystallise both the amorphous and micronised batches. X-ray PhotoElectron Emission Microscopy (XPEEM) of pharmaceutical compounds was attempted but, due to the higher beamflux required, sample damage and charging effects were too great to draw any meaningful conclusions at this time.

Declaration

No portion of this work, except that which is stated in chapter 6, in this thesis has been submitted in support of an application for another degree or qualification at this or any other university or other institution of learning.

Notes on copyright

(1) This thesis is subject to a confidentiality agreement with sanofi-aventis. No parts may be made public without the agreement of sanofi-aventis.

(2) Copyright in text of this thesis rests with the Author. Copies (by any process) either in full, or of extracts, may be made only in accordance with instructions given by the Author and lodged in the John Rylands University Library of Manchester. Details may be obtained from the Librarian. This page must form part of any such copies made. Further copies (by any process) of copies made in accordance with such instructions may not be made without the permission (in writing) of the Author.

(3) The ownership of any intellectual property rights which may be described in this thesis is vested in the University of Manchester, subject to any prior agreement to the contrary, and may not be made available for use by third parties without the written permission of the University, which will prescribe the terms and conditions of any such agreement.

(4) Further information on the conditions under which disclosures and exploitation may take place is available from the Head of Department of Chemical Engineering and Analytical Science.

Acknowledgements

I would like to thank my supervisor, Sven Schroeder, for his guidance, pearls of wisdom and general support with my research, especially for giving me the freedom to steer the project how I wished. His experience and help with surface science was also invaluable as was his encouragement, especially when things went wrong! And I have very nearly forgiven him for introducing me to synchrotron work.

I would like to thank everyone in SLMS labs who have all at some time given me either material or moral support. I especially wish to thank Simon Braun for helping with beamtimes, vacuum systems, soft X-ray cell related matters and all manner of other help, Tom Lonsborough for his work on ibuprofen formulations and Nikolaos Tsapatsaris for help with 2-D correlation spectroscopy. Synchrotron experiments are usually run continually but without help this would be impossible so thanks also go to those who have helped out at beamtimes; Simon Braun, Agnes Dauvergne, Hamid Esfahanian, Andy Ip, Angela Beesley, Norbert Weiher, and Anna Makarowicz. Also thanks go to Chris in the Chemistry mechanical workshops for help with making parts for the soft X-ray cell, John Walton for help with the XPS, Soufyane Tefahi for AFM, Dr Paddy Hill for help with ESEM, Dad and Dr Alick Deacon for help using L^AT_EX and proof reading.

I have spent considerable time at Daresbury Laboratory's Synchrotron Radiation Source (SRS) and without the help and support of staff scientists these experiments would have been all but impossible. I would especially

like to thank Dr John Purton (Beamlines 5U.1 and 1.1), Dr Sunil Patel (6.1) and Dr Ian Kirkman (1.1) for help with setting up, running experiments and maintainance.

I would like to thank Sanofi-Aventis for funding through a CASE award and providing samples of pharmaceuticals and formulations. I would also like to thank Dr David England and Dr Stephen Byard specifically for their help and support with the project, especially for fruitful discussions at our progress meetings which were the source of much of the direction of the project and Hanh Nguyen for SR 142801 samples. Also thanks go to Heather Jackson of AstraZeneca for providing indomethacin samples and BASF for ibuprofen samples and formulation information.

Thanks also go to PUPA Gilberts team at the Synchrotron Radiation Center for help with XPEEM experiments, especially Dr Mike Abrecht, Dr Ronke Olabisi and Rebecca Metzler for help with sample preparation performing experiments and data analysis, and for making me welcome in a strange and foreign land.

Finally thanks to Charlie, Mum and Dad and my friends and family for listening to my complaints and rants, pretending to know what I was talking about, and most importantly for the non-work things that kept me sane.

Abbreviations

- DVS - Dynamic Vapour Sorption
- ESEM - Environmental Scanning Electron Microscopy
- EXAFS - Extended X-ray Absorption Fine Structure
- FY - Fluorescence Yield
- NEXAFS - Near-Edge X-ray Absorption Fine Structure
- PXD- Powder X-ray Diffraction, Synonymous with XRPD
- SAXS - Small Angle X-ray Scattering
- TEM - Transmission Electron Microscopy
- TEY - Total Electron Yield
- XAFS - X-ray Absorption Fine Structure
- XANES - X-ray Absorption Near Edge Structure, Synonymous with NEXAFS
- XAS - X-ray Absorption Spectroscopy
- XEOL - X-ray Excited Optical Luminescence
- XPEEM - X-ray PhotoElectron Emission Microscopy
- XPS - X-ray Photoelectron Spectroscopy
- XRPD - X-ray Powder Diffraction

Chapter 1

Introduction

1.1 Objectives

The pharmaceutical industry is of key importance to the U.K. economy. It generates over £12 billion in exports and directly employs over 70,000 people¹. The cost of bringing a new pharmaceutical product to the market has been estimated at around £1 billion¹ and the vast majority of this cost arises from extensive testing and rejection of unsuitable compounds. Any method for improving the efficiency of testing or stopping the development of unsuitable compounds earlier will have an enormous impact on the cost to market and hence for the industry as a whole.

The purpose of this work is to develop the use of soft X-ray synchrotron and surface science techniques for the characterisation of new drug compounds and formulations. Soft X-ray surface science has rarely been used in the pharmaceutical industry, but other areas of pure and applied

material science have made considerable progress using these techniques. The project aims to evaluate how useful and how practical these methods are, and to determine the value of future studies for the pharmaceutical industry.

1.2 Outline

The thesis is organised around the following areas concerning the background and development of equipment suitable for *in situ* soft X-ray spectroscopy and the pharmaceutical systems studied with it.

- Surface science and soft X-ray spectroscopy for pharmaceuticals
- Surface sensitive spectroscopy and microscopy
- *in situ* soft X-ray cell design
- Polymer coating for improving bioavailability (SR 142801[Osanetant] and SSR 180575)
- Surface amorphous and crystalline content (SR 49059 and indomethacin)
- Suspension stability (ibuprofen)
- Additional work on inks and pigments, X-ray microscopy and other detection methods
- Conclusions

Chapter 1 features an introduction to surface science and a brief overview of pharmaceutical development and testing. It also covers previous developments in soft X-ray spectroscopy for pharmaceutical materials and formulations. The previous literature shows that X-ray Photoelectron Spectroscopy (XPS) has been used for several studies but X-ray Absorption

Spectroscopy (XAS) studies of drugs has been very limited and even then only applied to hard-XAS.

Chapter 2 addresses the theoretical background for the techniques used in the subsequent studies including synchrotron sources and the generation and focusing of X-rays, X-ray Absorption Spectroscopy (XAS), X-ray Photoelectron Spectroscopy (XPS), Scanning Electron Microscopy (SEM), Transmission Electron Microscopy (TEM) and X-ray PhotoElectron Emission Microscopy (XPEEM).

Chapter 3 describes the design, construction and testing of the vacuum chamber developed for the project. The cell was developed through several iterations and it incorporated predominantly off-the-shelf parts with a few custom built components.

Chapter 4 concentrates on two poorly soluble drug development compounds, which were treated with polymer surfactants to modify the surface-water interaction. Correlations between modified surface properties and dissolution were observed. The first drug substance, SR 142801, was modified with increasing levels of poloxamer and XAS showed that surface water corresponded to improved performance in trials. The second, SR 180575, was modified with different polymers and using XAS and XPS it was possible to determine how effective the coating polymer was in terms of coverage and adsorbed water. High relative humidity was used to probe the polymer morphology on the surface.

Chapter 5 deals with crystalline and amorphous content at the surface of a drug substance. XAS was used to determine differences in the surface spectra between amorphous and crystalline batches of SR 49059. These spectra were then used to determine that a third, micronised batch, had an ultra thin amorphous surface layer. The same technique was also shown to work for a different drug, indomethacin. It was also possible to observe humidity induced phase transitions by exposing the drug substance to high relative humidity.

Chapter 6 describes experiments to study the stability of ibuprofen suspensions. It was found that peak intensities in XPS, notably water and polymer (C-O) correspond to the performance of a formulation in stability tests.

Chapter 7 covers additional work on drugs and techniques which were largely unsuccessful, but may be of interest for further study. These include a study of ink adhesion which preceded this work and XPEEM of drug formulations.

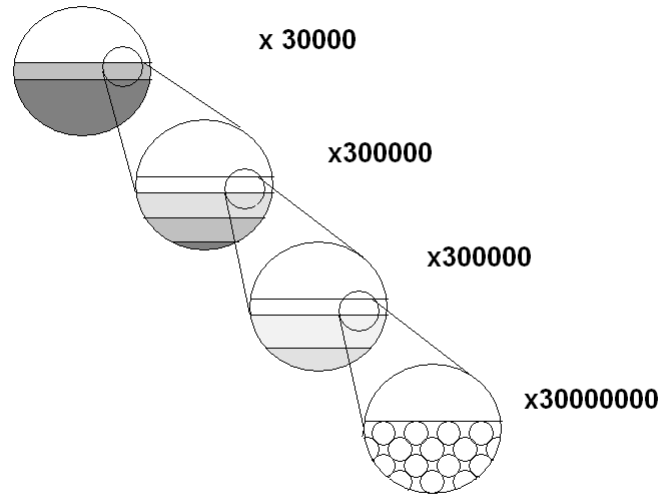
Chapter 8 concludes by addressing the impact the work could have on pharmaceutical development and future work that could be built upon it.

1.3 Surfaces

A surface is a discontinuity between two distinct phases. From an experimental point of view, a surface is usually considered to be the top few atomic layers of a material. The study of surfaces poses a number of potential problems to experimentalists.

The most important problem is the small size of the surface region compared to the bulk, as illustrated in Figure 1.1. For a piece of material approximately 1 mm^3 the ratio of surface atoms to bulk atoms is of the order of 1:1,000,000. This makes changes in surface properties far too small to detect using conventional bulk sensitive techniques. It is therefore necessary to have specialised techniques available to study the surface region. Two common approaches of doing this involve probing a substance mechanically, as in atomic force microscopy, or alternatively using a method with limited signal escape depth such as electrons or even heavy ions².

Bulk Analysis



Surface Analysis

Fig. 1.1: Contrasting surface analysis with bulk analysis. The diagram illustrates the scale of the surface region and the small volume it represents compared to the bulk³

There is also the problem of contamination, which is ever present in surface science. The time taken to form a monolayer on a surface depends on the flux of atoms striking a surface and the sticking coefficient, which is the fraction of atoms that will remain on the surface. The flux is proportional to pressure, and the sticking coefficient depends on several factors including the reactivity and temperature. At room temperature and pressure (1000 mbar, 25°C), assuming a sticking coefficient of 1, the time taken to form a contamination monolayer is of the order 10^{-9} s. At very low pressures (10^{-9} mbar) the time to form a monolayer is of the order 10^3 s. The need for Ultra High Vacuum (UHV) pressures comes from the need to maintain a clean surface over the course of a measurement and is the cause of many of the technical problems in designing and building surface sensitive

experiments.

Why, given the inherent problems, should we perform surface science at all? The study of surfaces is of fundamental importance in material science as it represents a unique region of a material where the structure and hence the properties vary, sometimes greatly, from that of the bulk. For example, in a crystalline solid the surface is where the crystal structure terminates and the nature of this discontinuity determines the surface properties. In chemistry it affects the adsorption of gas and the resulting reactions. In chemical engineering surface properties have a profound influence on such processes as agglomeration, flocculation and suspension. It is also of considerable importance to a wide range of industries. Catalysis depends fundamentally on the interaction between the catalyst surface and reactants³ as illustrated in Figure 1.2 which uses the example of carbon monoxide oxidation on gold, the exact nature of the reaction mechanism is still a point of debate and remains an active area of surface science research. The surface model is now widely used as the basis for catalytic mechanisms. The electronics industry has invested heavily in surface analysis instruments to characterise semiconductors⁴. Polymer manufacturers use such approaches to check that films are suitable for printing and packaging. Figure 1.3 shows the surface treatment of polypropylene and polyethylene films⁵⁻⁹. The films have poor printability due to their smooth, non-polar nature and additives from the production process. Corona discharge treatment modifies the surface region to produce properties more suitable for ink adhesion. Biomedical polymers for pacemakers and other implant devices are now routinely tested using

Object	Typical radius (m)	Surface to volume ratio (m^{-1})
Football	0.1	30
Orange	0.03	100
Pea	0.005	600
Grain of sand	0.0005	6000
Micronised particle	0.000001	3000000
Nanoparticle	0.000000001	3000000000

Table 1.1: Bottom up nanotechnology and the surface region. As size decreases surface to volume ratio increases and surface effects start to dominate the material's properties.

surface analysis techniques¹⁰. If we include the use of surfactants then petrochemical, food processing, pharmaceutical and other manufacturers could stand to benefit from developments in applied surface science.

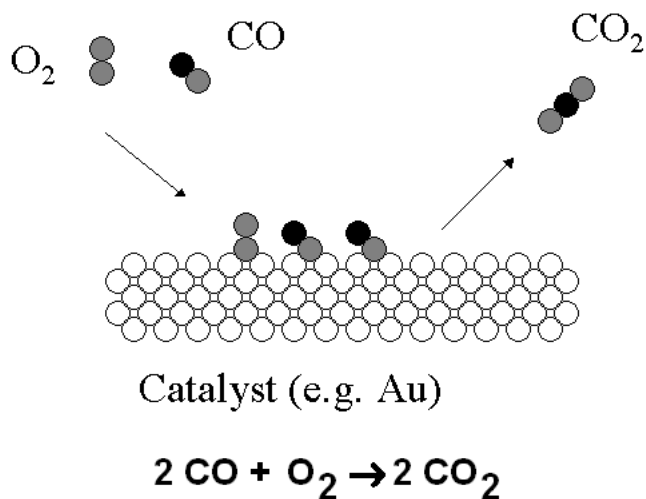


Fig. 1.2: A well studied surface mediated catalytic reaction. Carbon monoxide oxidation on a metal catalyst, gold being one of the most widely studied¹¹.

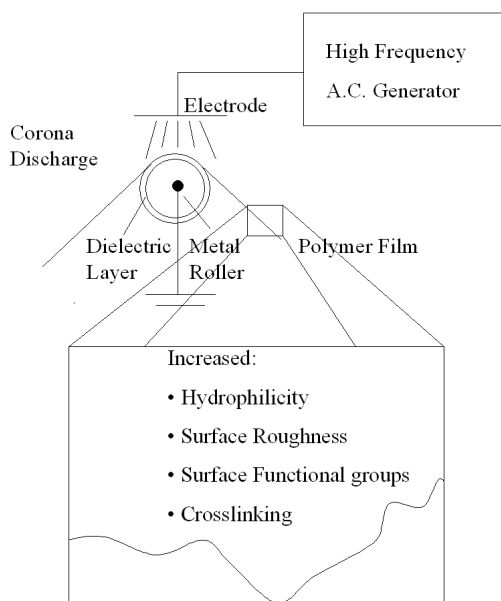


Fig. 1.3: Polypropylene and polyethylene are widely used as packaging materials but have poor printability due to their smooth, non-polar nature and additives from the production process. Corona discharge treatment modifies the surface region to produce properties more suitable for ink adhesion.

In addition, many of the techniques in surface science are often used in so-called bottom up nanotechnology. This is the building of new technology from molecular and supramolecular upwards, rather than miniaturisation of existing machines. Often the unique properties of nanoscale materials come from their high surface area to volume ratio (as shown in Table 1.1 for spherical particles), which surface analysis instruments are in a unique position to explore. The calculations can become less meaningful at very low sizes where an atom thick surface layer can start to comprise a significant volume compared to the total. The gradual introduction of nanomaterials in both drug materials and drug delivery systems¹² provides a further incentive for the adoption of more surface science techniques within the pharmaceutical industry. It is worth noting a difference in terminology between scientific fields. Typically in physics and chemistry ‘nanoparticle’

refers to a particle size of the order of a few nanometers (nm). In the pharmaceutical industry it typically refers to anything sub-micron sized so a 100 nm particle might still be referred to as a ‘nanoparticle’.

1.4 Drug Discovery, Development and Testing

It is necessary to have a brief overview of the process of producing a new pharmaceutical product to have a context in which to place the experimental results and their possible impact.

1.4.1 Drug Discovery

Traditionally drug discovery was a non systematic affair, with new drugs coming from investigations of traditional remedies and serendipitous discoveries. Aspirin, for example, is derived in part from an old herbal remedy for headaches involving willow tree bark¹³ (which contains salicylic acid) and penicillin was discovered due to accidental contamination by mould of a bacteria cell culture. An improved understanding of biology at the molecular level has led to the chance approach being largely superseded by so-called rational drug discovery as shown in Figure 1.4.

In the rational model of drug design, molecules are picked for their properties, usually a highly selective affinity for a particular biochemical receptor or target such as a protein, which has been identified as an important trigger or sensor for a particular disease or symptom. Suitable molecules are determined by combinatorial chemistry and high throughput screening. The lead compound is the one thought to be the most promising and usually there will be other backup compounds based on the same structure, should the

lead prove unsuitable. The candidate, as the most suitable molecule from the ‘batch’, will then go on to the drug trial process. Scientific knowledge obtained during the discovery and testing process also improves understanding of the underlying biology.

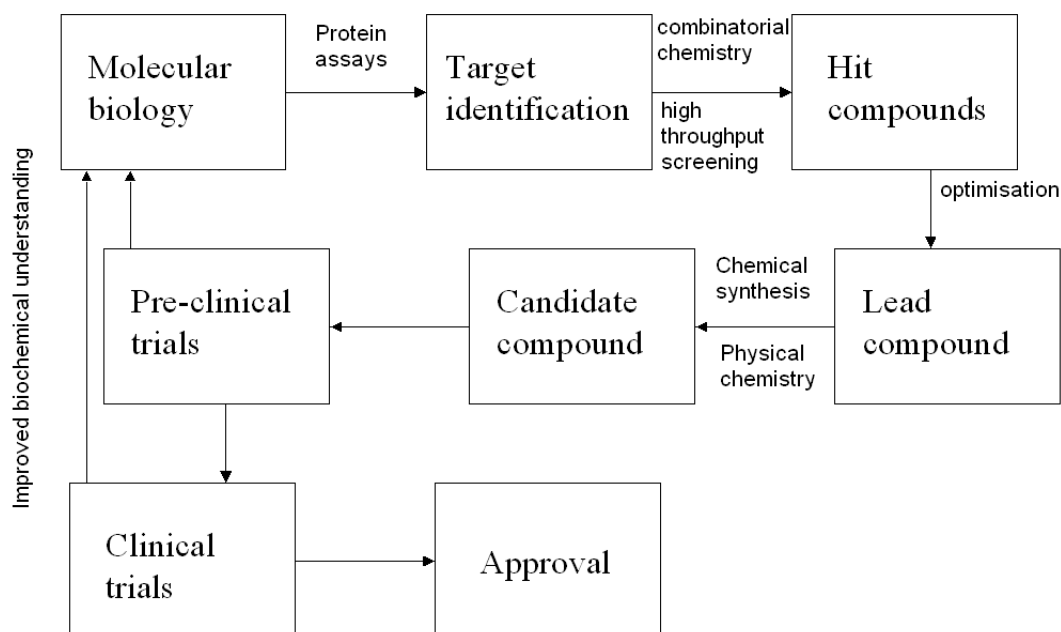


Fig. 1.4: A rational approach to drug design: Building on an understanding of biology at a molecular level potential drug molecules are found and optimised for a (protein) target.

1.4.2 Drug Testing

Pharmaceutical products require extensive testing due to stringent regulatory requirements¹⁴ and the medical principle of *Primum non nocere* “First, do no harm” is adopted to ensure they are safe for patients. Testing is the most expensive stage of developing a drug product so any improvements in efficiency here can drastically change the cost to market.

1.4.2.1 Pre-clinical

The purpose of pre-clinical testing is to ascertain safety limits for the clinical trials by determining the toxicity and pharmacokinetic properties of the candidate compound using animal models and tissue cultures. While rare anomalous cases show that pre-clinical screening is not always perfect, it is still necessary for estimating safe dosage limits. It is also a legal requirement in many countries that a compound has had sufficient animal testing before proceeding to human trials.

1.4.2.2 Clinical

Clinical trials refer to human testing for safety and efficacy purposes once the drug has passed the pre-clinical stage. Traditionally it is considered a 3 phase process with increasing numbers of patients at each stage although for completeness the so-called phase 0 and phase IV stages have also been included, as illustrated in Figure 1.5. At any stage of the testing a drug compound may prove unsuitable and be rejected. This rigorous testing and rejection is what causes the massive cost of developing a new drug product which has been estimated at around £1 billion.

While strictly speaking not a part of the traditional testing regime, testing of novel treatment methods or new drug delivery devices is sometimes considered to be phase 0 testing¹⁵.

Phase I trials are small scale trials on healthy subjects to determine the

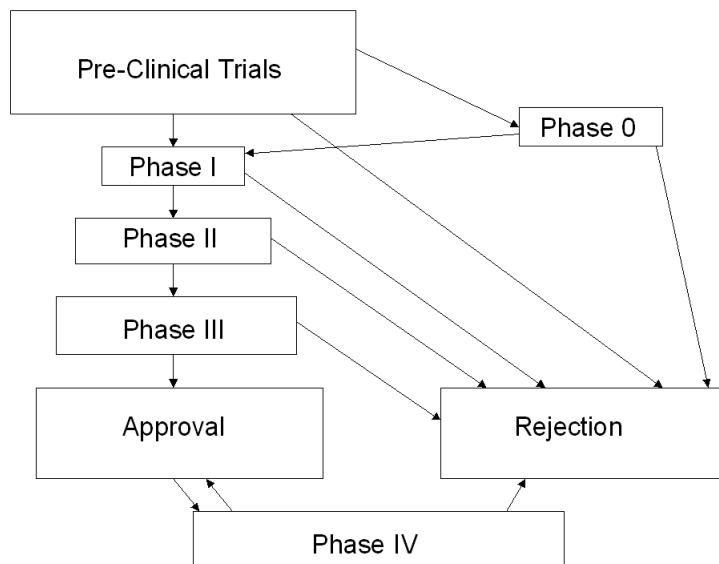


Fig. 1.5: Schematic of the drug testing process. Testing and rejection of new compounds accounts for most of the estimated £1 billion cost of developing a drug.

human safety of the drug. They are also used to gain initial pharmacological and pharmacokinetic data on uptake, absorption, metabolism etc.

Phase II trials frequently split into Phase IIa and IIb. Phase IIa are proof of concept tests and may be omitted. Phase IIb are the first tests in patients with the symptoms or disease the drug is intended to treat. They are small scale tests to determine efficacy and dosages for the drug.

Phase III trials are large scale tests on patients to obtain more statistically valid data than phase II. It is predominantly the phase III data that will determine if the drug is approved (The drug will have had to pass the previous phases before getting to phase III).

Once a drug has been approved by the relevant regulatory agency as safe and is in wide-spread use development can still continue. As part of product life-cycle management a drug product may be reformulation to improve and control release profile for improved patient safety and product optimisation. Safety information is still collected as there is a much larger pool of data to draw from. It is not unheard of to revoke a licence for a drug which has passed the phase I, II, III trials when a previously unforeseen side effect comes to light such as the case with thalidomide.

1.5 Soft X-ray Spectroscopy in the Pharmaceutical Sciences

This section will address previous work on pharmaceutical surfaces studied using the following soft X-ray spectroscopy techniques and some of the associated technical developments. The theoretical backgrounds to the techniques are discussed in further detail in Chapter 2.

Pharmaceuticals already have, through structural biology, a close connection to synchrotron science. Protein crystallography is one of the major tasks of most synchrotrons and plays a significant role in modern drug discovery. Synchrotron X-ray diffraction is widely used to determine crystal forms and structures for the pharmaceutical itself. The work is discussed from the perspectives of using;

- X-ray Photoelectron Spectroscopy (XPS)
- X-ray Absorption Spectroscopy (XAS)
- X-ray PhotoElectron Emission Microscopy (XPEEM)

1.5.1 Introduction

The surface properties of a pharmaceutical are not necessarily important at a biochemical level where the substance will most likely be in solution. However, they do impact on the physiological and pharmacokinetic effects, especially the initial interaction of the product with the body. They also

impact upon the physical properties of a formulation such as stability. Micro and sub-micrometer sized particle formulations increase the surface area and speed up (oral) incorporation into the body by aiding dissolution. Poorly water soluble drugs can be modified with surfactants to boost bioavailability, the fraction of the drug remaining at the site of action. Environmental extremes of humidity and temperature will affect the surface first. Amorphous material at the surface can affect formulation into tablets. XPS and soft-XAS are well placed to study these surface related issues but it is necessary to understand the limitations and problems associated with these techniques, see also Chapter 2.

There are several problems which make pharmaceuticals a poor choice for studying with XPS and XAS, and to a certain extent, have been responsible for the smaller body of work than would be expected for such an important set of materials. Most pharmaceutical products are based on active ingredients which are (i) organic, (ii) insulating and (iii) tend to outgas in vacuum.

(i) X-rays, especially around the relevant absorption edge, can be chemically reducing so care has to be taken to check that the sample can withstand the intensity without significant change over the course of an experiment. This problem tends to be more pronounced with more electronegative species, particularly fluorine containing compounds. The higher intensities required for suitable imaging make this a big problem with XPEEM, especially when dealing with biological samples.

(ii) Charging will affect the electron emission, which is critical to XPS and electron yield XAS. Charging can cause peaks and edges to shift. In XPS several systems have been developed to neutralise charging effects and are now common in commercially available machines. With *in situ* XAS the gas in the chamber will prevent charge build up due to ionised gas molecules migrating to charged areas on the sample. This problem is very pronounced in XPEEM because of the high electric field applied for imaging, the high intensity and the need for vacuum. Mixing with metal powder and coating with gold or platinum can reduce the effects but at the risk of changing the sample surface significantly.

(iii) Outgassing is when a material has volatile components which evaporate or sublime in the vacuum and raise the pressure in a similar way to a leak (sometimes called a virtual leak). Outgassing causes two problems; the first is that it makes it very problematic to maintain an Ultra High Vacuum (UHV) environment and secondly the outgassing may result in some damage to the sample which makes it unrepresentative of how it exists under ambient conditions. Outgassing is a problem with shared facilities and equipment because of the risk of contaminating the vacuum and in general, biological and pharmaceutical samples need to spend far longer in airlocks to achieve a sufficient vacuum. This was also a motivation for developing purpose built equipment for the project.

1.5.2 X-ray Photoelectron Spectroscopy (XPS)

X-ray Photoelectron Spectroscopy (XPS) uses (soft) X-rays to photoeject electrons. Due to their small inelastic mean free path these electrons have a limited escape depth meaning they originate from the surface layers (~ 5 nm). The kinetic energy of the electrons is measured and the binding energy is calculated. The positions of binding energy peaks allow the determination of elemental abundances. Shifts in the binding energy correspond to changes in the ejecting atoms local chemical environment and can be used for chemical state determination. The field of X-ray photoelectron spectroscopy was first developed from the mid 1950s^{3;4} with the first commercial instruments appearing in the late 1960s. Initially most studies were of idealised systems such as single crystals and other inorganic materials including metals, alloys, oxides and semiconductors, which are not damaged by Ultra-High Vacuum (UHV) or X-rays. The first studies of polymers in the mid 1970s were in part made possible by instrument improvements and other important developments such as low energy electron flood guns, which eliminated many of the problems caused by sample charging. By the mid 1980s it was a well established tool in polymer science and is still frequently used in material development¹⁶ and its use continues to improve¹⁷. A spin-off of the work in polymer sciences is the application for polymer films manufacturers, eager to ensure suitable printing properties in their packaging materials^{6;8;16;18–22} and it has been instrumental in addressing outstanding problems concerning the surface effects from various pretreatments²³. It was also the first area of research undertaken by the author in regards to this thesis.

The first applications to biomaterials came in part from the new polymer work and also from the earlier work on inorganic materials such as TiO_2 ²⁴. With the development of artificial implants in all areas of medicine, from the life changing such as pacemakers and artificial hips to the more mundane such as contact lenses, there came a need to understand how the body reacts to such materials. The adsorption of proteins on these materials is a direct result of the surface properties. The protein layers themselves are of the order of 1-10 nm thick which is within the realm of soft X-ray surface science. Thanks to Castner and Ratner, work such as this has since become routine²⁵⁻²⁹, and the American Food and Drug Administration (FDA) often use XPS obtained information to assess the suitability of medical devices. A commonly studied material in biomedical surface science is the widely used PMMA (Polymethyl methacrylate). It has a high biocompatibility due to its hydrophilicity³⁰⁻³². When an implant material is used it provokes a response from the immune system, the first part of which is the adsorption of a protein, fibrinogen, to the implant material as shown in Figure 1.6. The active site of the protein, where it reacts with a substrate, is hydrophobic as it needs to remain in solution (blood) until it can attach to the foreign material and this response is minimised with PMMA, leading to its wide spread use.

With XPS proving useful in many aspects of polymer science, it was then applied as a complementary technique to polymer-pharmaceutical mixtures. Carli and co-workers³³⁻³⁶ chose XPS partly because of similarities

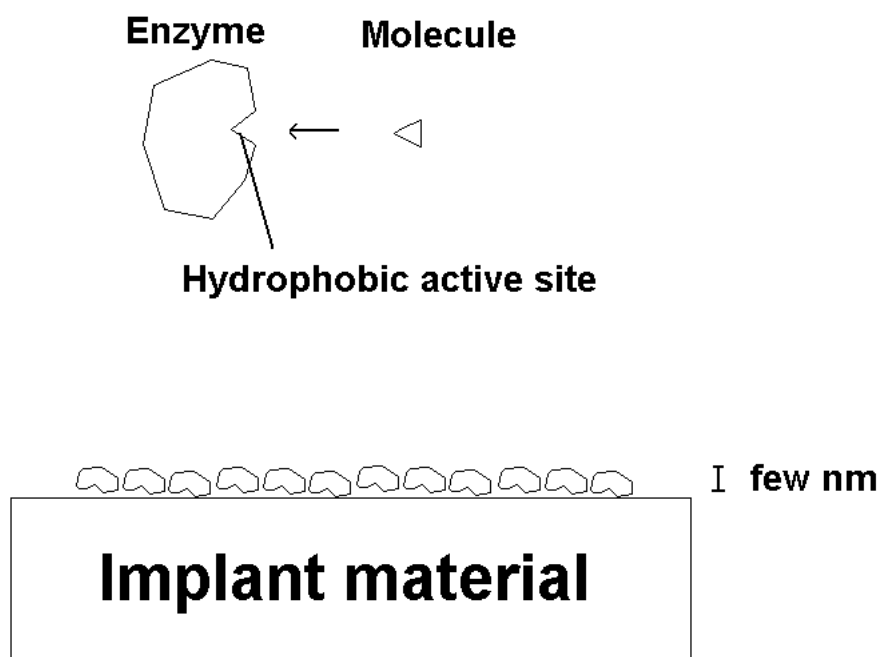


Fig. 1.6: Enzyme and implant material interaction is governed by the surface properties of the material and the protein (the active site).

between the polymer-drug systems they were studying and metal supported catalysts which had previously been successfully studied with XPS. They used swelled cross-linked polyvinylpyrrolidone to incorporate drug material and then compared expected elemental abundances with measured values to work out how much drug was present at the surface. As a result they were able to determine that one of the compounds had almost entirely coated the polymer. Although they did some chemical state assigning, they did not use this information in the quantitative analysis and they made no allowance for the hydrocarbon contamination that is almost always seen in XP spectra. This method was used by other workers^{37;38} who also looked at drug-polymer systems, including nanoparticle systems, to investigate surface enrichment and they were able to determine the emergence of a core-shell structure in

their formulations (see Figure 1.7).

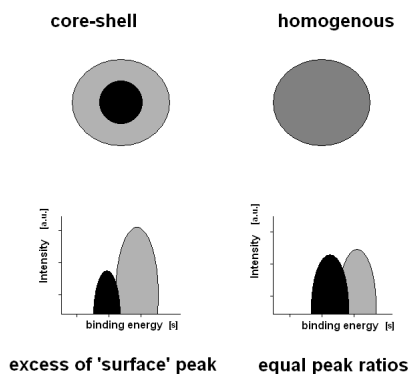


Fig. 1.7: A core-shell structure leads to surface spectra where one component is enhanced relative to the other.

Feng^{39–41} and his group studied Taxol, a very potent anti-cancer drug. They used XPS as a complementary technique to other surface techniques such as Scanning Electron Microscopy (SEM) and Atomic Force Microscopy. They formulated PLGA (poly(lactic-co-glycolic acid)) nanospheres in an attempt to improve uptake of the drug and used the XPS to determine the resultant surface chemistry of the formulation and combined this with morphological information from the SEM and AFM. They were able to compare methods of nanoparticle encapsulation and determine which was the best method for incorporating the drug into the formulation.

Davies and co-workers^{42–48} used XPS and Secondary Ion Mass Spectrometry (SIMS) to study the surface structure of polymers used in more complex drug delivery systems and related this to degradation. They used polyethylene oxide (PEO) as a model drug compound and grafted it to polystyrene colloids. They followed the specific peaks in the carbon envelope

(C-O) to identify the drug model and this correlated well with increasing levels in the polystyrene and this approach circumvents the problem of C-C contamination.

Buckton⁴⁹ investigated pure drug substances instead of formulations. They looked at barbiturate powders and pressed tablets where they found variations in surface energies that did not correspond to changes in chemical composition as measured by XPS. This work was important in showing that XPS of pharmaceuticals can address a whole manner of surface problems and need not be limited just to polymer or formulation studies.

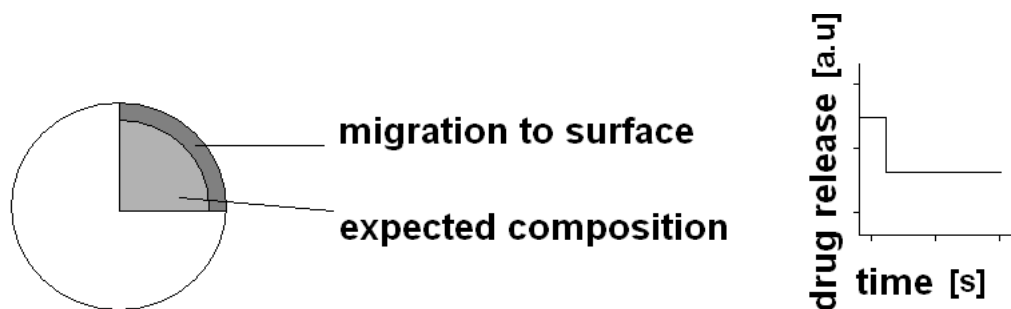


Fig. 1.8: Variations in cross-sectional drug concentration can affect the release profile.

John⁵⁰ used combined XPS and SIMS to study drug incorporations into a drug delivery system for sustained release and they noticed that drug inclusion along a cross-section of the polymer (hydroxypropyl cellulose) was not constant which, would lead to unwanted variations in dosage. Figure 1.8 shows an initial spike in a drug release profile corresponding to surface enrichment in the formulation.

Westwood⁵¹ studied the use of a cationic polymer to hold an anionic drug substance and deliver this to eye. By using XPS he was able to confirm that a suitable reaction between the drug and polymer had occurred, binding it to the polymer surface.

1.5.3 X-ray Absorption Spectroscopy (XAS)

X-ray absorption edges were measured by Mosley at Manchester, who used them to confirm that atomic numbers, Z , were physically meaningful (corresponding to nuclear charge) and predicted the existence of unknown elements from gaps in plots of measured X-ray spectra. X-ray Absorption Fine Structure (XAFS) was first discovered in the mid 1920s. Kronig⁵² offered the first explanation of this as the outgoing photoelectron scattering off neighbouring atoms but it was not until 1971 that it was first used in a structural determination by Lytle, Sayers and Stern⁵³. For practical purposes X-ray Absorption Spectroscopy (XAS) is divided into two regions, namely Extended X-ray Absorption Fine Structure (EXAFS) and X-ray Absorption Near Edge Structure (XANES)/Near Edge X-ray Absorption Fine Structure (NEXAFS). EXAFS, extending from about 40 eV past the absorption edge to several hundred eV, provides structural information such as bond lengths, coordination numbers and unlike X-ray diffraction, it requires no long-range order. XANES/NEXAFS, up to 40-50 eV past an edge, provides information on bond angles, bond lengths, oxidation states and electronic structure, and is highly sensitive to the presence of

adsorbates. In most (but by no means all) cases the acronym XANES is used for hard X-rays and in chemistry and earth science literature, while NEXAFS is used for soft X-rays and is also commonly used by physicists and surface scientists. Throughout this work NEXAFS is the preferred term. See Chapter 2 for further details.

XAFS has been dominated by studies with hard X-rays. This allows data collection using the bulk sensitive transmission mode as well as removing problems associated with using soft X-rays and the accompanying vacuum systems. Heavy atoms are also better at scattering the outgoing electron wave. For pharmaceutical studies this means that almost all the work has been on compounds based around a central metal atom⁵⁴⁻⁵⁸ despite the large number of pharmaceutical compounds with only light elements. One of the first pharmaceutical systems studied using XAFS was of the coordination chemistry of complexes in anti-arthritis drugs⁵⁹. EXAFS, especially when combined with other crystallographic techniques, provides valuable insights into the local molecular structure around an X-ray absorbing atom (Figure 1.9). This was used to look at structure around a central gold site of several drugs^{55;56}.

This approach has been used on similar metal containing pharmaceuticals such as platinum anti-cancer drugs (Cisplatin and Carboplatin)^{57;58}, Bouvet⁶⁰. There were suggestions that Carboplatin, a much less toxic drug than Cisplatin, might be unstable in solution and could convert to a more toxic degradant. XAS in solution showed that this could indeed

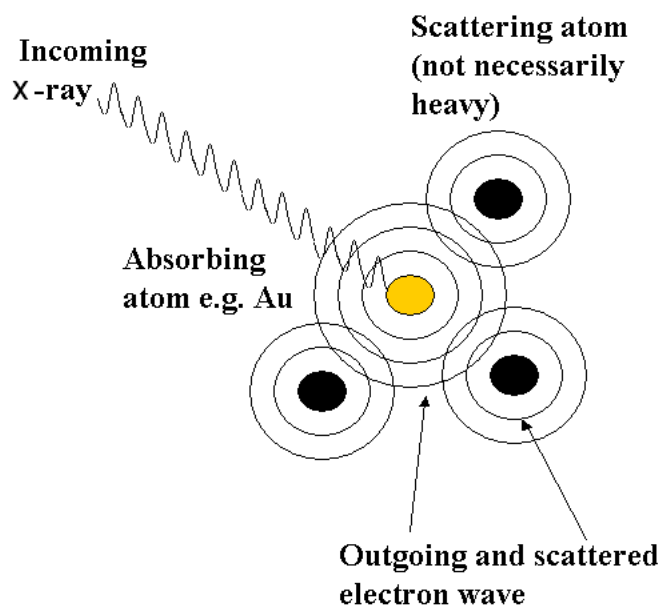


Fig. 1.9: An incoming X-ray can eject a core electron from a central atom, the outgoing electron wave scatters and interferes with neighbouring atoms.

happen, and it was observed using NEXAFS reference spectra from each form to synthesise the intermediate spectra and observe the reaction (Figure 1.10). It was possible to show that this problem was only important at low pH values. The studies illustrated how effective XAS can be as an *in situ* tool. This is comparatively easy for high atomic number (Z) materials as X-rays with energies at their absorption edge are highly penetrating.

Arsenic pharmaceuticals⁶¹ have been studied and NEXAFS shifts were used to identify the chemical state of an injected solution where it could potentially exist in a number of different forms. Comparison with a reference solution of arsenic acid confirmed that the chemical state of

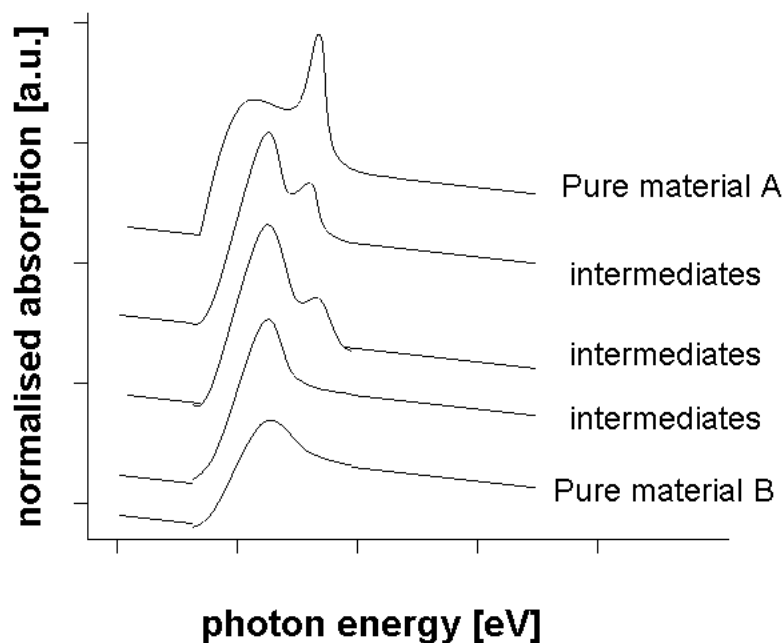


Fig. 1.10: A common method for Near edge spectra; the endpoints of a reaction or concentration are identified or reference spectra are made for known chemical states of a given element.

the main component in the injected form was similar. This is a common approach in other fields such as geology, catalysis and environmental science where shifts are identified from known model compounds and used to determine the oxidation state in an unknown sample.

Other similar compounds studied include contrast agents for Magnetic Resonance Imaging to examine the structures they form in aqueous solutions, and radiopharmaceuticals, which were studied to compare bond lengths between heavy elements. This approach can only provide information about the heavy element and its near neighbours. Although very useful in these cases it does not address light elements and cannot be used for samples

without a heavy atom to act as the absorbing atom⁵⁴.

Soft-XAS studies of pharmaceuticals however have not been as wide spread as those in the hard X-ray region because of the technical problems covered in section 1.5.1. The first NEXAFS spectra at the carbon (285 eV), nitrogen (405 eV) and oxygen (532 eV) K-edges had to wait until the late 1970s⁶² and the development of the first monochromators that were capable of reaching from 100 - 1000 eV. Most of the earlier studies were adsorbates on single crystals, although later work included studies of polymer films⁶³ and wide application to catalysis to investigate *in-situ* surface reactions^{64;65}. As with XPS, the improvements in monochromators and brightness have made it more practical to study more complicated systems and NEXAFS has now been widely used in geology, environmental and polymer chemistry.

Use of NEXAFS for pharmaceuticals has not been widespread. One reason for this is that NEXAFS cannot easily be applied to samples in solution, unlike hard XAS. Also the spectra would be very complicated. Instead of being based around a single central atom as in the hard XAS examples there would be multiple contributions from each atom of the element being studied. Ade and Dhez⁶³ have studied a wide range of common polymers some of which are important for drug formulations. Researchers have also studied several biomedical polymers⁶⁶⁻⁶⁸ and these have shown that it is perfectly feasible to study drug delivery devices to provide complementary information to that provided by XAS.

Several researchers are working on making measurements in solution using liquid microjets and spectra from liquid water and salt solutions have been measured⁶⁹⁻⁷¹. With new higher flux beamlines measurements from moist samples and even samples in solution could become common. With higher flux there are fewer problems with signal attenuation from water vapour and there are a wide range of possibilities. NEXAFS has recently been used to examine drug solubility⁷². NEXAFS is very sensitive to hydrogen bonding influencing local electron structure. It is thought that this could be used to probe the surface interactions of poorly soluble drugs and they are currently working on equipment that would allow measurements in solution.

1.5.4 X-ray PhotoElectron Emission Microscopy (XPEEM)

The current emphases in the design and development of new soft X-ray beamlines are improvement of the beam footprint; higher intensity; and a small, well defined spot size for the beam. This, together with combined efforts in improving analytical instruments such as those for XPEEM, has pushed the spatial resolution limits lower and lower. The current range of XPEEM microscopes on 3rd generation synchrotrons are easily capable of generating NEXAFS spectra with a spatial resolution of 50 nm and as low as 15 nm has been reported⁷³. The potential uses for this technique are huge and it seems to fit the ideal parameters of a surface science

technique as shown in Figure 1.11 of high spatial resolution combined with high chemical sensitivity. It has already found applications across the whole range of materials that NEXAFS has been used for, including semiconductors and magnetic materials^{74;75}, mechanical wear studies⁷⁶, geology and environmental science⁷⁷, polymers where studies have been able to observe phase separation in polymer melts making use of previous detailed NEXAFS spectra^{32;67;68;78;79} and biomaterials^{30;31;80;81} where preferential absorption of protein (fibrinogen) onto the less biocompatible polymer in a two polymer melt has also been observed. The ability to study materials down to these scales could prove very important with the shift towards nano-particle incorporating formulations.

1.5.5 Conclusions

Extensive studies of biomedical materials have shown that wide scale use for pharmaceutical materials is feasible, and the popularity of recent reviews in biomedical surface science show that these types of applied systems are of increasing interest to surface science workers. With advances in instrumentation it now seems that XPS could become a routinely used technique for formulation development. XAS and XPEEM will be slower to be adopted mainly due to constraints of obtaining experimental time but they can still provide valuable supporting data for specific problems where the one-off cost could be justified.

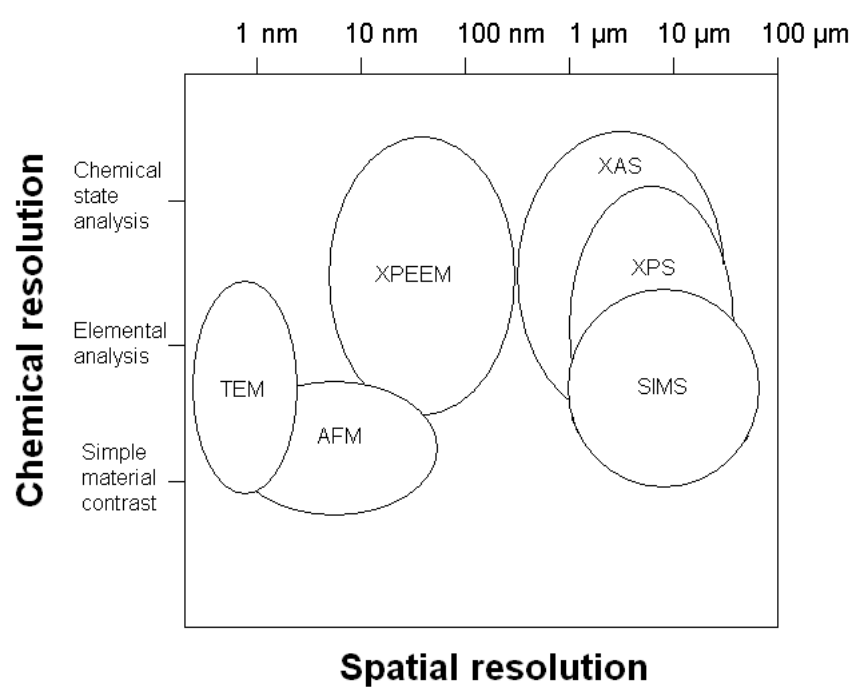


Fig. 1.11: Surface sensitive techniques are a trade off between spatial and chemical/structural resolution.

Chapter 2

Experimental: Theory, Methods and Techniques

2.1 Introduction

No ‘magic bullet’ exists in surface science which can provide all the information about a sample. Experimental solutions are trade-offs between spatial resolution, spectral and structural resolution, *in situ* use and availability of equipment. In order to interpret results correctly it is important to have a good understanding of how the technique works, what information it can provide and what their limitations are. The following chapter covers the theoretical background of the techniques used later in the thesis.

Soft X-rays are generally considered to be those with photon energies in the range $100 \text{ eV} \leq h\nu \leq 1\text{-}2 \text{ keV}$ which overlaps the vacuum ultra-

violet region (VUV), hard X-rays are those with higher energies. They are important experimentally because electrons ejected by soft X-rays tend to have short mean free paths in matter and the region encompasses the absorption energies of carbon, nitrogen and oxygen. The exploitation of soft X-rays for experimental purposes has many significant problems that can broadly be divided and discussed along the following lines:

- Generation (X-ray tubes and synchrotrons)
- Vacuum Requirements (pumping and pressure measurement)
- Manipulation (monochromating and focusing)

2.1.1 X-ray Tubes

X-ray tubes have been available as laboratory sources since the 1900s. They work by having an electron beam decelerate into a target material as shown in Figure 2.1. The target then emits an X-ray. The electron beam ejects a core electron from a target atom which then relaxes by emitting an X-ray with a characteristic energy, which is dependent on the material used, and filling the core hole with a higher level electron as shown in Figure 2.2. For an XPS instrument the characteristic energy should be high enough to eject a wide range of core electrons from the surface and the line width should be narrow enough that it allows deconvolution of the spectra. Due to the heat load the material also has to have suitable thermal properties such as high conductivity. Aluminium and copper are the two most common materials used^{3;4}.

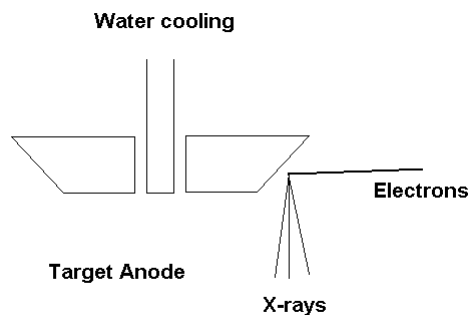


Fig. 2.1: An X-ray tube in an XP spectrometer uses a rapidly rotating water cooled target (to dissipate heat load) and an electron beam which is decelerated into the target to produce the X-rays

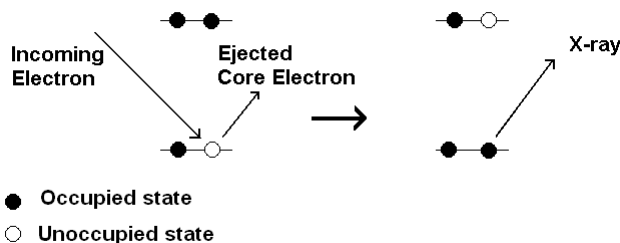


Fig. 2.2: X-rays are produced by using the incoming electron beam to eject core electrons and put the atom in an excited state which then relaxes by emission of an X-ray and filling the core hole with an electron from a higher energy level.

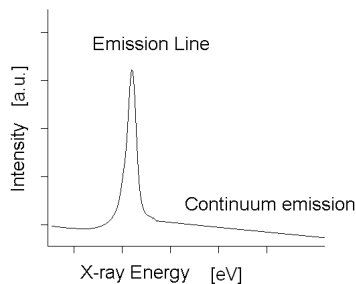


Fig. 2.3: Typical spectra from an X-ray tube with a high flux of photons coming from the K_{α} peak. Also present will be additional peaks from any impurities and a brehmsstrahlung background from the decelerated electrons.

X-rays are emitted at a characteristic energy (Figure 2.3) there are additional lines from impurities in the target and satellite emissions from less intense lines. There also exists a continuous background from brehmsstrahlung emission that contributes nothing to the signal but increases

the noise level and can contribute to sample damage.

2.1.2 Synchrotron Radiation Sources

Synchrotron radiation, so called because it was first identified in a synchrotron particle accelerator, occurs when relativistic electrons are accelerated in a magnetic field. The radiation emitted has a very high brilliance and is in a highly collimated beam tangential to the acceleration due to relativistic effects. Initially this was a problem for particle physicists causing energy loss in accelerated electron beams. Workers in other fields, however, realised that such an intense source of radiation over a wide range of wavelengths, including soft X-rays, would be highly beneficial in other areas of research. Synchrotron radiation was first used parasitically by Tomboulion and Hartman⁸² in 1956 for measuring the transmission of thin metal foils. This 1st generation of parasitic synchrotron radiation experiments was so successful that accelerators became purpose built for synchrotron radiation users; the 2nd generation of sources. The continued growth and progress in accelerators as shown in Figure 2.4 has led to the development of a 3rd generation of sources which build on previous experience to produce even higher radiation fluxes due to better insertion magnets such as undulators and wigglers. Exponential increases in brilliance are leading scientific breakthroughs in material, chemical and biological science. The high flux and tunable nature of beamline optics make synchrotron sources the tool of choice for soft X-ray techniques, but the expense in constructing and

running one means that most industrialised countries can only afford to operate a few and as such experimental time is highly valued.

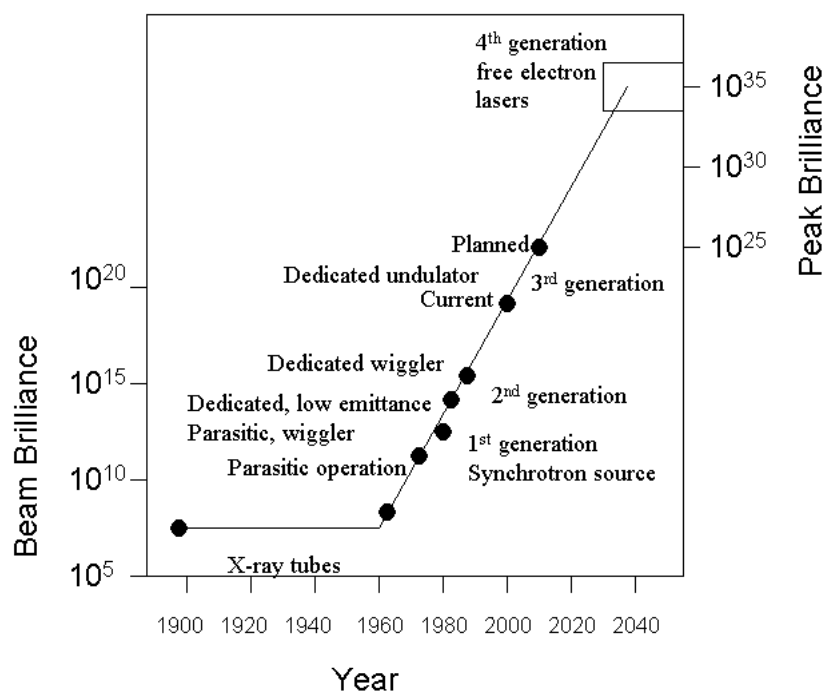


Fig. 2.4: The rise and rise of synchrotron radiation.

2.1.2.1 Electron Ring

A main storage ring is used to cycle an electron beam which will emit synchrotron radiation as it passes through a magnetic field. In order for the electron beam to reach a sufficiently high energy it will periodically be injected from a progressive series of linear and circular accelerators as shown in Figure 2.5. For Daresbury laboratory an electron gun injects a beam of electrons into a linear accelerator which accelerates the beam to 10 MeV, then a booster synchrotron cycles the beam up to 600 MeV, this is then injected in the storage ring where it is accelerated to 2 GeV. The beam loses energy through (desired) synchrotron radiation at each magnet. Radio frequency cavities are used to boost the beam energy back up. The beam slowly loses intensity so it periodically (every 12-24 hours) needs to be reinjected anew, or topped up continuously.

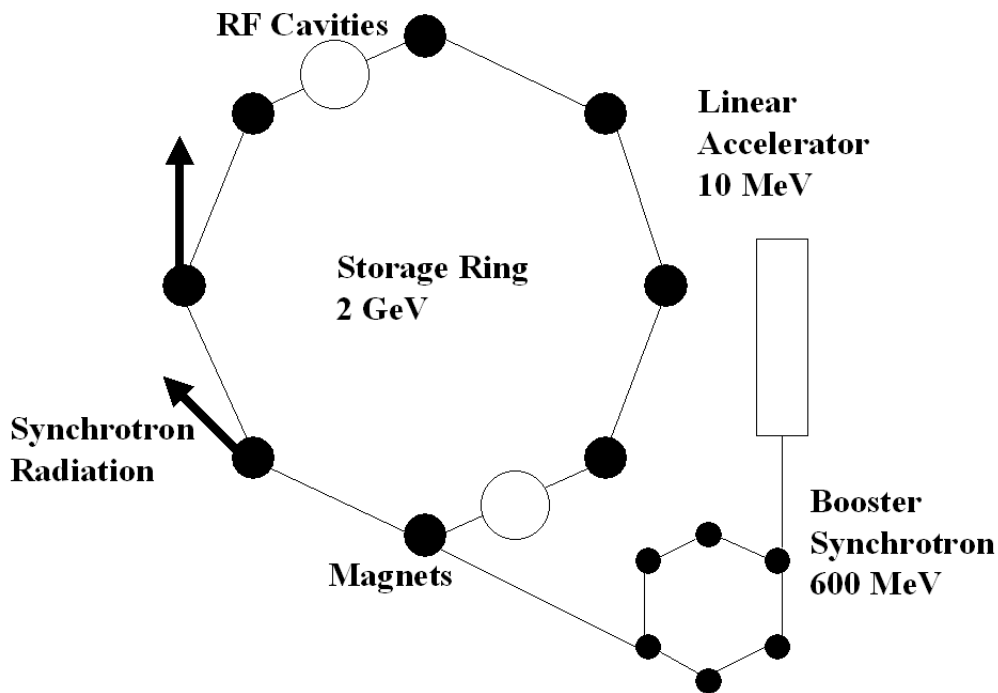


Fig. 2.5: Schematic of a system of accelerators to produce synchrotron radiation.

2.1.2.2 Magnets and Insertion Devices

When a relativistic electron beam passes through any magnetic field it will emit synchrotron radiation (see Figure 2.6). Due to the relativistic nature of the electron beam the resultant radiation is very highly collimated (compressed by an angle $1/\gamma$). In earlier synchrotrons the magnets used for steering the beam were also used as the primary source of radiation but more sophisticated devices have now been developed which allow greatly improved fluxes or polarisation control.

The emission spectrum of a typical Daresbury bending magnet (calculated using the Advanced Photon Source (APS) program⁸³) is shown in Figure 2.7.

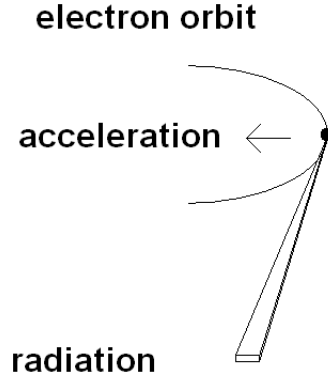


Fig. 2.6: Accelerated charges emit electromagnetic radiation, such as the electron beam passing through the magnetic field of a bending magnet or insertion device. The radiation field is compressed by an angle $1/\gamma$.

The characteristic energy is the energy at which the flux is greatest. The operating and design parameters of a synchrotron are often optimised to produce radiation at the most commonly used wavelengths for the research community using it. The characteristic wavelength, λ is dependent on the Lorentz factor, γ , and the electron radius of curvature, r ⁸⁴. The characteristic wavelength is given by,

$$\lambda_u = \frac{2r}{3\gamma^3} \quad (2.1)$$

where the Lorentz factor for relativistic effects is given by,

$$\gamma = \frac{1}{1 - v^2/c^2} \quad (2.2)$$

where v is the speed of the object and c is the speed of light in vacuum.

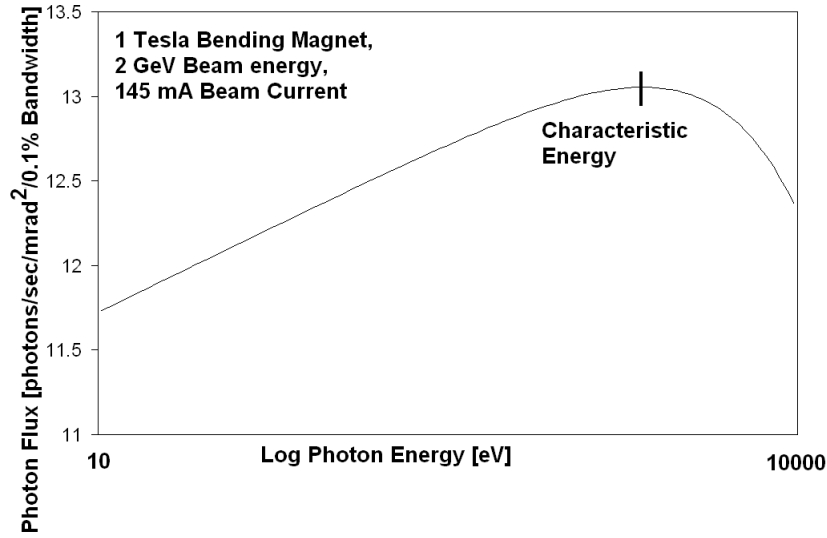


Fig. 2.7: The spectrum produced for a typical bending magnet at Daresbury Synchrotron Radiation Source (SRS).

Insertion devices are arrays of magnets opposing each other to maximise the acceleration the electron beam undergoes but with no net deflection of its path. The operation of insertion devices is determined by a dimensionless parameter, K which depends on the undulator wavelength, λ_u , the magnetic field B , the electron mass and charge⁸⁴ and is given by,

$$K = \frac{eB\lambda_u}{2\pi mc} \quad (2.3)$$

When $K \gg 1$ then each pole contributes independently to the flux to give N times the flux of a single magnet where N is the number of poles. If $K \ll 1$ then the poles constructively interfere which produces sharp harmonic peaks and gives a resultant flux of N^2 compared to a single magnet^{84;85}. The bandwidth of the harmonics is given by,

$$\Delta\lambda/\lambda = 1/nN \quad (2.4)$$

where n is the n th harmonic. The very narrow band and very high brilliance result in a very efficient insertion device only producing radiation in the narrow harmonic which can then be tuned over a wider range as in Figure 2.8. The magnets are often set up in an array similar to Figure 2.9.

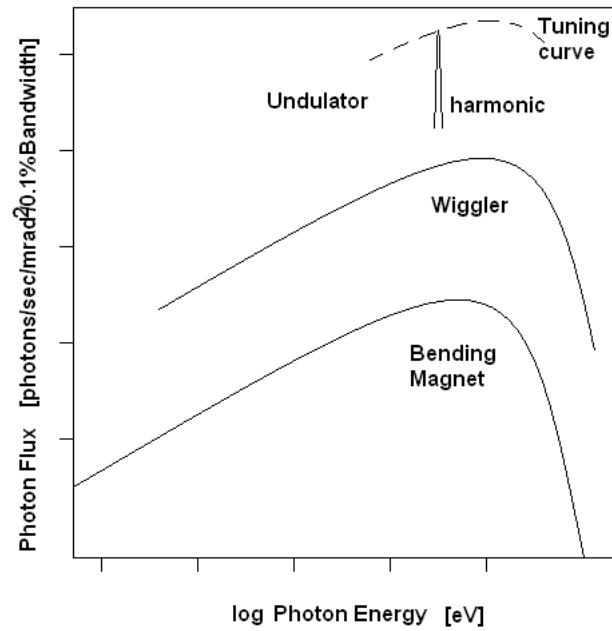


Fig. 2.8: Comparison of Flux from a bending magnet, a wiggler and an undulator.

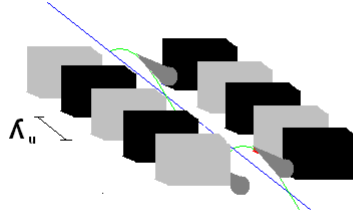


Fig. 2.9: A generalised insertion device consisting of an array of magnets opposing each other to maximise the acceleration the electron beam undergoes but with no net deflection of its path

2.1.3 Vacuum Conditions

Soft X-rays have a short inelastic mean free path in air and their use requires vacuum conditions. It was not until high quality vacuum systems had improved that surface analysis instruments using soft X-rays were practical. A typical XPS machine with a distance of the order 10-100 cm between the X-ray source and the sample requires a pressure of 10^{-5} mbar or lower to ensure enough photons reach the sample surface. While this pressure is several orders of magnitude greater than that required to prevent surface contamination, it still presents problems for making *in situ* measurements. At a synchrotron the pressure inside the main ring is typically 10^{-9} mbar or less in order to reduce the number of collisions between the electron beam and residual gas molecules which reduce the beam stability.

2.1.4 Focusing and Monochromatisation

The optics of X-ray tube do not need to be as sophisticated as those of a synchrotron source. As discussed previously the dominant line is not the only emission encountered, however the use of a monochromator can eliminate the problems associated with this. A monochromator is usually a crystal diffraction grating or monochromator that uses Bragg diffraction to select a specific wavelength, λ given by:

$$2d \sin \theta = n\lambda \quad (2.5)$$

where λ is the wavelength, θ the incident angle and d the atomic spacing. For soft X-rays polished silicon or quartz crystals have an appropriate d -spacing for normal use. The monochromator can also focus the resultant beam in a small spot size that is useful in microanalysis and imaging (Figure 2.10). A Rowland sphere monochromator uses a crystal bent around a hypothetical sphere such that the photons of a given order and wavelength will be focused onto one spot. The development of suitable monochromators and the subsequent reduction in sample irradiation was an important catalyst for the rapid uptake of XPS in the study of polymer surfaces.

For the broad spectrum emission in a synchrotron source (Figure 2.7) monochromating and focusing are a necessity for most experiments rather than a luxury. The development of suitable monochromators and optics in the soft X-ray region was the main stumbling block in the use of soft X-rays. It was not until the late 1970s⁶² that a suitable crystal was adapted to act

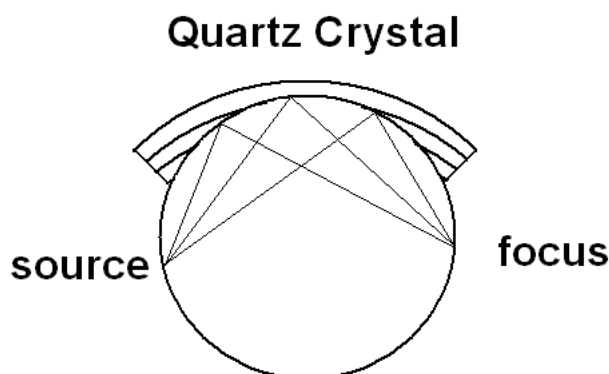


Fig. 2.10: A common monochromator used in XPS. A Rowland sphere monochromator uses a crystal (Quartz) bent around a hypothetical sphere such that the photons of a given order and wavelength will be focused onto one spot (sample).

as a monochromator and even today none exists that encompasses the whole range from 100 - 2000 eV. In addition the glancing angles used, as shown in Figures 2.11, mean that the smallest layer of contamination on the optics will have a dramatic effect on the useful flux received. This flux reduction depends on wavelength and this introduces additional structure into spectra, especially around the carbon K-edge which needs to be removed using a normalisation process. This usually entails using a gold mesh (I_0) to record the flux at a given wavelength which is then used to remove artifacts in the spectra. Later improvements in focusing mirrors have allowed spot sizes to be massively reduced on recent soft X-ray beamlines. Improvements such as these have led to high resolution spectromicroscopy and it is now possible to record spectra with a spatial resolution down to at least 50 nm⁷⁸ and measurements down to 15 nm have been reported⁷³.

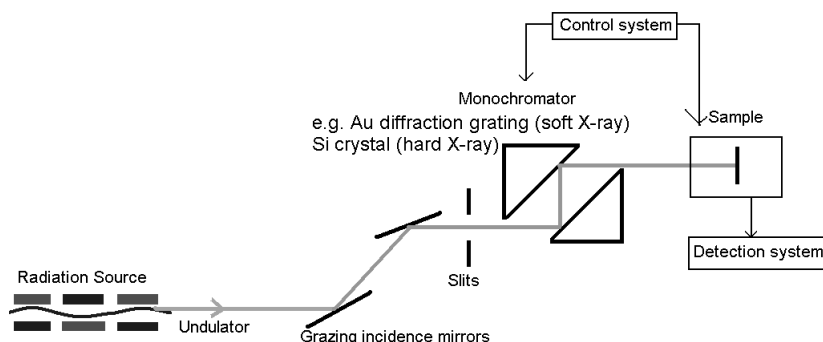


Fig. 2.11: A schematic of the layout of a typical beamline (not to scale). Mirrors and slits bring a collimated focused beam to the beamline area. Remote control and detection systems are necessary where the beam presents a radiation hazard.

2.2 X-ray Spectroscopy

2.2.1 Spectroscopic Notation

X-ray Absorption Spectroscopy spectra are labelled by the absorbing shell using the K,L,M... notation for each principal quantum number, n , starting with K for the core shell. Transitions from the core levels to molecular orbitals in Near Edge X-ray Absorption Fine Structure are labelled as $1s \rightarrow \pi^*$ or simply π^* . X-ray Photoelectron Spectroscopy peaks are identified by using the s,p,d notation for the subshell from which the ejected electron originates. Auger peaks are identified using the K,L,M notation and label the core level ejected initially, the level which falls into the core hole and the level the auger electron is emitted from, e.g. O KLL would be an auger electron from the L shell caused by another L shell electron replacing a core hole in the K shell of an oxygen atom.

2.2.2 X-ray Absorption Spectroscopy (XAS)

X-ray Absorption Spectroscopy (XAS) measures the absorption coefficient μ of tunable monochromatic X-rays as a function of incoming photon energy. Sharp increases in absorption occur when the incoming photons have sufficient energy to ionise core electrons. X-ray Absorption Fine Structure (XAFS), which refers to oscillations, peaks and other features in the absorption edge, is divided into two regions. The extended region (EXAFS) is dominated by scattering of the outgoing electron wave from neighbouring atoms and provides structural information on bond lengths, coordination number and type. The near-edge (NEXAFS) region probes electronic structure and gives information on bond lengths, angles and chemical state.

2.2.2.1 X-ray Absorption Coefficient

The absorption of an X-ray beam passing through a material can be described using the Beer-Lambert law. For the example in Figure 2.12 an incoming beam of intensity I_0 , passing through a material of thickness x the transmitted intensity I is given by,

$$I = I_0 e^{-\mu x} \quad (2.6)$$

where μ is the absorption coefficient, which is dependent on the material.

X-ray absorption spectroscopy measures μ as a function of energy. In

the simplest case the absorption coefficient should slowly decrease as a function of energy as shown in Figure 2.13. Very high energy X-rays are more penetrating than hard X-rays which are more penetrating than soft X-rays.

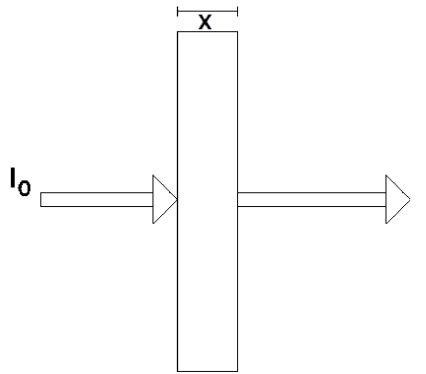


Fig. 2.12: The model of transmission used in the Beer-Lambert law, the absorption of X-rays is a function of the flux, thickness and a coefficient, $\mu(E)$.

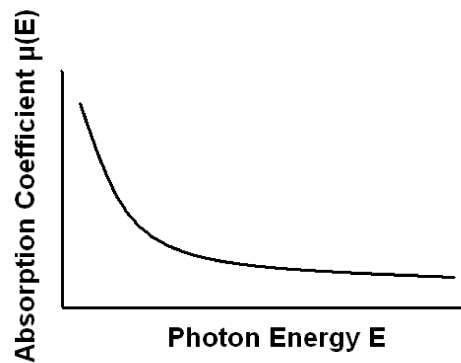


Fig. 2.13: The expected change of $\mu(E)$, a gentle decrease in the absorption with energy.

The absorption coefficient also shows discrete edges which correspond to the energy required to eject a core-level electron as shown in Figure 2.14.

Once this threshold is crossed the absorption coefficient increases sharply because photo-ejection of core electrons is now available as a process to absorb the incoming X-rays.

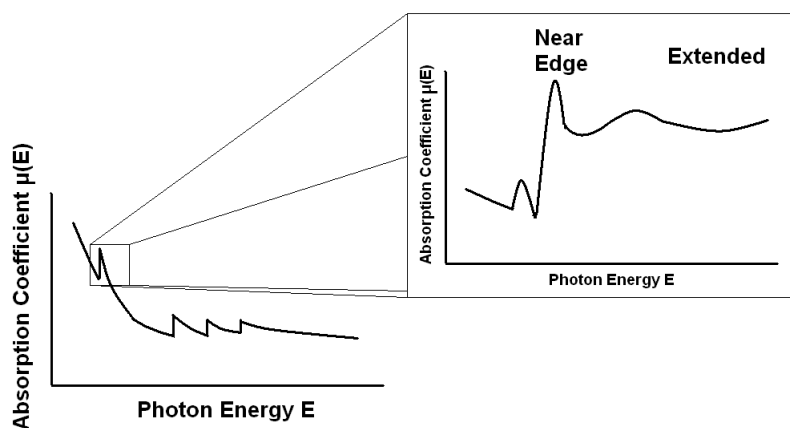


Fig. 2.14: Discrete jumps in $\mu(E)$ referred to as absorption edges are caused by the incoming X-rays having sufficient energy to eject a core electron to the vacuum level.

Further detail is also present in the X-ray absorption spectra (Figure 2.14). This is caused by scattering of the ejected electrons of neighbouring atoms and electrons being promoted to unoccupied molecular orbitals. This fine structure can be used to elucidate structural, chemical and electronic details from the material. The fine structure is divided into two regions, the near-edge which extends up to 40 eV past the absorption edge and the extended region which extends from about 40 eV to several hundred eV past the edge.

2.2.2.2 Extended X-ray Absorption Fine Structure (EXAFS)

The EXAFS oscillations are caused by the ejected electron wave scattering off neighbouring atoms (Figure 2.15). It provides local structural information without the need for long range order. The scattering and hence the EXAFS oscillations, depend on the scattering atoms, their number and distance from the absorbing atom and the thermal disorder of the system.

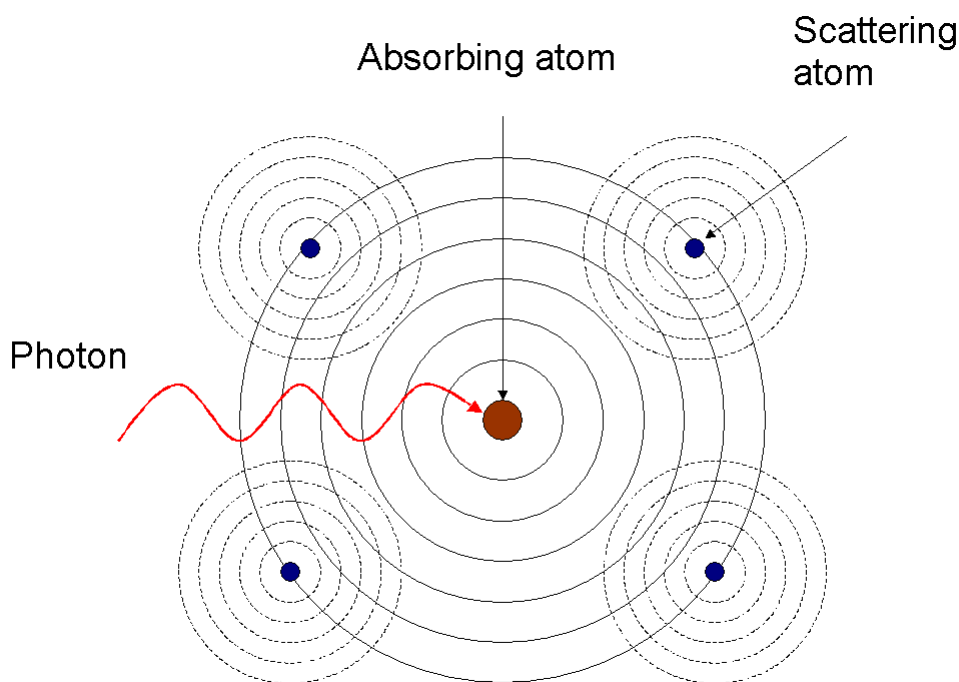


Fig. 2.15: EXAFS originates from interference caused by the out-going photoelectron ejected by the absorption event. Reproduced from⁸⁶.

The EXAFS equation describes the oscillations from the contributions of the various scattering atoms and it is possible to extract useful information by fitting a parameter in the equation to the fine structure. EXAFS data are experimentally harder to acquire due to the necessity of obtaining good

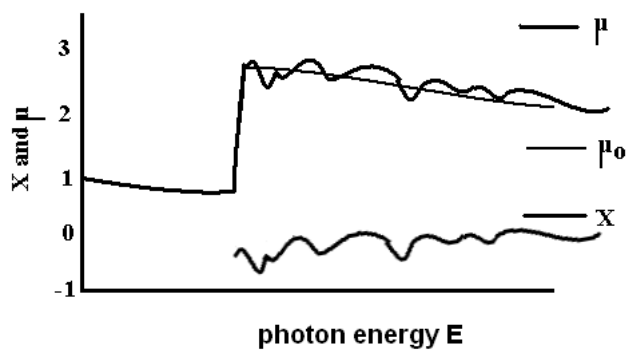


Fig. 2.16: The measured absorption spectrum, μ , is subtracted from the basic background absorption, μ_0 , to leave the fine structure, χ , which can then be analysed.

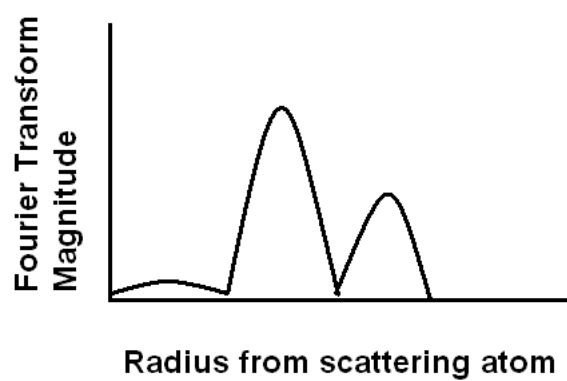


Fig. 2.17: A Fourier transform of χ as a function of radial distance from the absorbing atom.

counting statistics for the fitting approach to data analysis and the useful oscillations can extend hundreds of eV past the absorption edge. The equation (derived in^{62;87}) gives the extracted fine structure, χ (Figure 2.16), in terms of the sum of the contributions of every neighbouring shell of atoms to the fine structure,

$$\chi = \sum \frac{n_X S_0^2 f_X(k) e^{-2k^2 \sigma^2}}{k r^2} \sin(2kr + \alpha_{MX}(k)) \quad (2.7)$$

where n_X is number of atoms in that scattering shell, S_0^2 is the amplitude reduction factor, $f_X(k)$ is the amplitude function, $-2k^2 \sigma^2$ is the Debye-Waller factor for thermal disorder in the system, k is the electron wavevector, r is the interatomic distance and α_{MX} is the phase term. This model uses the plane wave approximation which assumes that the distance to the nearest atomic neighbour is much greater than the radius of the absorbing atom, this allows the outgoing spherical electron wave to be modelled as a plane wave. A Fourier transform of χ gives a radial distribution of scattering atoms (Figure 2.17). Due to phase shifts which vary with the electron wavevector, k these are not the physical distance of the neighbouring atoms.

2.2.2.3 Near-Edge X-ray Absorption Fine Structure (NEXAFS)/X-ray Absorption Near-Edge Structure (XANES)

The near-edge region (historically referred to as NEXAFS for soft X-rays and XANES for hard X-rays) is considered to be easier to measure than EXAFS but harder to interpret. There is no equivalent formula to the EXAFS

(2.7) for the near edge. The EXAFS is dominated by single scattering events but the near-edge is dominated by multiple scattering and transitions to unoccupied molecular orbitals (Figure 2.18), the observed resonances correspond to the dipole allowed transitions of a core (1s) electron to an antibonding orbital⁶².

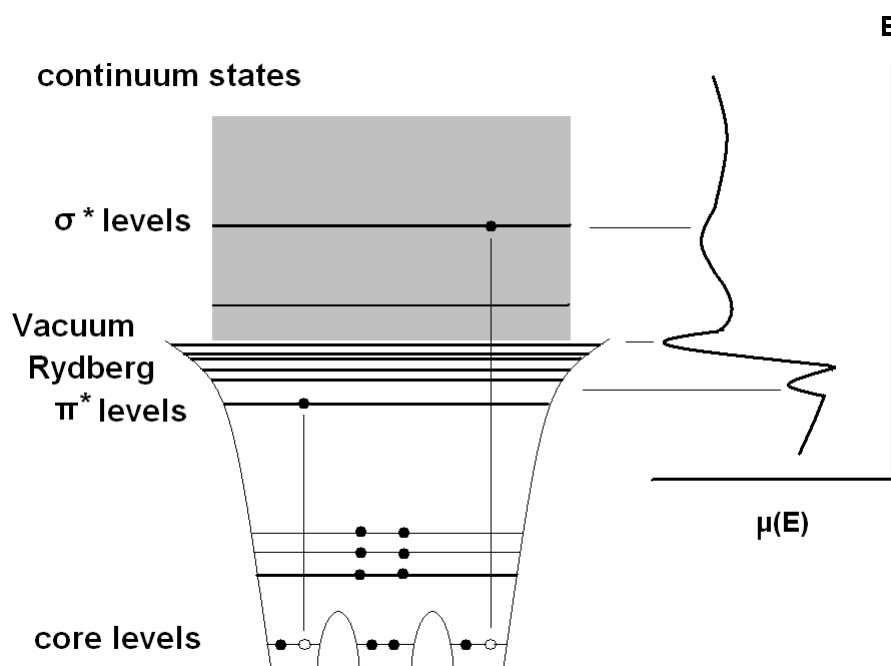


Fig. 2.18: NEXAFS spectra: In addition to promotion to the vacuum level which causes the existence of absorption edges they can also be promoted to unoccupied molecular orbitals allowing NEXAFS to probe the electronic structure of atoms and molecules. The observed resonances correspond to the dipole allowed transitions of a core (1s) electron to a antibonding orbital⁶².

Synchrotron radiation has a very high level of linear polarisation; by changing an ordered sample's orientation with respect to the polarisation of the beam it is possible to determine angular dependences of π^* and σ^* orbitals (Figure 2.19), the resonance intensity of an orbital is largest if the E vector points in the direction of that orbital⁶². This has been used to

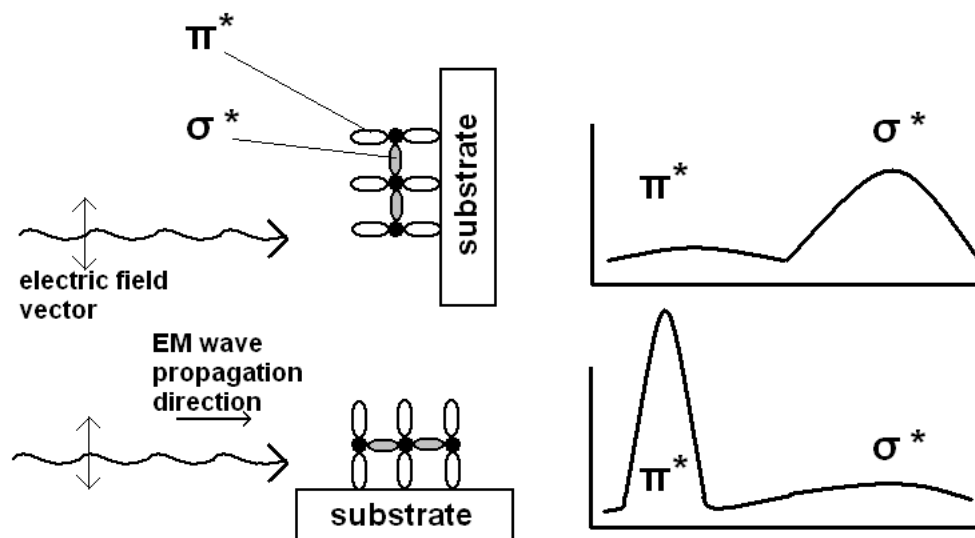


Fig. 2.19: Angular dependence of NEXAFS spectra: Due to the nature of some planar molecules and the polarised nature of synchrotron radiation, the orientation of molecules can be determined by the relative intensities of the π^* and σ^* peaks in NEXAFS spectra taken at different angles.⁶².

determine how some planar molecules such as benzene adsorb onto different surfaces. NEXAFS can also give an indication of bond length. The distance (in energy) between the π^* and σ^* peaks is inversely proportional to the bond length, so a greater energy separation means shorter bonds. For large molecules and polymers what is known as the building block approach is sometimes used. This model proposes that the overall spectrum is the sum of diatomic spectra from those species making up the molecule, and has been successful especially when comparing gas and adsorbed gas spectra to polymers⁶².

2.2.2.4 Data acquisition

The common methods of data acquisition are shown below and the choice is usually dependent on the concentration of sample and the need for bulk/surface sensitivity. Fluorescence yield and electron yield arise from the relaxation of excited atoms by the process shown in Figure 2.20.

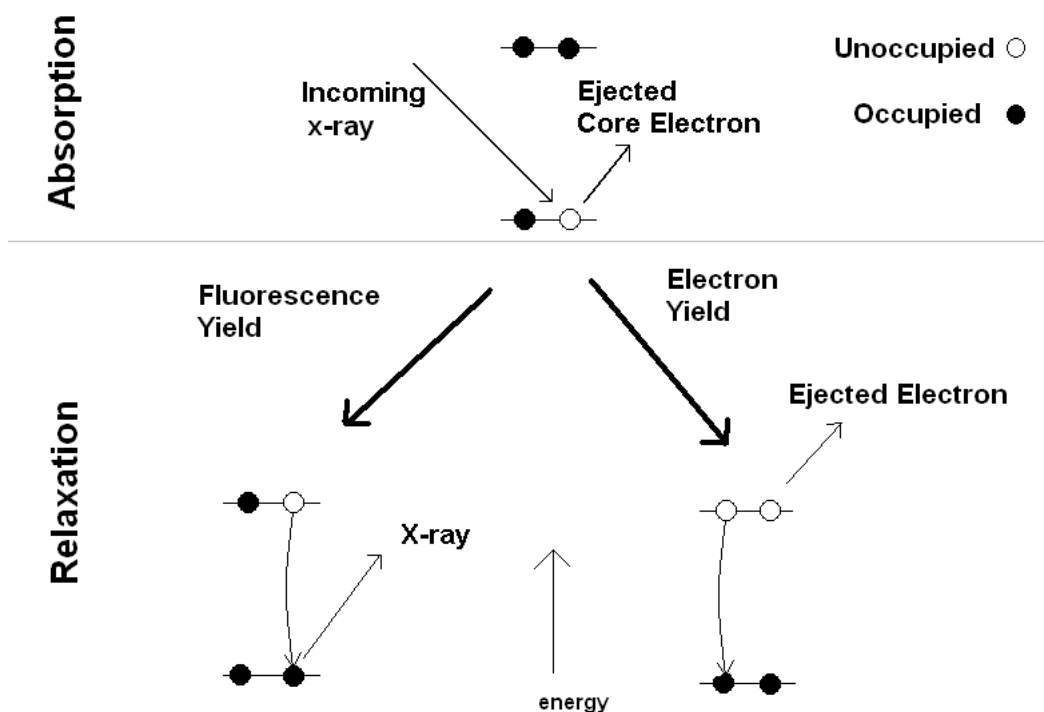


Fig. 2.20: The absorption event ejects a core electron and excites an atom which can then relax by emitting an X-ray (Fluorescence Yield) or an auger electron (Electron Yield.)

Transmission measures the beam intensity and the transmitted beam directly by using gas ionisation chambers (Figure 2.21). The chambers are filled with a mix of noble gases and a high electric potential is applied, an absorption event in the chamber ionises the gas and is recorded as a count.

The ion current produced in the chambers is proportional to the beam passing through the chamber and the thickness and intensities are related to the absorption coefficient μ , by the Beer-Lambert law (Equation 2.6). Due to the need for the beam to pass through the sample, transmission is almost only used for experiments with hard X-rays which have sufficient energy to penetrate a sample of a reasonable thickness. It has occasionally been used for soft X-rays⁶³ although this requires the casting of very thin films (~ 100 nm).

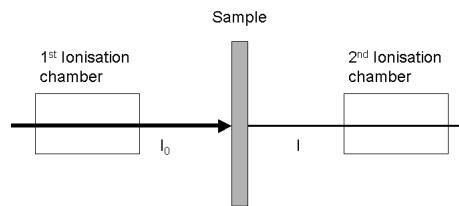


Fig. 2.21: Transmission mode measurements use two chambers to measure the intensity of the beam before and after passing through the sample in the same way as Figure 2.12.

Fluorescence yield (FY) uses a X-ray fluorescence detector to detect photons emitted from the sample. It is easier for high Z atoms which have a higher yield than low Z atoms. This is caused by the atoms relaxing after an X-ray has ejected a core electron. Photons have a much longer mean free path than electrons so FY represents bulk sensitivity, approximately $1\ \mu\text{m}$ in the soft X-ray range.

Electron yield uses a picoammeter to measure the number of electrons

ejected from the sample (photoejected or Auger electrons) which is proportional to the absorption coefficient. A bias voltages is applied to collect the total signal (total electron yield) or to selectively count electrons within a given kinetic energy range (partial electron yield). The sampling depth of total electron yield detection depends on the Bethe range (the total distance the electrons travel in matter) as unlike XPS, electron yield also has contributions from inelastically scattered electrons as well as elastically. The Bethe range has a Z dependence due to the increased back scattering at higher atomic numbers (which also helps to make hard-XAS easier) and the energy dependence is analogous to the universal curve for inelastic mean free paths⁸⁸.

X-ray Excited Optical Luminescence (XEOL) allows for the XAS signal to be detected by optical emission from a fluorescent material. As the energy of the optical photon will depend on nature of the emitting electron it is possible to get site specific EXAFS/NEXAFS information from a sample.

2.2.2.5 Normalisation

Because of variations in the X-ray intensity caused by instabilities in the cycling electron beam and contamination of the beamline optics it is necessary to normalise the absorption coefficient, μ . Most beamlines have an intensity monitor (called an I_0 grid) consisting of a gold mesh which is placed in the path of the X-ray beam. Most of the beam passes through and the rest hits the mesh causing photoionisation. The current produced by this is

recorded to track the beam intensity and artifacts can then be removed from the spectra. Throughout this work data have been normalised to an I_0 mesh.

2.2.3 X-ray Photoelectron Spectroscopy (XPS)

X-ray Photoelectron Spectroscopy (XPS) uses monochromatic X-rays to eject core electrons from a sample surface (Figure 2.23, 2.22). The kinetic energies of the ejected electrons are measured and the binding energy is calculated. The binding energy indicates the element the ejected electron originated from and small shifts in the binding energy are used to identify the chemical state that element is in.



Fig. 2.22: A typical commercial XPS instrument (Kratos Axis Ultra) at Manchester University, showing the instrument X-ray sources and monochromator (center), electron analyser (top) and vacuum and pressure and control systems (left).

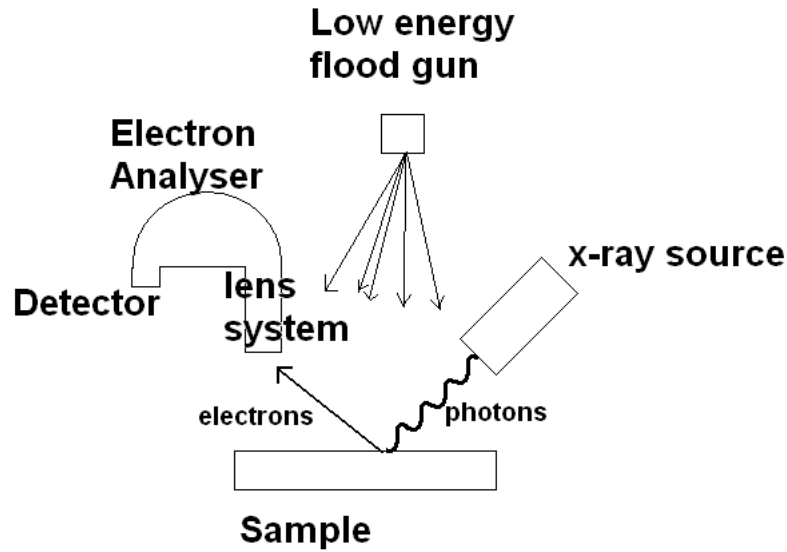


Fig. 2.23: Schematic of an XPS instrument. An X-ray source bombards a sample with X-rays; ejected electrons are collected by the lens system and then measured in the electron analyser; an electron flood gun is used to prevent a build up of charge on the sample surface.

2.2.3.1 The photoelectric effect

The photoelectric effect was first discovered by Hertz and the theoretical explanation won Einstein the Nobel prize. The photoelectric effect can be described by the formula,

$$E_K = h\nu - E_{Bind} - \phi_w \quad (2.8)$$

where E_K is the kinetic energy of the ejected electron, E_{Bind} is the binding energy, ϕ_w the work function and $h\nu$ is the photon energy. In a typical XPS experiment $h\nu$ is kept constant, the kinetic energies of electrons ejected from the sample are measured and the binding energy is inferred from the photoelectric equation.

Kinetic energy is measured using a hemispherical analyser which measures the deflection of an electron's path between two hemispheres held at different potentials, V_1 and V_2 (Figure 2.24). The deflection depends on the energy of the electrons and this will determine where the electron arrives at a position sensitive detector then records the count and hence the energy.

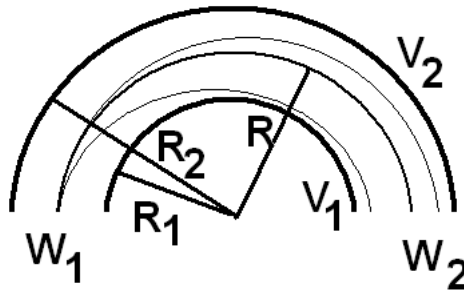


Fig. 2.24: An Electron analyser. Two spheres of radius R_1 and R_2 kept at potentials V_1 and V_2 . Electrons enter at W_1 and are deflected by the electric field from the two voltages. The deflection depends on the energy of the electrons and this will determine where at W_2 the electron arrives, a position sensitive detector then records the count and hence the energy.

2.2.3.2 Sampling Depth

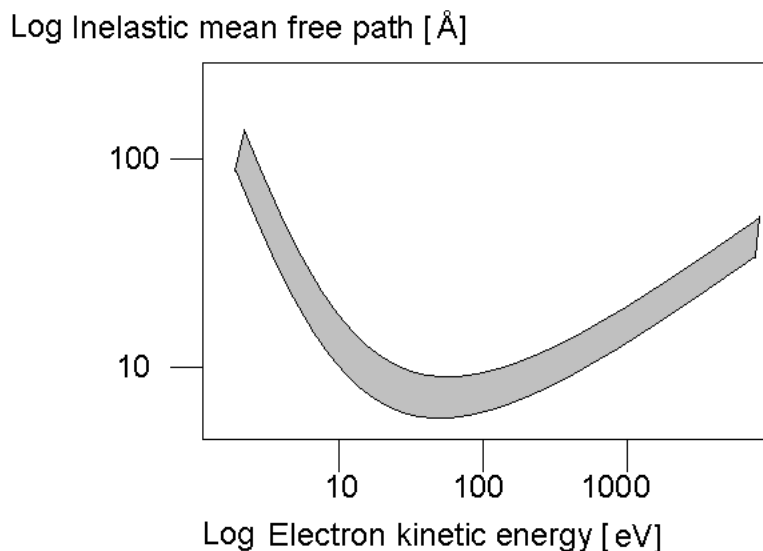


Fig. 2.25: The so called 'universal curve'. Empirical data on inelastic mean free paths falls within the shaded area. XPS and carbon K-edge electron yield NEXAFS are close to the bottom of the IMFP curve explaining their high surface sensitivity, redrawn from ⁸⁸.

Like electron yield detection in XAFS the short mean free path of the electron is the cause of the high level of surface sensitivity. As the kinetic energy of the outgoing electron is measured then only unscattered or elastically scattered electrons contribute to the signal⁸⁹. Typical sampling depths for laboratory based instruments are 2-5 nm. Using a tunable X-ray source, such as a synchrotron, the sampling depth can be varied as $h\nu$ is being increased, so for a given binding energy the kinetic energy will be different, providing a non-destructive depth profile allowing variation in line with the universal energy curve (Figure 2.25) described by Seah and Dench⁹⁰. The inelastic mean free path (Figure 2.26) is the length for which

$1/e$ electrons travel after undergoing a collision in which energy is transferred and is the reason for the surface sensitivity of XPS. It is a fraction of the signal reacting the surface so some electrons from 2 or 3 times the inelastic mean free path can reach the surface and contribute to the signal.

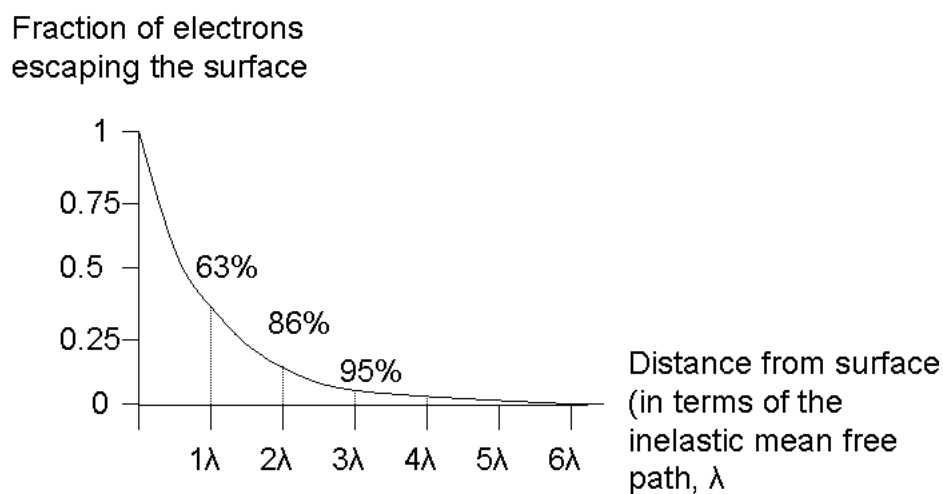


Fig. 2.26: The inelastic mean free path is the length for which $1/e$ electrons travel after undergoing a collision in which energy is transferred and is the reason for the surface sensitivity of XPS.

2.2.3.3 Spectra

Scans over the whole accessible energy range are used to ascertain elemental abundances. Restriction of the pass energy of the electron optics allows the sensitivity to be increased but at the expense of energy resolution so it is common practice to record high sensitivity spectra of the whole

energy range then high resolution spectra of the most important regions, Figure 2.27 shows some of the different spectra. Different elements have different photoemission⁹¹ cross sections so this is corrected for by empirically determined relative sensitivity factors which weight the elemental abundances accordingly.

The background in XP spectra is dominated by inelastically scattered electrons, which cause the background to be higher on the high binding energy side of a peak giving XP spectra their distinctive shape. For analysis the back-ground can be modeled as a linear back ground or a more accurate model can be used. The two most widely used are the Shirley and Tougaard backgrounds. The Shirley method uses iterative fitting to determine the background at a point to make it proportional to the intensity of the peak area above that point³. The Tougaard⁹² background attempts to remove all the inelastic process to leave the photoelectron peak. The Tougaard background is one used throughout this thesis as it more accurately matches the background in the data obtained.

The primary peaks observed in the XP spectra emanate from core level electrons. Peak positions are determined by the binding energy of a core electron as shown in Equation 2.8. Shifts in the peak position are caused by the local chemical environment of the ejecting atom. The peak shape is a mix of a Lorentzian from the emission line and a Gaussian from various factors in measuring and recording. The ratio depends on the instrument being used; throughout this work a GL ratio of 30% was used based on

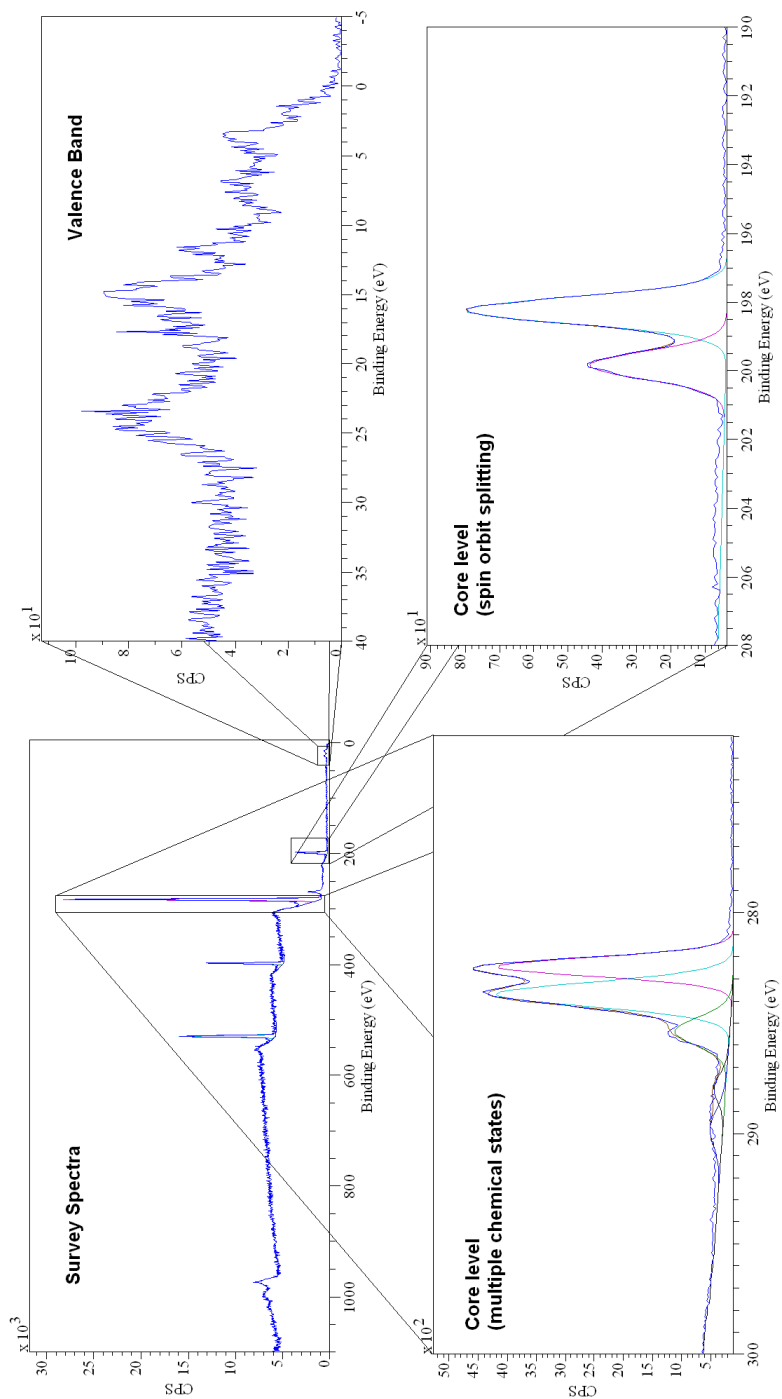


Fig. 2.27: The context of different spectra with respect to the survey spectra. Survey spectra show a wide range of energies with high sensitivity. Core levels have higher resolution allowing different chemical states to be determined.

fitting the GL ratio to a single peak sample (polypropylene).

The core level energy positions are sensitive to the local environment of the emitting atom. The local environment can perturb the electron cloud around the atom causing an ejected electron to perceive a change in the nuclear shielding (Figure 2.28), effective charge and hence its energy level. For carbon 1s peaks a shift will be seen in the peak to higher binding energy as the carbon atom becomes more electro positive due to being bound to more electro negative species. Quantification of this energy shift allows the chemical state of the emitter to be determined.

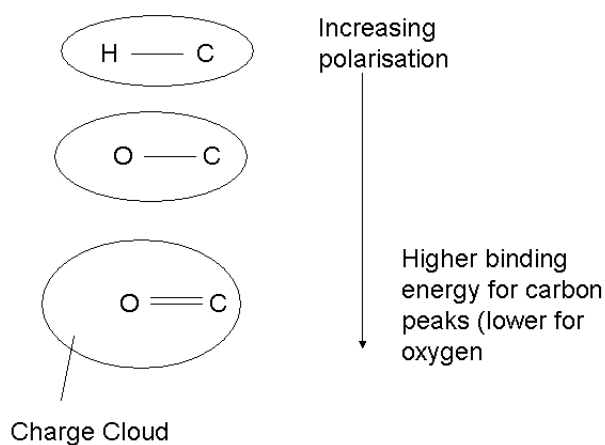


Fig. 2.28: Origin of binding energy shifts in XPS: For carbon 1s peaks a shift will be seen in the peak to higher binding energy as the carbon atom becomes more electro positive due to being bound to more electro negative species.

For electrons ejected from orbitals with non-zero orbital angular momentum, the spin-orbit interaction causes the emergence of two peaks for

a given chemical state. The ratios of the two peaks are fixed and it provides a further constraint for peak fitting.

Shake-off features are commonly found in samples with aromatic ring systems and they are caused when a valence electron is ejected with a core level electron. The energy for the valence ejection is then no longer available for the core ejection which causes the corresponding peak to be several eV lower than expected. Shake-offs can be up to 10 % of the primary peak.

Very low binding energy electrons are emitted from the valence band rather than core levels. Valence bands contain information from all the elements in the samples and are thus much harder to interpret fully, but they are widely used as a finger print to identify unknown material in a sample. Due to the fact that they have the lowest binding energy they have the highest kinetic energy hence the greatest sampling depth for a given photon energy.

Angle-resolved XPS allows the sampling depth to be further reduced by changing the geometry of the experiment. The sample surface is tilted with respect to the electron analyser to increase the effective path electrons have to travel to reach the surface (see Figure 2.29). The change in spectra can be quantified and used to form a non-destructive depth profile. ARXPS only allows the sampling depth to be reduced not increased, so it cannot be used to probe deeper than normal XPS.

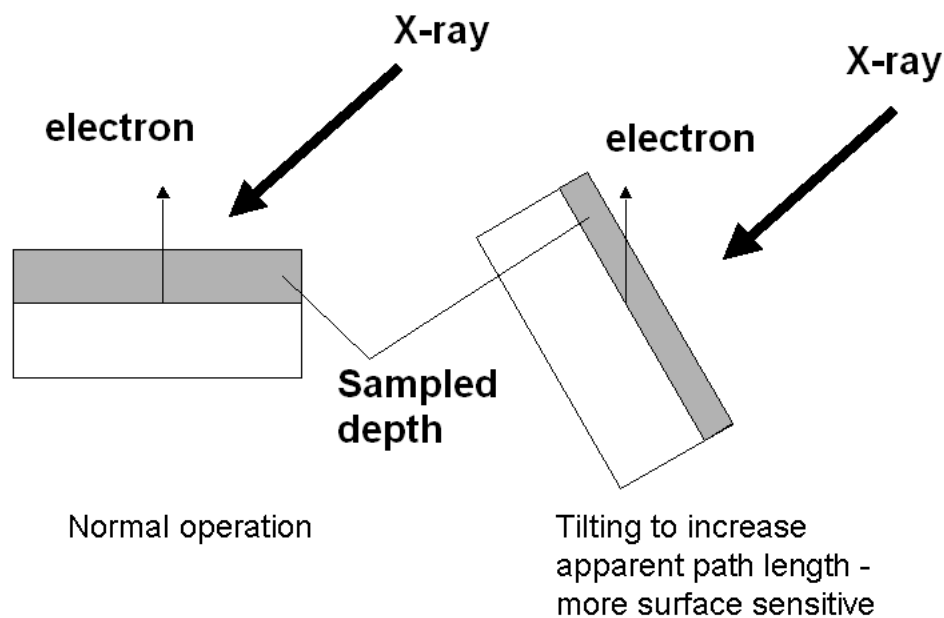


Fig. 2.29: Angle Resolved X-ray Photoelectron Spectroscopy increases the surface sensitivity by increasing the effective length of material the photoelectron travels through.

The sample surface can be destructively depth profiled using ions such as Ar^+ to bombard the surface and strip off layers. This is rarely used for organic samples due to the sample damage often caused by this process. Secondary Ion Mass Spectrometry (SIMS), another widely used surface science technique, is based on this principle whereby the removed (secondary) fragments are analysed using mass spectrometry.

2.3 Microscopy

2.3.1 Introduction

The resolving limit of an optical imaging system is the distance between two points at which they can still be resolved as two distinct points. This is, in the diffraction (far field) limiting case, approximately half the wavelength, λ , of the light used. This means that any optical microscope can only have a maximum resolution of around 200 nm in an ideal case and any features below this scale will not be resolved. Electron microscopy has become very popular as a method of probing structure far below the resolution limit imposed by optical photons. It is also possible to use X-ray microscopes to increase spatial resolution due to the shorter λ .

Scanning probe techniques are not diffraction limited and are also popular methods for probing nanoscale structure. A tip rasterises the sample surface and an image can be produced from many sources, for example mechanical (Atomic Force Microscopy), electrical (Scanning Tunnelling Microscopy) or optical (Scanning Near-Field Optical Microscopy). The resolution is limited by the size that the tip probes and the smallest distance it can be moved, for example an AFM is limited by the sharpness of the tip in contact with the sample and the piezoelectric actuators moving the tip.

2.3.2 Electron Microscopy

It is trivial to accelerate electrons to a sufficient energy to have a wavefunction with a wavelength much smaller than that of light (550 nm for red light). Further manipulation of the beam is possible using both electric and magnetic fields. Lens systems function as they do for optical systems, with magnetic fields being used as a large magnetic field is much safer than a large electric field. The quality of an electron lens in terms of chromatic and spherical aberration is very poor compared with optical lenses. Electrons will interact with matter in the following ways to produce detectable signals (Figure 2.30). These physical processes provide contrast for imaging (transmitted vs others, backscattered and secondary and auger vs. others) information about the crystal structure (diffracted) and chemical and elemental information (Auger and X-ray emission):

- Transmission
- Back scattering
- Absorption
- Secondary-electron emission
- Diffraction
- Auger-electron emission
- X-ray emission

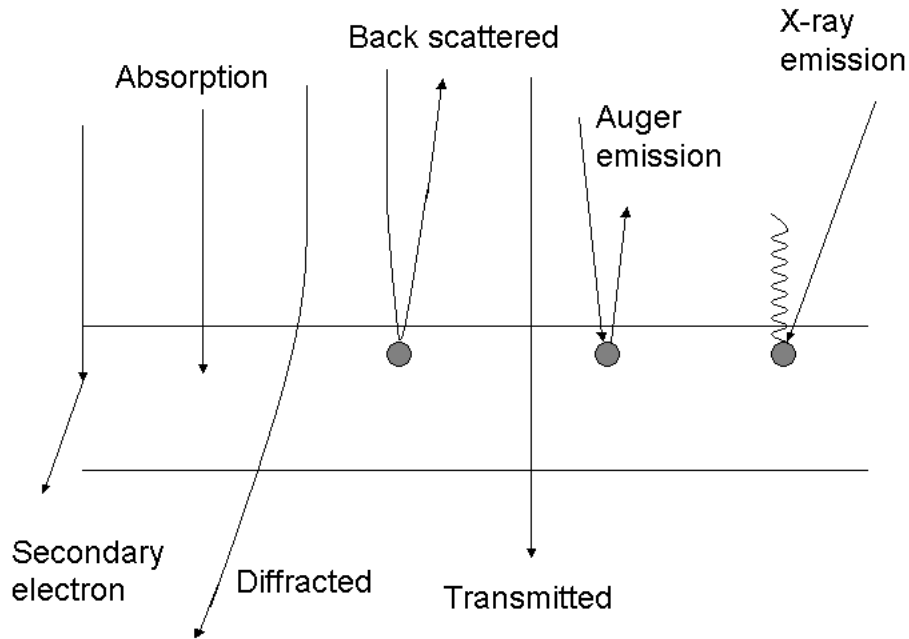


Fig. 2.30: Interactions of electrons with matter. These physical processes provide contrast for imaging.

2.3.3 Scanning Electron Microscopy (SEM)

Scanning Electron Microscopy uses a focused electron beam to raster scan a sample surface and an image is formed from backscattered and secondary electrons. Scanning coils move the beam (which has been focused by other electromagnets further up the optics column) so the detection side does not require spatial resolution. The primary electron beam can also excite atoms and the subsequent relaxation can emit X-rays with a characteristic energy dependent on the material. This is frequently used for elemental analysis (EDAX - Energy Dispersive Analysis of X-rays). A schematic of an SEM is shown in Figure 2.31.

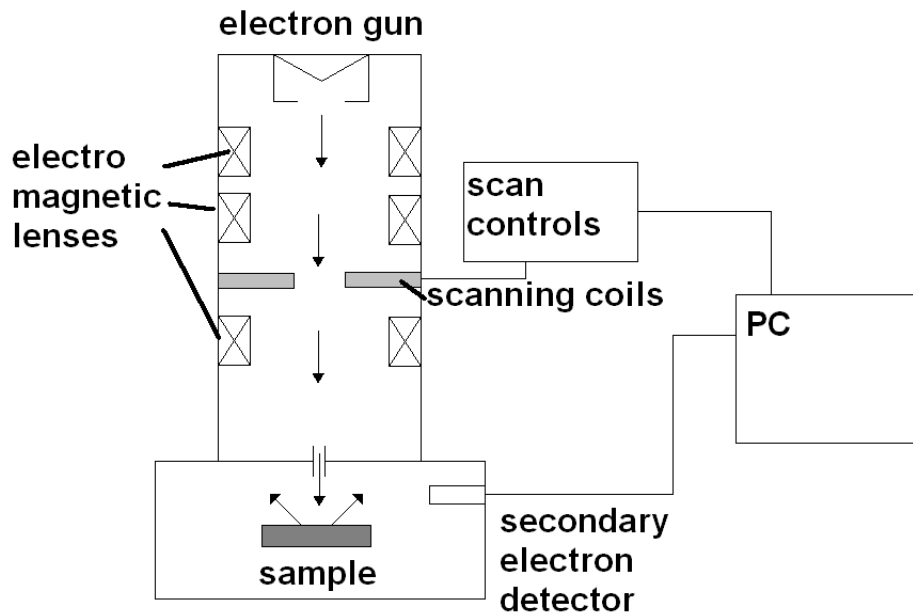


Fig. 2.31: Scanning Electron Microscopy (SEM) schematic: Electrons are emitted from a cathode and accelerated and focused onto a small spot on a sample, the beam is then rasterised over the sample, the image being formed from the backscattered and secondary electrons.

2.3.3.1 Environmental Scanning Electron Microscopy (ESEM)

Charging effects and vacuum problems with standard SEM led to the development of the so-called environmental SEM (ESEM). Differential pumping is used to keep a pressure gradient over the length of the microscope to obtain a high pressure in the analysis chamber (~ 10 mbars) while keeping as much of the system as possible under high vacuum. Figure 2.32 shows pressure limiting apertures (effusive rather than diffusive flow) in an ESEM which allow different sections of the machine to be maintained at different pressures. This allows the maximum number of electrons to reach the sample while still allowing the sample to be kept at a relatively high pressure. Water is used to raise the pressure in the analysis chamber and by cooling

the sample it is possible to achieve 100% relative humidity. The water also acts as a charge neutraliser to prevent the build up of charge on the surface distorting the image. It also amplifies the signal as a high energy electron can ionise multiple water molecules similar to conversion TEY XAS. This removes the need for coating the sample with gold or platinum which is sometimes necessary with standard SEM of insulating samples. It does however attenuate the primary electron beam so images tend to be of lower quality than SEM.

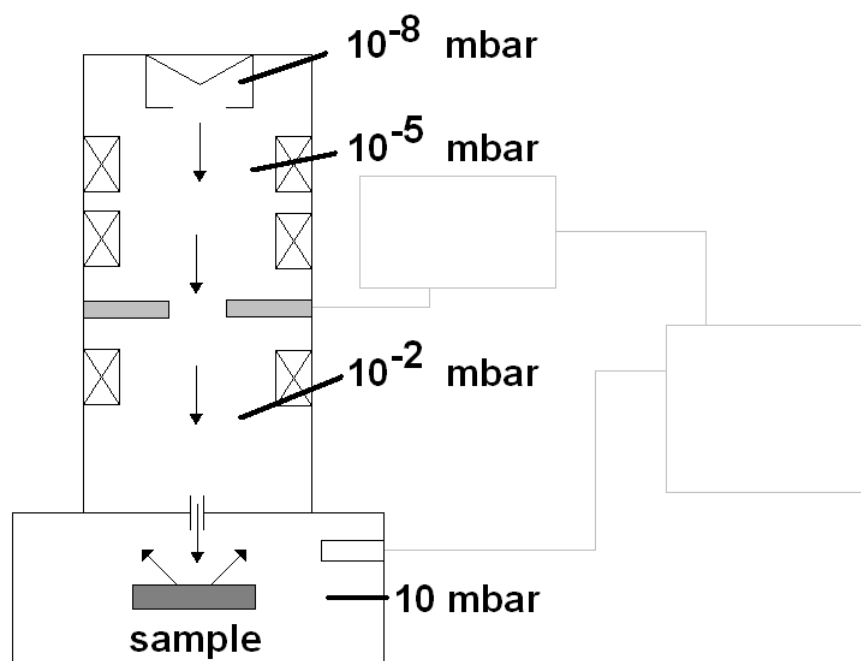


Fig. 2.32: Environmental Scanning Electron Microscopy (ESEM) schematic. Pressure limiting apertures allow different sections of the machine to be maintained at different pressures.

2.3.4 Transmission Electron Microscopy (TEM)

Transmission Electron Microscopy (TEM) images a focused beam of electrons which has passed through a thin sample (Figure 2.33) transmitted (or diffracted) electrons are then focused downstream to form an image. This image is then projected onto a phosphor screen to form an optical image which can then be captured using film or a CCD. Image contrast comes from different transmissions of electrons and structural information can be obtained by imaging diffracted electrons. Electrons are highly attenuated by matter necessitating very thin samples, typically of the order of 100 nm or less. For obtaining diffraction data the thickness required is even less because of the smaller proportion of diffracted electrons compared to those transmitted. Commercial instruments can achieve resolutions $\leq 2\text{\AA}$.

2.3.5 X-ray PhotoElectron Emission Microscopy (XPEEM)

X-ray PhotoElectron Emission Microscopy (XPEEM) uses a tunable beam of (soft) X-rays from a beamline focused onto a sample surface, photoejected electrons are caught in the high electric field (as in Total Electron Yield NEXAFS) and focused using an electron optics column onto a phosphor screen (as in TEM). As the X-ray beam energy is increased a NEXAFS spectrum is generated for each pixel point (Figure 2.34) to record a spectrum made up of image slices.

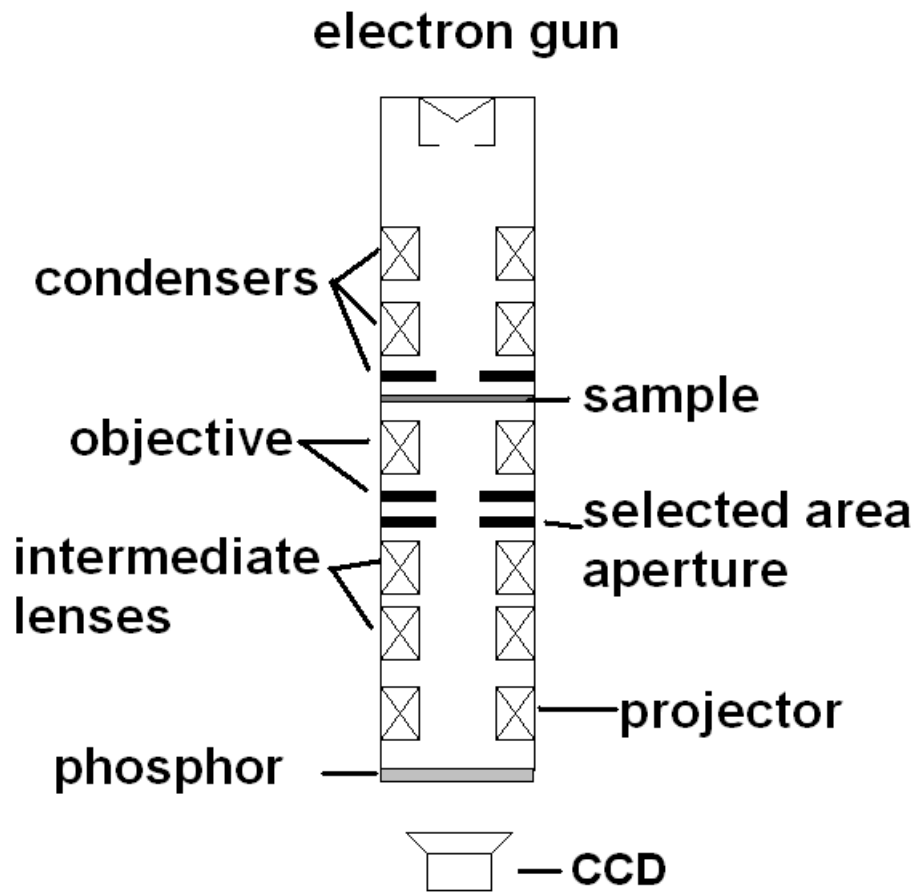


Fig. 2.33: Transmission Electron Microscope (TEM) schematic.

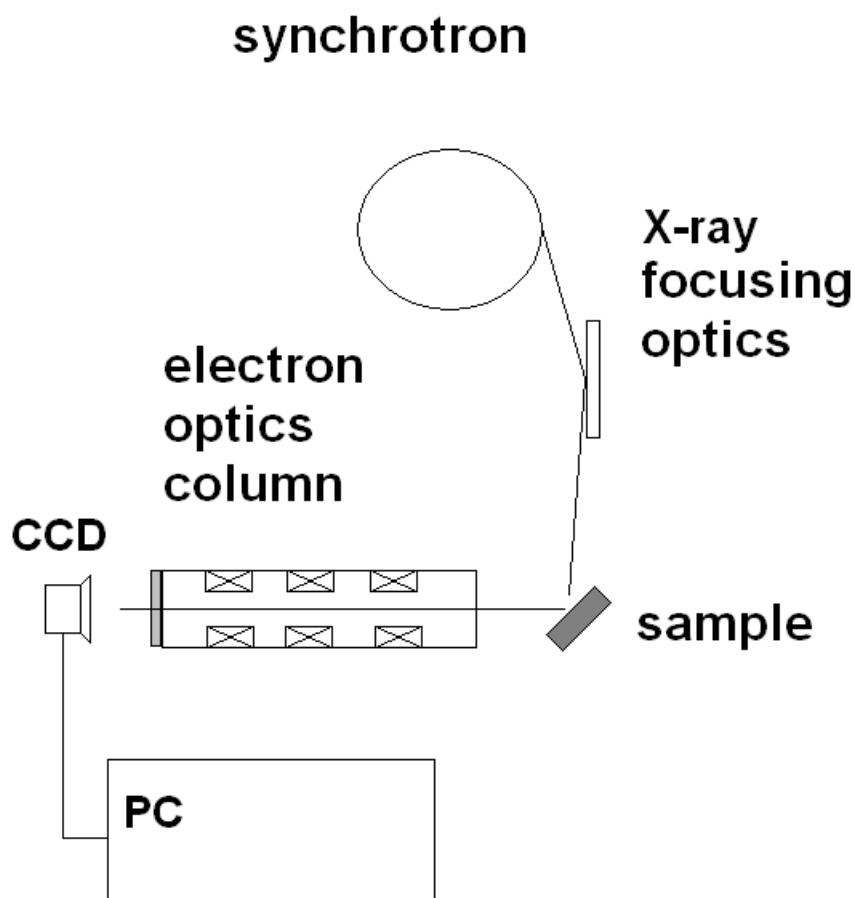


Fig. 2.34: X-ray PhotoElectron Emission Microscopy (XPEEM) Schematic.

Images are often dominated by topological effects as they have the greatest effect on electron deflection, but these effects can be mitigated by comparing two image slices at different points on the spectra axis. The amount of data is very large compared to conventional NEXAFS so it is commonly used in one of two ways; extracting a spectrum from an interesting feature or region, or mapping an interesting spectral feature.

To allow an image of a small area to be formed it is necessary to have

the X-ray beam small and focused. This increases the intensity of the beam and in turn increases the radiation damage suffered by the sample. This is a major concern for organic samples where sample damage occurs even at much lower doses. Charging problems are also significant due to the absolute need for UHV coupled with the high (20 kV) electric field used for capturing electrons into the optics column.

2.3.6 Imaging XPS

Newer XPS instruments have the ability to form an image from the ejected photoelectrons. By restricting the energy window of electrons used to make the image it is possible to produce an image at a specific core level peak providing element specific images or even chemical state specific images.

2.3.7 Atomic Force Microscopy (AFM)

Atomic Force Microscopy (AFM) uses piezoelectric controllers to rasterise a tip in contact or near-contact with a sample surface (Figure 2.35). A tip which is sharp on the atomic scale allows the AFM to have such a high resolution, down to atomic scale has been reported⁹³. Forces AFM can measure include Van der Waals, mechanical force, electrostatic and magnetic. Forces acting on the tip are recorded by either measuring the deflection of the tip or the force required to keep the tip at a constant height. This is done using a laser to illuminate the tip and a photodiode to monitor

the reflected light which drops when the tip is deflected. The tip can also be vibrated while measuring to reduce the tip damage to the material. Differences in the phase of the vibrations with respect to the driving force correspond to material changes in the surface, although only comparative assessments can be made.

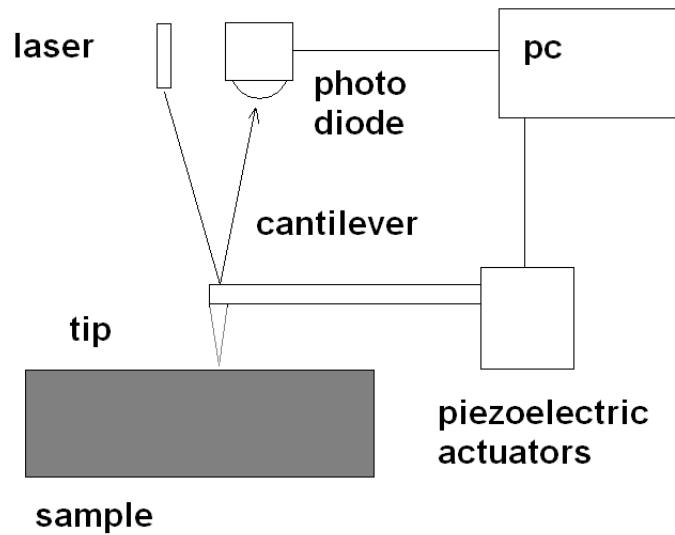


Fig. 2.35: Atomic Force Microscopy (AFM) Schematic. The interaction between the tip and the sample is measured by the deflection of a cantilever using a laser. The tip is rastered over the samples and a deflection map is produced.

Chapter 3

Soft X-ray Cell Development

3.1 Introduction

The vacuum requirements of using soft X-rays, electron spectroscopy and studying surfaces require specialised equipment and materials. Many surface science instrument suppliers now exist to produce Ultra High Vacuum (UHV) equipment and associated parts to several standard types. It is still common, however, for experimental chambers to be purpose built for a particular type of experiment. The use of soft X-ray absorption spectroscopy for *in situ* studies is still relatively new compared to other areas of surface science and in general each experimentalist will have their own design of chamber for this. Another consideration for the *in situ* experimentalist is the possibility of contaminating UHV clean equipment which provides another impetus to developing a dedicated chamber. The different levels of vacuum can approximately be described by the pressure ranges shown in Table 3.1 and the mean free paths of the gas molecules relative to the vacuum chamber

Name	Pressure (mbar)	Mean free path
Low vacuum	1	MFP \ll 1 m
Medium vacuum	$> 10^{-4}$	MFP < 1 m
High vacuum	$< 10^{-4} - < 10^{-7}$	MFP ~ 1 m
Ultra high vacuum	$< 10^{-8} - < 10^{-12}$	MFP > 1 m
Extreme high vacuum	$< 10^{-12}$	MFP $\gg 1$ m

Table 3.1: The different levels of vacuum. As the pressure drops the mean distance between collisions of gas molecules increases and gas-gas interactions are replaced by gas-wall interactions as the dominant feature.

size, a nominal 1 m.

3.2 Requirements

The *in situ* cell had to meet a number of requirements:

- All components need to be UHV compatible
- Cell environment needs to be isolated from the beamline vacuum
- Fine pressure control
- Temperature control compatible with UHV and reactive gas mixtures
- Small volume for fast pumping and minimal dosing gas usage
- Signal collection for total electron yield and fluorescence yield
- Inexpensive as reasonably possible and with as many ‘off-the-shelf’ parts as possible

The chamber went through several iterations, initially being ‘cannibalised’ from various parts then evolving based on experience and incorporating more purpose built parts.

3.3 Initial Design

There are several high and ultra-high vacuum (UHV) standards available for off-the-shelf construction. The most commonly found are KF (high vacuum), Conflat (CF) and ISO (CF and ISO are both UHV). The Conflat system was chosen primarily because it is the most widely used at Daresbury where the cell would be predominantly used and many companies produce a wide range of parts using this system. A typical conflat flange is shown in Figure 3.1.

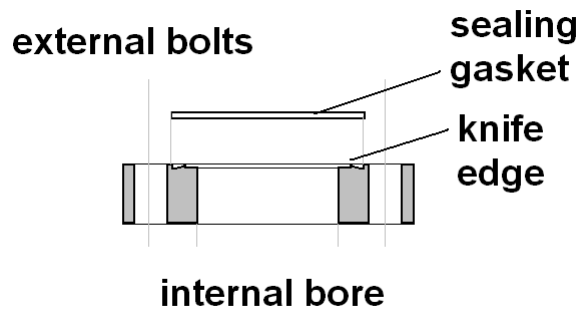


Fig. 3.1: The Conflat flange and gasket system as used in the cell design. Made to several standard diameters they are used to connect and seal UHV parts to a system. The seal is formed by stainless steel ‘knife-edges’ in each flange cutting into a softer copper (or occasionally silver coated or viton) gasket.

The seal between the flanges is made using a stainless steel ‘knife-edge’ to cut into a copper gasket. For non-UHV vacuums we have also used viton (a synthetic rubber) gaskets for the sample loading flange which have the advantage of being reusable.

To isolate the cell environment from the UHV of the beamline and synchrotron ring two pressure windows were used. The beamline had a

contamination barrier of ultra thin boron (1400 Å) which was rated to take a pressure of 10^{-2} mbar against vacuum and was there in case of a minor leak in the cell window. There was also a polyimide pressure window connection to the cell via the differential pumping system to the beamline. The polyimide window, while causing more spectral artifacts than the boron one, was rated to 10 mbar and was used as the primary method of protecting the beamline from the pressure in the chamber. It is worth noting that a major break in the cell polyimide window has a good chance of breaking the boron window as a result of the pressure wave causing a sudden change. A variety of windows are commercially available and it is possible to have the polyimide re-enforced with a tungsten mesh. This increases the upper pressure limit to 100 mbar or even atmospheric pressure but causes a drop in flux reaching the sample of up to 60% so a trade off can be made with respect to flux and pressure/safety which is easily variable with this design.

The system of pumping and venting, shown in Figure 3.2, was the same for all the cells designed. To pump the chamber down (or vent it) both turbo molecular pumps are fully used so valves V_1 (window by-pass) and V_2 (turbo pump throttle) are open V_3 (gas dosing inlet) and V_4 (beamline valve) are closed. To avoid breaking the pressure windows while pumping or venting W_1 is opened and the by pass operated by V_1 ensures the pressure is equal on both sides of W_2 . To dose gas into the system the bypass V_1 is closed and the gas pressure in the chamber is controlled downstream by using V_2 to throttle the turbo pump and upstream by V_3 to introduce gas into the chamber. While measuring V_4 must be open and W_1 closed.

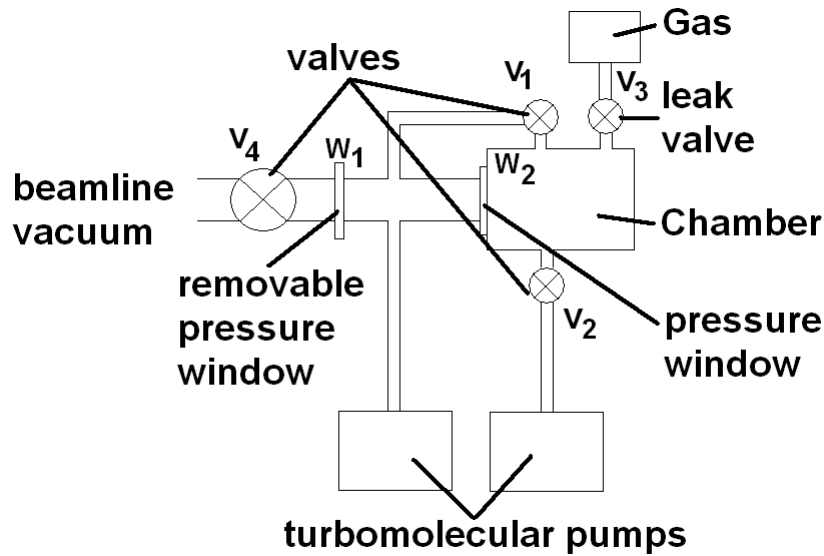


Fig. 3.2: Schematic of the vacuum system common to all the cells.

Pressure up-beam (toward the synchrotron) of the boron window was all controlled and monitored by the beamline control system and kept at a pressure of 10^{-9} mbar or lower. Between the boron (beamline) and polyimide (cell) window there was a differential pumping section which was pumped by a turbo-molecular pump at 10^{-7} mbar or lower and could be connected to or isolated from the cell vacuum. The cell pressure was controlled upstream by a precision all metal leak-valve connected to helium and any other gases required, and downstream by a throttled turbo-molecular pump. For UHV a pressure by-pass could be opened and both turbo pumps could be used to pump the main chamber.

Data was collected for both electron yield and fluorescence yield (see Figure 3.3). Total Electron Yield (TEY) data was measured as a drain

current using an electrically isolated sample holder and an isolated, biased (+90 V) ring in front of the sample, electrically connected via a special flange to a power supply. This was then connected to two picoammeters, one connected to the sample (Drain current) and the other connected to a biased conducting ring in front of the sample (Collector current). Fluorescent Yield (FY) data was obtained using a novel gas microstrip detector⁹⁴ developed by the detector group of the Rutherford Appleton Laboratories. The picoammeters produce a voltage (with a gain usually around $10^9/10^{10}$) which is fed into a voltage-to-frequency converter then recorded using an voltage-to-frequency converter connected to a computer. Picoammeters are very sensitive to electrical noise and all cables were heavily shielded with aluminium foil to act as a faraday cage.

The gas microstrip detector uses a series of long parallel electrodes in a helium environment behind another (polyimide) pressure window to maintain the difference between the cell and detector environments (Figure 3.4). When a photon enters the detector it ionises a helium atom and the electron and helium ion produced are attracted to the electrodes and are registered as a count. In order to protect the electronics from damage from sparking (electrical discharges), another gas is added as a quenching agent. Isobutane was initially used but this has the problem of signal attenuation at the carbon K edge. This can be replaced with methane which gives a 4 fold improvement in C K-edge signal (due to having 1/4 of the carbon atoms) but it is less effective as a quench and can leave the detector electronics vulnerable.

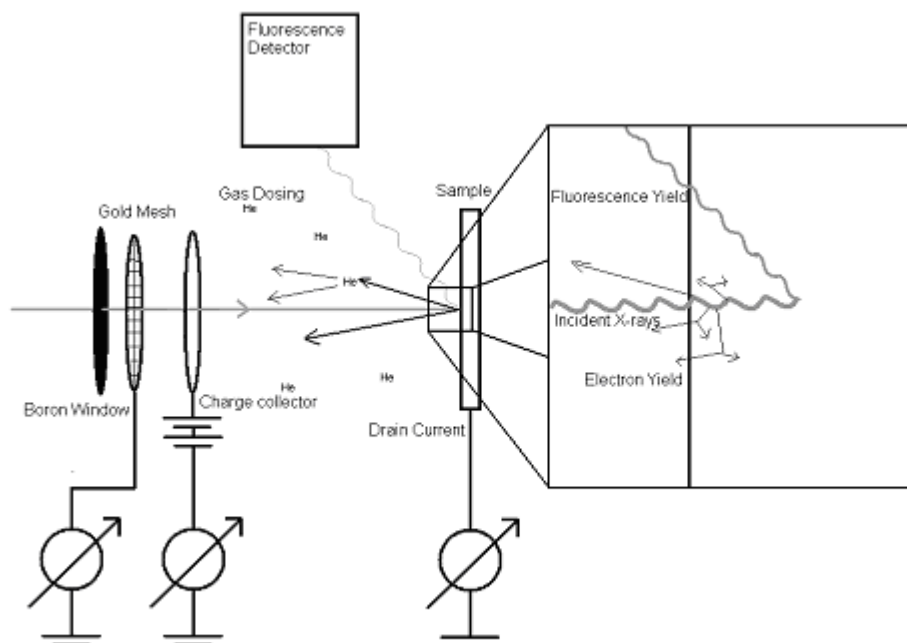


Fig. 3.3: Schematic of data collection. Surface sensitive Total Electron Yield (TEY) and beam intensity (I_0) are measured using picoammeters, each ionisation event producing a cascade of ions in the gas which is recorded.

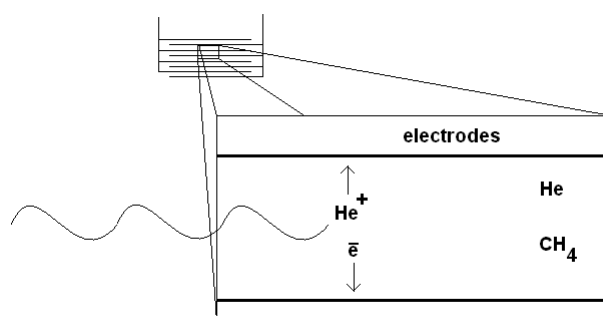


Fig. 3.4: Gas microstrip fluorescence detector. The detector is formed from an array of microscopic electrodes in a gaseous environment (helium for detection plus another to reduce sparking).

3.4 Cell Versions

3.4.1 Mark I

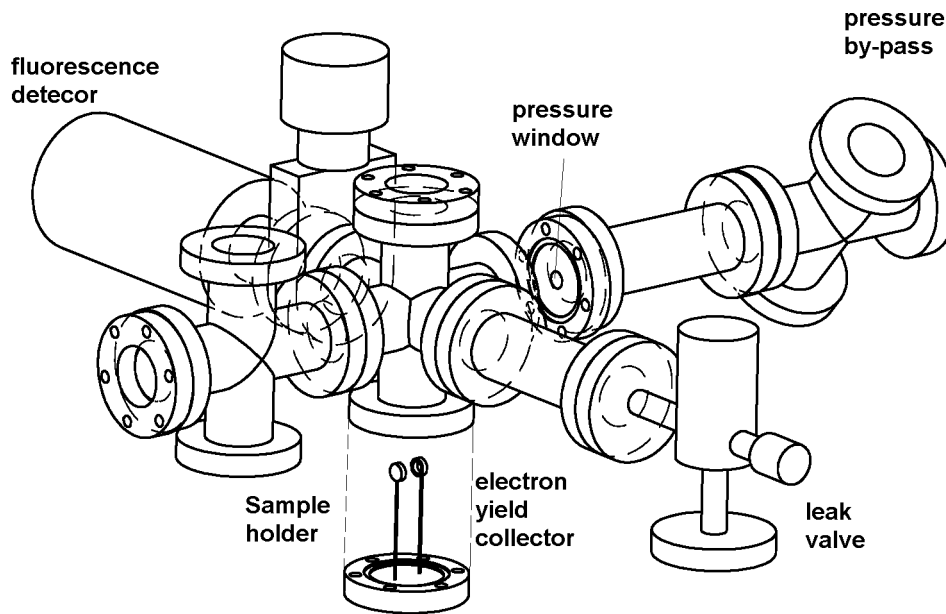


Fig. 3.5: Partially exploded view of the initial soft X-ray cell (Mark I), constructed from cannabilised parts.

The cell was initially constructed from cannabilised parts at a synchrotron, this first version (Mark I, Figure 3.5) had no heating capacity and samples were held in place by making them into a paste or sticking them onto double sided conducting carbon tape. This was then attached to a gold sample holder which was connected to an electrical feed through. A biased +90 V ring was directly in front of the sample holder which was mounted on the same flange, which needed to be removed for sample changes. The cell only had a single leak valve which was used to dose helium into the sample

chamber. The data taken using this cell iteration is shown in section 4.3.

3.4.2 Mark II

The next modification (Mark II, Figure 3.6) was to use a linear-rotary manipulator, to allow angle-dependent spectra to be taken and a new sample holder was devised. The cell can be used on its side to allow powders to be held in the sample caddy without carbon tape, or vertically so that samples can be tilted with respect to the linear polarisation of the synchrotron X-rays. The number of leak valves for gas dosing was increased for use with catalysis experiments to allow simultaneous dosing of several gases such as helium, oxygen and carbon monoxide for catalysis studies. An example of data take at different pressures using this cell is shown in Figure 3.7⁹⁵, showing a prominent CO peak at higher pressures.

The sample holder consisted of an electrically isolated metal (aluminium or steel) plate connected to the outside via an electrical (BNC) feedthrough for a drain current. A boron nitride resistive heater, power connectors and thermocouple were mounted on the metal plate to allow heating, even in a reactive atmosphere. An example of data take using this cells temperature control is shown in Figure 3.9⁹⁵. The sample itself is placed in a snap-on caddy which fits over the metal plate (Figure 3.8). The biased electron yield collector was mounted on a teflon inset which was electrically connected via a (BNC) separate from the manipulator feedthroughs.

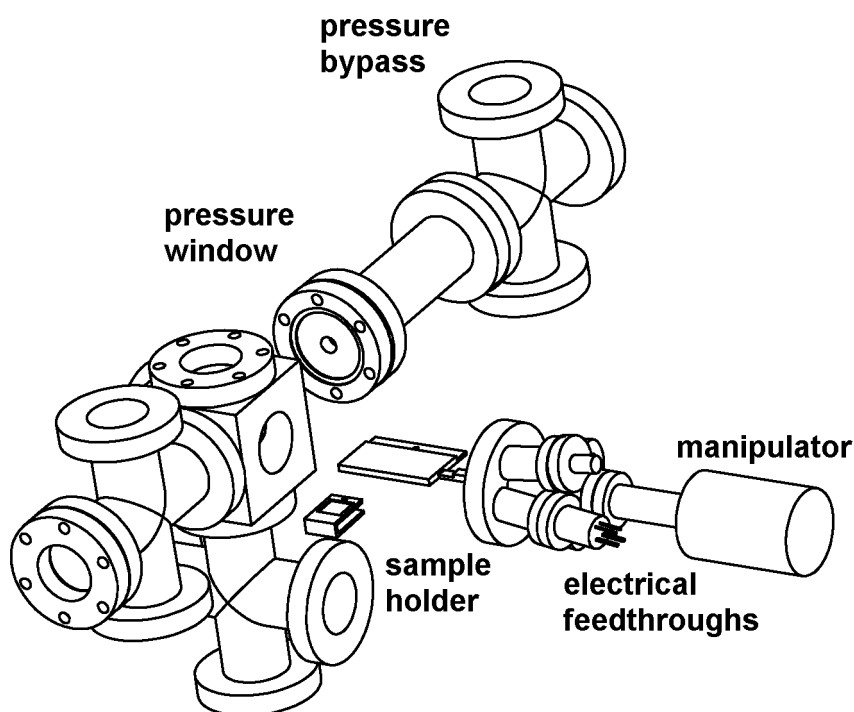


Fig. 3.6: Partially exploded view of the second iteration of soft X-ray cell (Mark II). The snap-on sample holder and the use of a manipulator to mount most of the feedthroughs are the main difference.

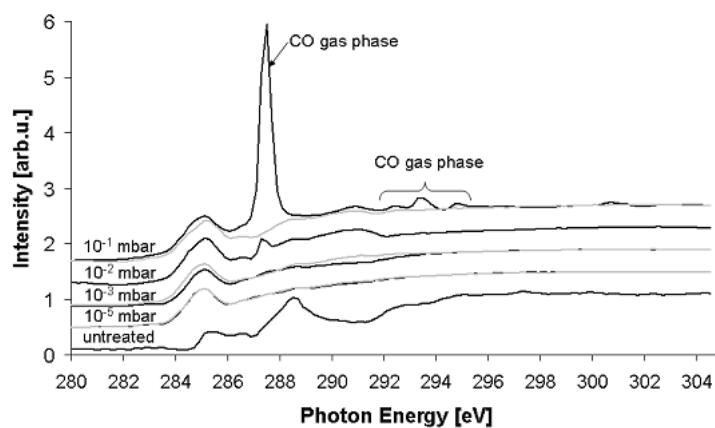


Fig. 3.7: Carbon K-edge NEXAFS of CO over gold at different pressures⁹⁵.

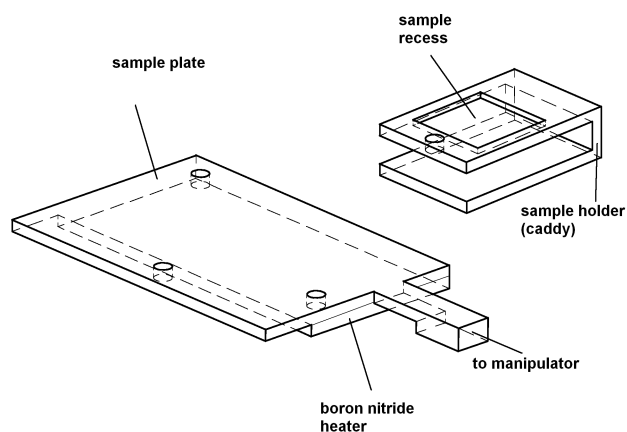


Fig. 3.8: The sample mounting system developed consists of a caddy with a recess for powders or single crystals and a recess for a thermocouple and a connector for electron yield drain currents. The caddy slides onto another metal plate which houses the heating (or cooling) device and is connected to the manipulator.

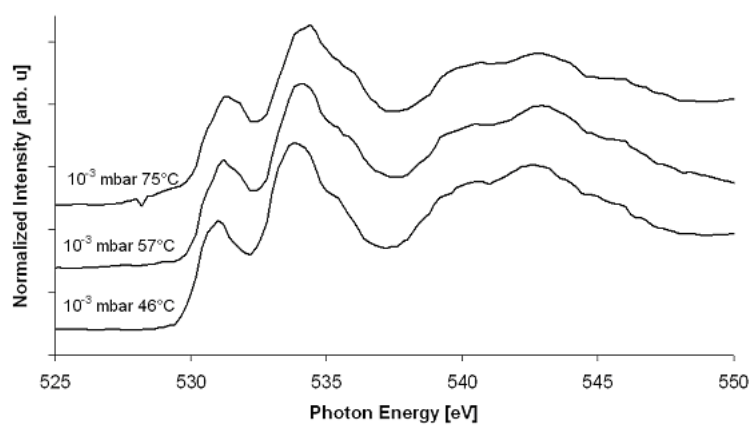


Fig. 3.9: Carbon K-edge NEXAFS of CO over gold at different temperatures⁹⁵.

3.4.3 Mark III

The final iteration of the soft X-ray cell (Mark III, Figure 3.11) utilises the same manipulator and caddy sample mounting system as the Mark II and the variable path length window design. There are two main chambers, one for measurement and another which can be used for pre-measurement treatment such as sputtering although this is not very applicable to pharmaceuticals.

In the case where the absorption edge being studied is present in both the sample and the gas environment it is useful to be able to determine which signal is from the sample and which is from the gas. The window section designed for the final version utilises an earlier cell design by Schroeder⁹⁶ (Figure 3.10) to allow the gas path to be varied by adjusting the position of the pressure window. This in principle allows variation the ratio of gas to sample signal and elucidate which features occur from which. The vacuum is preserved as long as possible by mounting a pressure window on a tube inside the chamber. It also uses several pieces of gold mesh after the pressure window to allow normalisation to remove window effects more easily. In principle they can also be placed at differing potentials to allow the performing of partial electron yield experiments. A comparison of the different designs is shown in Table 3.2.

The sample holder was manufactured by the workshop of the Chemistry department at Manchester University and the window section was built by PSP vacuum⁹⁷. The rest of the cell was made from standard off-the-shelf

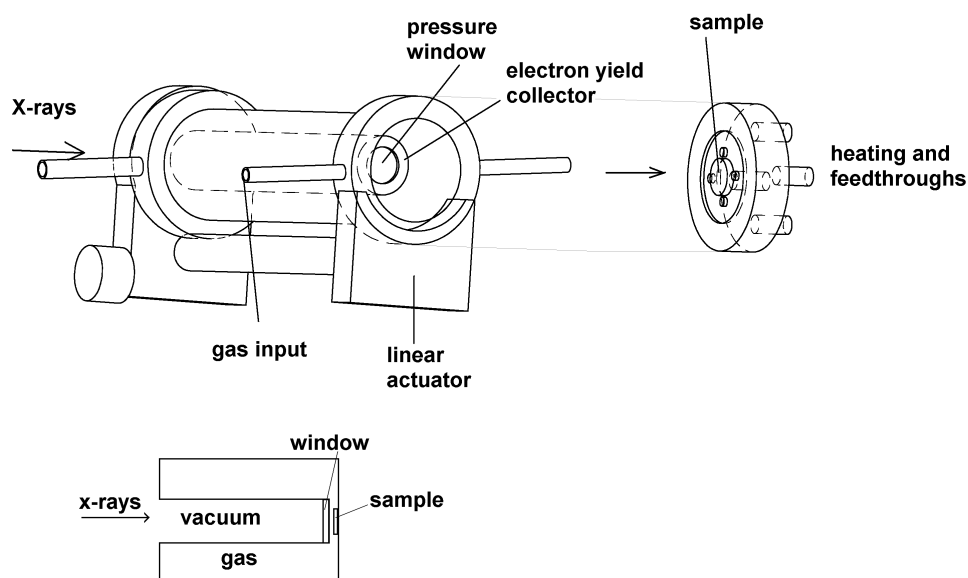


Fig. 3.10: A previous cell design by Schroeder uses an approach that allows a variable gas path length for the incoming photons. This allows the discrimination of the signal of the gas from that of the sample if they both have the same element.

parts from Hositrad⁹⁸ and Caburn⁹⁹ from the CF 35 and 16 range.

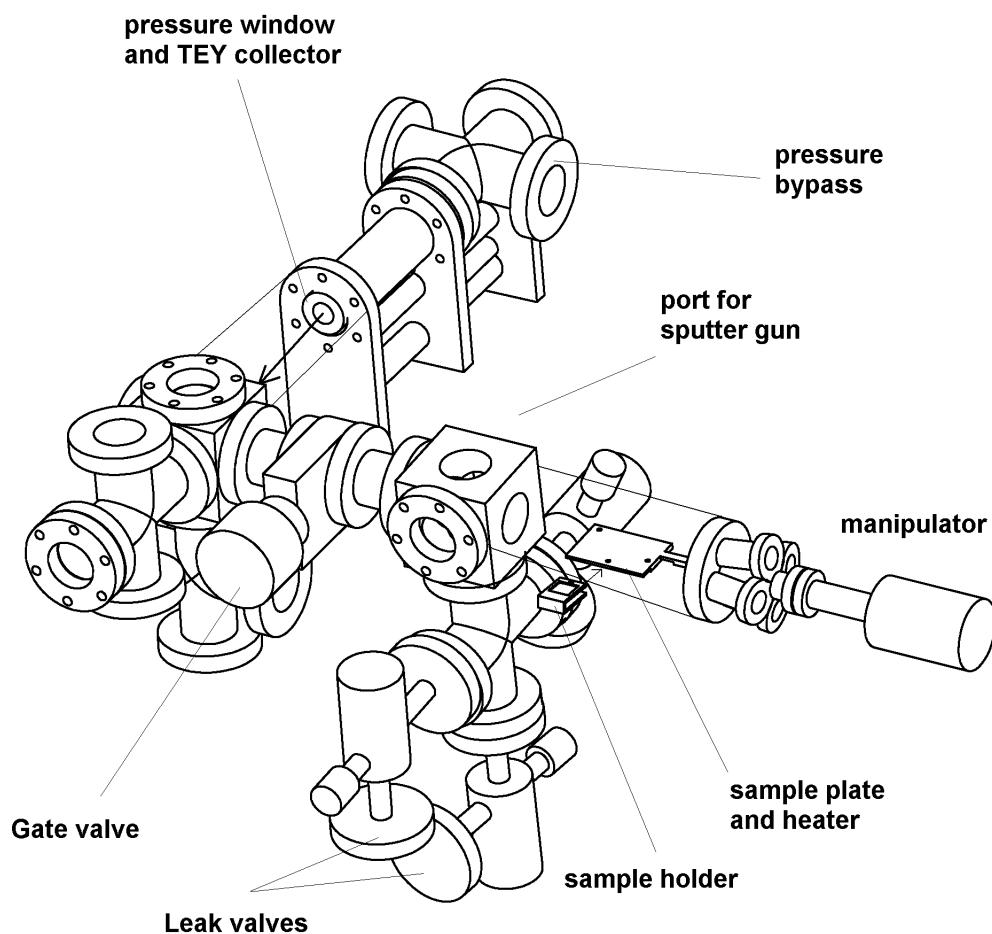


Fig. 3.11: The final design for the soft X-ray cell (Mark III).

Cell	Advantages	Disadvantages
Mark I	Cheap, only one custom part	Only one dosing gas, no sample movement, no temperature control
Mark II	Temperature Control, multiple gas dosing, can move sample	Higher cost due to custom parts and manipulator
Mark III	Temperature Control, multiple gas dosing, can move sample, partial electron yield detection, can sputter sample	Higher cost due to custom parts and manipulator, lower flux due to gold mesh

Table 3.2: Cell Comparisons

Chapter 4

Polymer Coatings for Improving Bioavailability

4.1 Introduction

The human body is approximately two thirds water and hence poor water solubility in a drug product poses serious problems in terms of bioavailability. In the initial stages of drug development the emphasis is placed on suitable biochemical properties such as selective affinity for a particular receptor, or toxicity. This approach initially fails to consider physical properties which may be important^{95;100–102}. This problem is becoming increasingly common with new drugs being developed and currently 60% of new compounds in development show poor solubility in water. This is due to increasing molecular weights of new development compounds.

The bioavailability represents the fraction of the active pharmaceutical

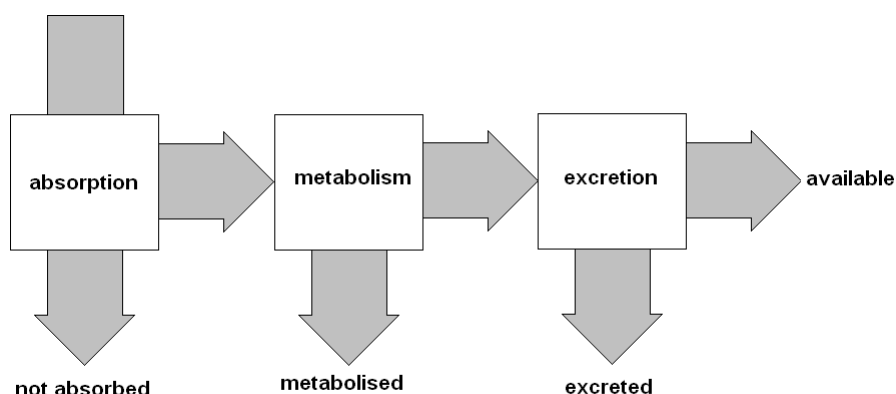


Fig. 4.1: Bioavailability is the fraction of the drug available at the target. Surface modification of poorly soluble drugs with water soluble polymers can increase the fraction being absorbed by the body and hence the bioavailability.

ingredient (API) which reaches the blood stream and is available at the target site¹⁰¹. This is reduced by fractions of the drug not being absorbed into the body, being excreted and being metabolised (Figure 4.1). It can be compared relative to other formulations of the same API or as a comparison between intra-venous (straight to systemic circulation) and oral delivery. Bioavailability is primarily influenced by the rate of absorption through the gastro-intestinal tract, the rate of metabolic breakdown by the body and the rate of excretion by the body.

Methods to improve poor bioavailability caused by low solubility in water include micronisation to reduce drug particle size and increase surface-to-volume ratios, and the use of surfactants to improve solubility¹⁰². Synthetic additives to drug formulations are subject to the same testing as the API^{14;103} so it is usual to use standard additives which are well understood and tested such as polyethylene-polypropylene oxide (poloxamer) and poly-ethylene

glycol (PEG). Wherever possible natural ingredients are used for inactive parts of the formulation such as cellulose and corn starch for bulking agents.

Poloxamer (polyethylene-polypropylene oxide co-polymer) has proved to be a very useful synthetic polymer^{104–107} and is frequently used to make a variety of drug delivery systems such as solid solutions, solid dispersions and coatings. Solid solutions have an amorphous drug and dispersions have a (micro) crystalline drug in the polymer matrix¹⁰⁸. The systems studied here are coated microcrystalline formulations more akin to core-shell drug delivery systems. The mechanism proposed consists of two stages: one of swelling of the polymer, followed by dissolution of the API⁹⁵ which may or may not involve forming polymer-drug complexes¹⁰². The dissolution profile is the instantaneous dissolution rate over time. Ideally this should move to a maximum and remain there to provide the optimum therapeutic dose. If the dissolution profile is constant then the surfactant is probably forming some form of complex which continually aids dissolution, if it shows an initial spike then the surfactant is probably only aiding the dissolution of the top few layers.

Each formulation still needs to undergo *in-vivo* studies which represent the most expensive stage of producing a drug product¹. With the growth in poorly soluble drug compounds it is becoming increasingly important to understand formulation development. A better understanding would allow predicting of optimal formulations before proceeding to trials. This is an area of growing importance in which surface science can be employed.

The surfactant coating can represent a sufficiently small overlayer which is unsuitable for study by conventional bulk study techniques. Any way of reducing the range of formulation which should be used in clinical trials will potentially have a huge implication on the final cost of bringing a drug product to market. The use of surfactant and coatings also helps to produce more consistent dissolution rates which improve patient safety.

Sections of this work have been presented at XAFS XIII (13th International Conference on X-ray Absorption Fine Structure) and SRMS-5 (5th International Conference on Synchrotron Radiation in Material Science) and have been published in^{109;110}.

4.2 SR 142801, Osanetant

Neurokinin receptors are proposed targets for the treatment of schizophrenia. SR 142801 (Figure 4.2), trade name Osanetant, was the first non-peptidic antagonist of the NK3 receptor and is highly selective¹¹¹ making it an excellent candidate for treatment. However, the drug exhibited low oral bioavailability which was poorly reproducible so it was decided to modify the drug with a commonly used surfactant, a polyethylene-polypropylene oxide co-polymer (poloxamer) shown in Figure 4.3 to increase the instantaneous dissolution rate and hence improve bioavailability.

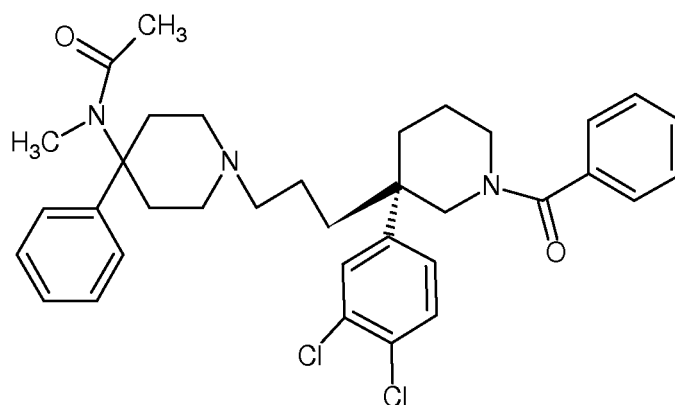


Fig. 4.2: SR 142801 Molecular Structure

Trials conducted by Sanofi-Aventis showed that the 50 mg/L preparation performed best, not the samples with the greatest amount of surfactant as expected. A series of formulations were prepared with increasing quantities of poloxamer and micronised crystals of the API. Samples were prepared by making an aqueous solution of the poloxamer at the following concentrations; 0, 10, 50, 100, 150, 200 mg/L. 4 g of the API was then added to 200 mL of

the surfactant solution and left to equilibrate for 6 hours and the resulting suspension was then filtered and dried at room temperature.

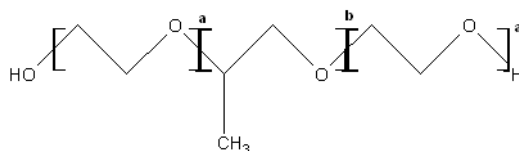


Fig. 4.3: Poloxamer Molecular Structure

The drug was chosen as the first problem of interest to be studied by the project and Near Edge X-ray Absorption Spectroscopy (NEXAFS) was used as a method to study the coating surface and explain why the 50 mg/L sample gave better trial results than the others, and discover if there was anything else of interest which could be determined using NEXAFS.

4.3 Near Edge X-ray Absorption Fine Structure (NEXAFS)

Carbon, nitrogen, and oxygen K-edge measurements were made on the 5U.1 undulator beamline of the Daresbury laboratory Synchrotron Radiation Source (SRS) using the Mark I cell shown in Figure 3.5. Data were collected using total electron yield (TEY) and fluorescence yield (FY). Electron yield in the energy range covering the K-edge adsorption for oxygen (530 eV), nitrogen (400 eV) and carbon (270 eV) gives a sampling depth of approximately 1-5 nm depending on the edge⁸⁸, making it highly surface sensitive. Fluorescence yield in the soft X-ray range has a sampling depth of 500-1000 nm making it essentially bulk sensitive when compared to electron yield⁹⁴. The chamber was pumped down to 10^{-6} mbar or lower, then the turbo pumps were throttled and back filled with helium to 2 mbar. Spectra were measured for the ranges 395-450 eV, 280-325 eV and 520-560 eV with 0.1 eV steps and 1 s measuring times. Repeated measurements were made of a single sample to check for radiation damage. No change of spectra over time was observed, so either damage did not occur or any damage occurred very quickly on the timescale of a single scan. Data have been normalised to an I_0 mesh.

4.3.1 Nitrogen K-edge

The nitrogen K-edge has no fluorescence yield data because of extreme attenuation near the nitrogen edge caused by a polyimide pressure window both in the detector and chamber, compounded by the small number of nitrogen atoms in the sample and the low yield for fluorescence for low Z atoms. Electron yield data in Figure 4.4 show two pronounced peaks at 402 eV and 406 eV assigned to π^* transitions and a σ^* transition at 416 eV. The 402 eV peak is thought to originate from the centre tertiary amine and the 406 eV peak from the two nitrogen atoms bonded to a amide group. The intensity of both peaks drops as the coating level increases due to attenuation of the nitrogen signal from the drug substrate with a great coverage of polymer. Specifically, there is a big drop between the 10 mg/L and 50 mg/L sample. There is also a drop between the relative heights between the 10 mg/L and 50 mg/L sample which may be due to some form of orientation effect. The samples are powders so if the difference in π^* and σ^* transition ratios is an orientation effect it could be from the surfactant preferentially adsorbing at one crystalline face.

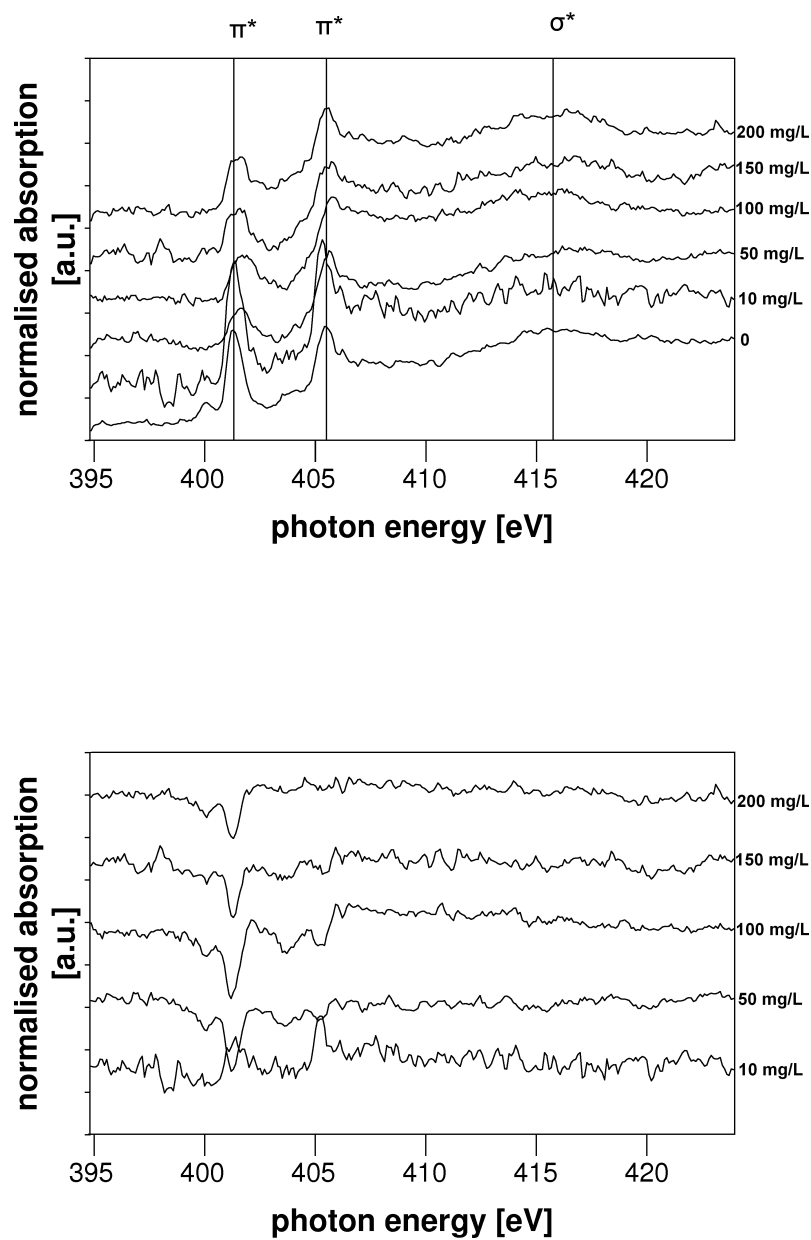


Fig. 4.4: SR 142801 nitrogen K edge total electron yield NEXAFS, top: normal spectra, bottom: difference spectra relative to the pure drug. The π^* peak at 402 eV decreases relative to the other π^* and σ^* peak. The biggest change being between the 10 mg/L and 50 mg/L samples.

Difference spectra were made to illustrate the changes between samples more clearly. The difference spectra are relative to the pure drug. It clearly shows the 50, 100, 150 and 200 mg/L samples with a drop in intensity around 402 eV which corresponds to a depletion of that peak relative to the pure drug, but no drop around 406 eV confirming a change in the relative intensities between the 402 eV and 406 eV peaks.

4.3.2 Carbon K-edge

The carbon K-edge total electron yield data is heavily influenced by absorption from the X-ray pressure window and the ubiquitous carbon contamination. Carbon contamination is also present on the beamline optics and causes a dramatic drop in flux around the carbon edge but this effect is mitigated in the data by I_0 normalisation and the presence of so many carbon groups in the drug and coating. The 150 mg/L sample, Figure 4.5, shows a big drop in intensity compared to the other samples. The pure drug, 50 mg/L and 200 mg/L showed an increase in the resonance at 288 eV. While the relative differences between samples can be pointed out it is difficult to say with any certainty to what they should be assigned. Structure in the spectra is also introduced by the beamline pressure windows but should be constant between samples. Frequently sputtering of the surface with Ar^+ ions^{3;4} is used to remove the top layers of carbon contamination from the surface but this method is far too destructive for complex organic samples such as pharmaceuticals.

The carbon K-edge data in Figure 4.6 showed no discernible variation between the samples in the fluorescence data. However the problems associated with the carbon edge fluorescence make the data somewhat unreliable. There is a large difference between the electron and fluorescence data. The most prominent π^* and σ^* do not match. Although some differences between the surface and the bulk might be expected, the differences are far greater than at the oxygen K-edge. This suggests that

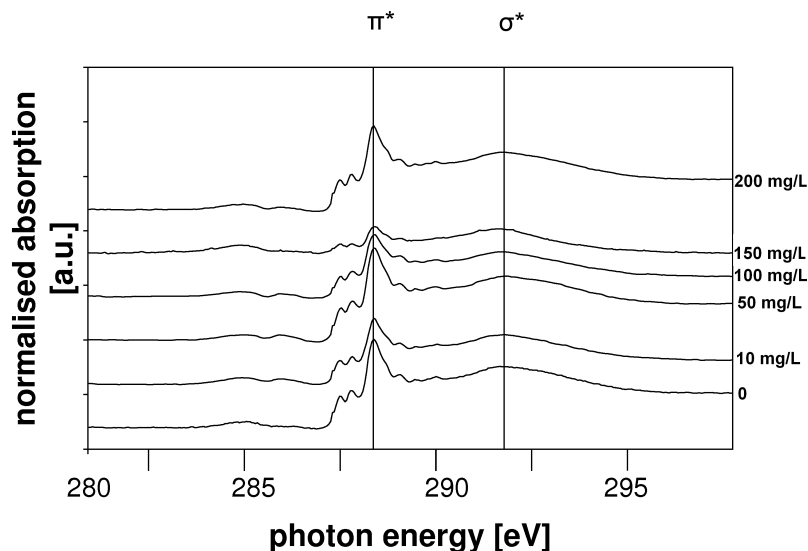


Fig. 4.5: SR 142801 carbon K-edge total electron yield NEXAFS. Due to carbon contamination of surface and beamline optics it is difficult to assign meaning to the spectra.

either the electron yield data are wrong, the fluorescence data are wrong or they both are. The detector used was a prototype and had not been optimised for the carbon K-edge, it was also behind a second pressure window which would have had different absorption characteristics to the primary window, additionally there will be absorption from the isobutane gas in the detector. This suggests that the problem is with the fluorescence. Given the large differences between the FY and TEY and the problems often encountered at the carbon edge no conclusions can be drawn from the data.

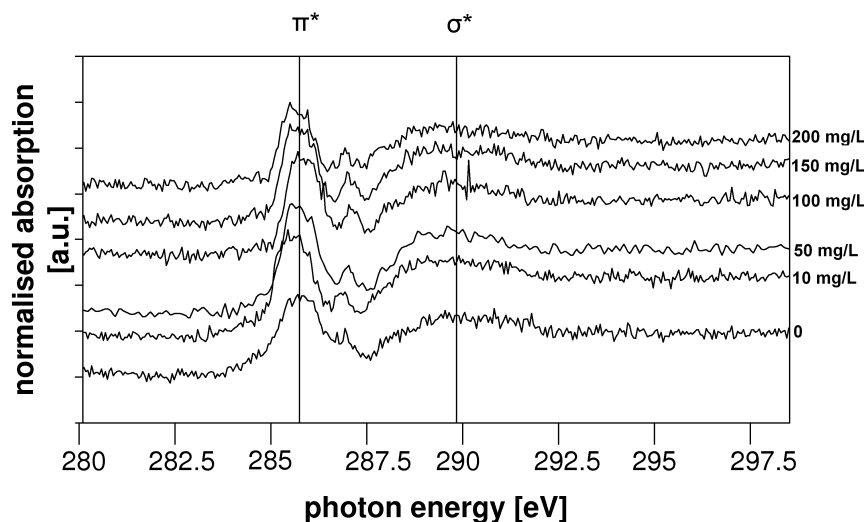


Fig. 4.6: SR 142801 carbon K-edge fluorescence yield NEXAFS. The fluorescence data do not match the electron yield data.

4.3.3 Oxygen K-edge

The oxygen K-edge data were the most interesting in terms of both the difference between the bulk and surface, and the differences between the samples. The bulk sensitive fluorescence yield data, Figure 4.7, show little variation between samples which is expected, as the underlying drug substrate which constitutes the majority of the bulk material should not change with coating levels. There are three easily identifiable resonances, the first a π^* resonance at about 532 eV and two σ^* resonances, one at 537 eV and one at 547 eV. The high energy resonance is associated with the shorter length amide carbonyl bonds. The low energy resonance is probably being detected from the surface layer with the single bond oxygen in the coating (Figure 4.9), explaining why the resonance is much weaker than in the

surface sensitive electron yield. The difference spectra show minor shifts in the position of the π^* transition which is probably caused by some slight drift in the monochromator. There is a slight increase in the 537 eV resonance in the 100 mg/L sample and of the 547 eV resonance in the 150 mg/L sample.

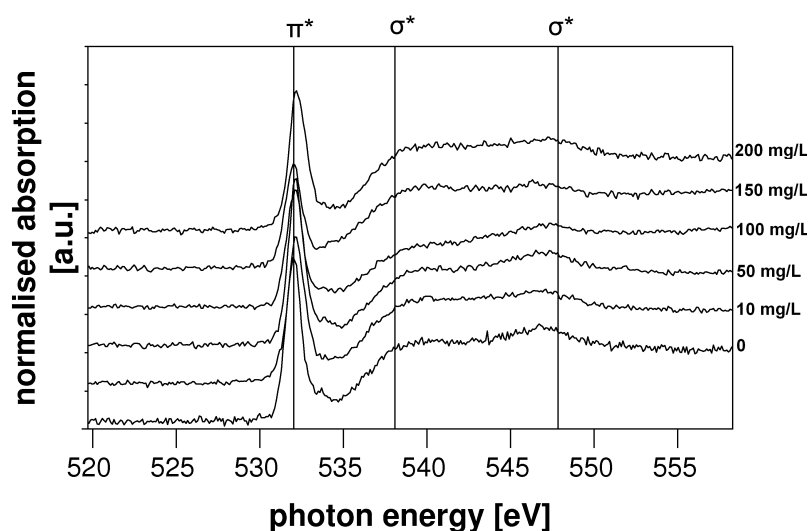


Fig. 4.7: SR 142801 oxygen K-edge fluorescence yield NEXAFS. The samples are virtually identical which suggests that the coating does not change the drug bulk. The high energy σ^* is thought to be from double bonded oxygen in the drug.

The surface sensitive total electron yield data (Figure 4.8) show the same π^* resonance as the fluorescence data and a far more prominent σ^* resonance at 537 eV which is caused by the poloxamer coating present on the surface (Figure 4.9). The high energy σ^* resonance at 547 eV is not present. Most interesting are the smaller resonances between the π^* and σ^* resonances identified as adsorbed water, which reach a peak at the 50 mg/L

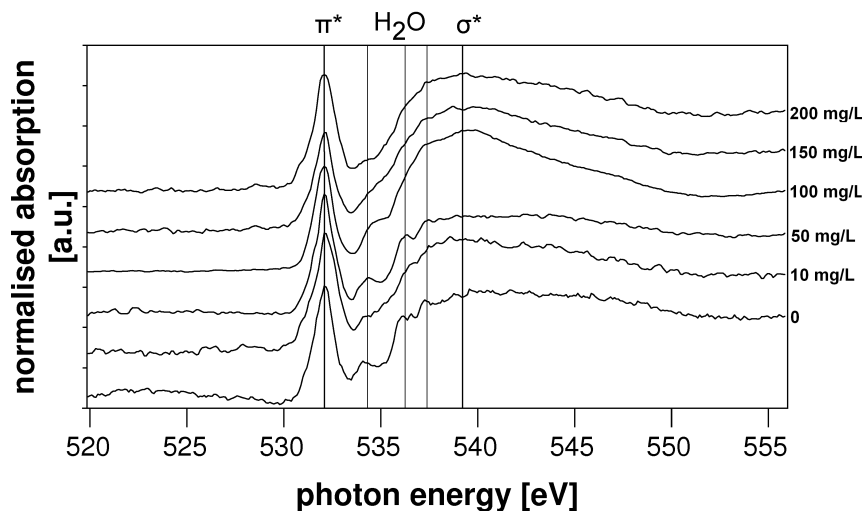


Fig. 4.8: SR 142801 oxygen K-edge total electron yield NEXAFS. The spectra show a far more prominent low energy σ^* bond than the fluorescence data and this is due to single bonded oxygen in the coating polymer and it rises with coating level. There are also smaller resonances between the π^* and σ^* which are identified as adsorbed water. The most prominent adsorbed water peaks in the 50 mg/L sample correspond to the best performing formulation.

sample and are also present to a lesser extent in the pure drug and 10 mg/L and 100 mg/L samples.

Figure 4.10 shows the difference spectra created from each sample's electron and fluorescence yield data and should represent the differences in that sample between the bulk and surface composition. Owing to the comparative lack of difference in the fluorescence yield data when compared to the electron yield data, surface differences dominate this set of spectra. All the difference spectra show a depletion at the π^* resonance which is most pronounced in the 50 mg/L sample. The σ^* is observable in most of the samples particularly in the 100 mg/L sample.

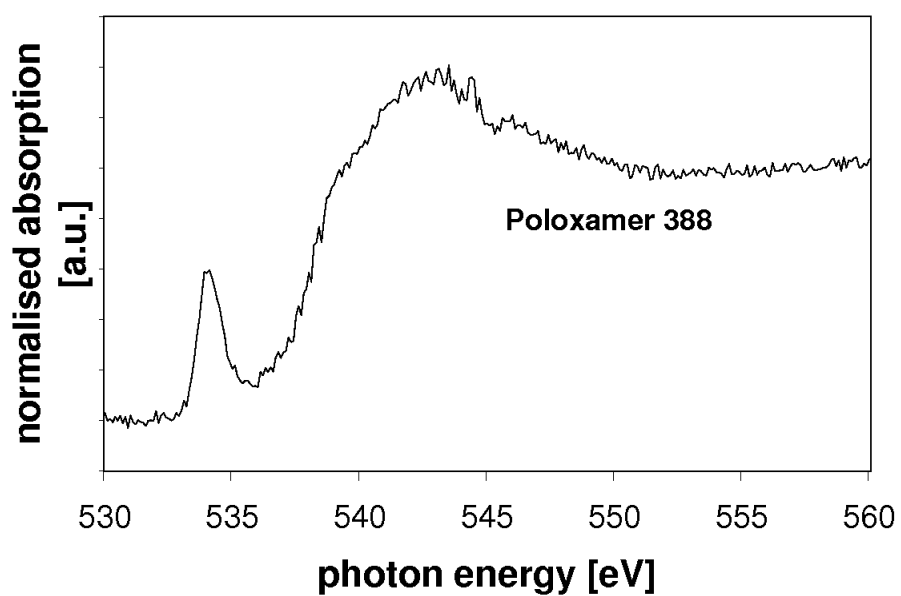


Fig. 4.9: Poloxamer 388 oxygen K-edge total electron yield NEXAFS. Notable is the small π^* resonance compared to the σ as seen in the formulation spectra.

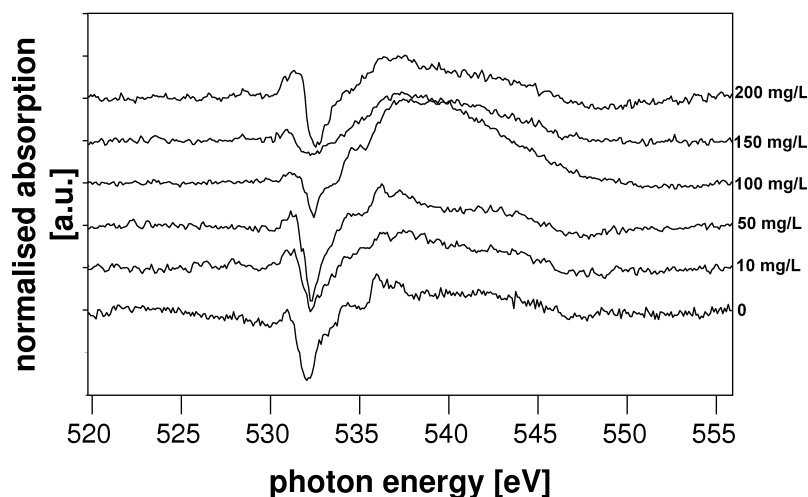


Fig. 4.10: SR 142801 oxygen K edge difference spectra, surface - bulk NEXAFS. The difference spectra are dominated by the drop in relative π^* intensity and a corresponding enlargement in the σ^* resonance associated with the surface.

4.4 Discussion

in-vitro dissolution results from Sanofi¹¹² showed that the 50 mg/L sample gave the best results, not as one would perhaps expect, the 200 mg/L sample due to its higher coating level. Discussing each edge in turn we are able to build up a picture of why this might be. The nitrogen edge electron yield spectra are surface sensitive and are only measuring the drug substrate, not the coating. They show a large drop in their intensities between the 10 mg/L and 50 mg/L samples, which suggests that the amount of physical coating on the drug shows a large increase for that coating level suggesting that the concentration of polymer in the initial solution has crossed some critical level. The change in the relative intensities of the π^* and σ^* peaks suggests

an orientation effect. This could be the coating preferentially absorbing along one face of the crystal structure or towards one side of the molecule as shown in Figure 4.11 changing how much of that face is exposed at different coating levels. The large number of carbon atoms in both the drug and coating, combined with the problems of carbon contamination and window absorption make it very difficult to use the spectra to conclude anything about the samples.

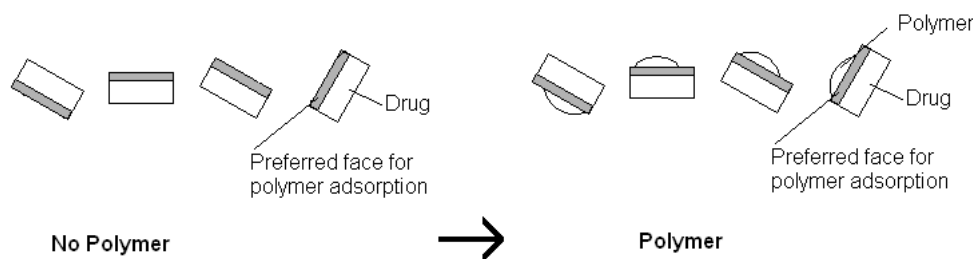


Fig. 4.11: Possible orientation effect

At the oxygen edge it is possible to clearly distinguish between the bulk and surface of the samples thanks to the fluorescence detector. The similarity of the bulk spectra illustrate that it is surface differences which are the deciding factor with these formulations. The surface spectra are clearly able to pick up on the deposited poloxamer coating. The oxygen spectra also show small resonances, which are in the correct position and are the correct shape for adsorbed H_2O gas^{113–115}. It seems to be the case that the water adsorption is not linearly dependent on coating levels. Also notable is the fact that the H_2O resonance position is slightly shifted in the 50 mg/L and 100 mg/L samples. Interestingly the 50 mg/L sample also

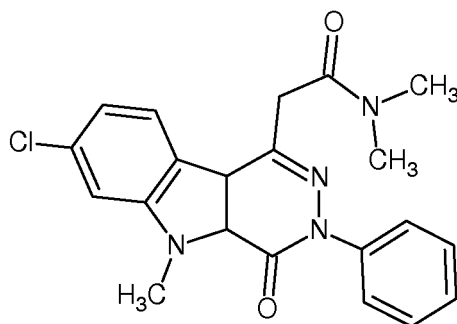
shows the greatest difference in π^* between the surface and the bulk and the 100 mg/L sample showed the greatest surface/bulk difference with the σ^* .

The improved results in the 50 mg/L sample seem to correspond with the most prominent adsorbed water peaks. The presence of water on the sample after being in the low vacuum of the cell shows that it is tightly bound this in turn suggests that the reason for its superiority in trials is that it is more water soluble and hence is more readily taken up into the blood stream. The fact that the water is only present in the surface spectra and not the bulk would suggest that normal bulk sensitive techniques would not have been able to distinguish this.


4.5 SSR 180575

SSR 180575 (Figure 4.12), a peripheral benzodiazepine receptor (PBR) ligand, is undergoing phase I clinical trials for activity in neurodegenerative diseases such as parkinsons and arthritis¹¹⁶. The drug shows poor water solubility and the purpose of this study was to examine the effects of different polymers being used for the coatings.

A sample of the drug provided by Sanofi-Aventis had been milled to give a particle size of a few microns. Water soluble polymers (Figure 4.13, 4.3) for coatings were obtained from Sigma-Aldrich; (i) Polyethylene glycol (PEG) 3350 (ii) Polyethylene-polypropylene glycol (Poloxamer) 388 (iii) Polyvinylpyrrolidone (PVP) 50 (iv) Poloxamer 188 (v) Polysorbate (Tween) 80. Coated samples of the drug were produced by making a 5%(wt) aqueous solution of each polymer and placing 15%(wt) of the micronised drug in solution and allowing it to equilibrate. The resultant suspension was then filtered. Additional Samples were prepared with a 2.5%(wt) of polymer solution (the two batches of samples are referred to as 5% and 2.5%).



PEG


HO[CH2CH2O]nCH2CH2OH

PVP



CC1(CCCC1=O)N[C@@H](C)CC

Fig. 4.13: Coating Polymers Molecular Structure

X-ray photoelectron spectra were measured using a Kratos Axis Ultra machine with a monochromated Al-K α source, hybrid (electrostatic and magnetic) lens system and charge neutralisation. A pass energy of 80 eV was used for surveys and 20 eV for high resolution scans. Survey scan was measured from 1100 to -5 eV with 0.5 eV steps and 200 ms dwell time. High resolution scans were taken around the peak of interest with 0.1 eV steps 300 ms dwell times and 3 (carbon and oxygen), 5 (nitrogen and valence band) or 10 (chlorine) repeats. Spectra were exported as VAMAS files.

Analysis was carried out using the commercial CasaXPS software. Repeated measurements were made on a single sample to check for radiation damage. No change of spectra over time was observed, so either damage did not occur or any damage occurred very quickly on the timescale of a single scan. After 3 complete sets of measurements (all core levels) some sample degradation was noticeable in the spectra and they had a yellowish appearance (changed from white)

4.6.1 Valence Bands

The valence band spectra show electrons ejected from the valence region rather than core electrons. As they have the lowest binding energy they are ejected with the highest kinetic energy, giving the valence band a greater sampling depth than the core level electrons (although the difference is \sim nm). The valence bands have a lower intensity than the core levels making them harder to measure. The structure is caused by all of the electrons involved in bonding in the material, making detailed analysis impossible for such a complex molecule (although density functional theory has been used to predict valence bands for simple polymers¹¹⁷ and other materials). Its main use here is as a finger print to identify a specific material. Figure 4.14 shows valence spectra from pure drug, coating and coated drug. The coated sample spectra all appear closer to the pure drug spectrum than their respective polymer spectra.

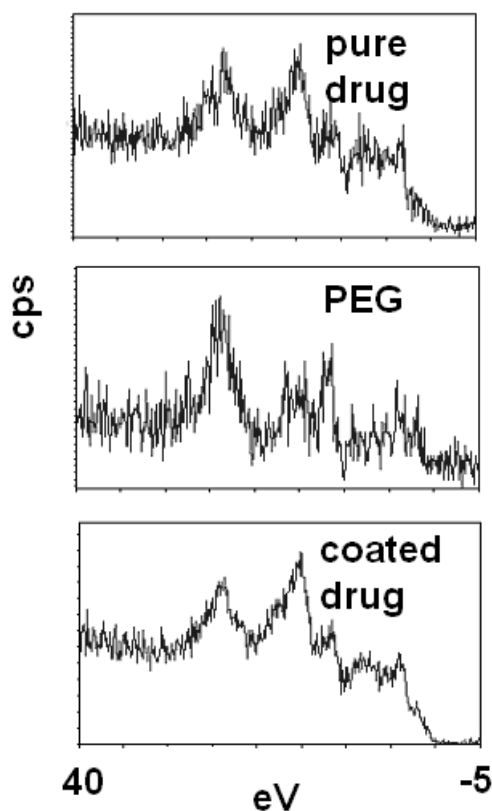


Fig. 4.14: Valence Band X-ray Photoelectron Spectra, Top: Pure Drug, Middle: Polymer (PEG), Bottom: Polymer Coated Drug. The coated spectrum appears to be very similar to the pure drug spectrum.

4.6.2 Survey Spectra

Survey spectra (Figure 4.15) show the whole energy range in a single spectrum. They are taken with a large pass energy which gives a higher sensitivity to peaks than a scan of a single peak, but the trade off is energy resolution so they cannot be reliably used to pick out different chemical states. They are used to determine elemental compositions using the area of each peak and a relative sensitivity factor (R.S.F.) which is a function of the element, the core level it came from and the instrument it was measured on. Tables 4.1 and 4.2 show the relative elemental concentrations

Material	C 1s	O 1s	N 1s	Cl 2p
PEG 3350	75.3	24.7	-	-
Poloxamer 388	75.3	24.7	-	-
PVP 50	80.4	11.0	8.6	-
Poloxamer 188	75.0	25.0	-	-
SSR 180575	77.7	8.5	9.5	4.3

Table 4.1: Relative percentage elemental abundances for drug substance and coating polymers

of the pure materials (polymers and drug substance) and the coated samples.

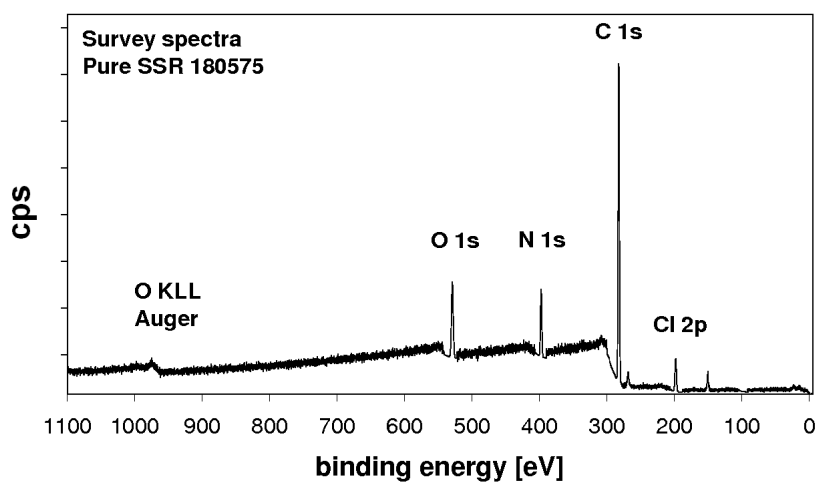


Fig. 4.15: SSR 180575 Survey spectra showing peaks from oxygen, nitrogen, carbon and chlorine, an oxygen KLL auger peak is also visible to the far right.

The chlorine signal is the only element that is always only from the drug (the nitrogen peak is the same excepting the PVP coated samples). This means that it can be used as an indicator to determine the physical coating level for a sample. The reduction in the chlorine peak between the different

Coating	C 1s	O 1s	N 1s	Cl 2p
PEG 3350	79.3	8.4	8.7	3.7
Poloxamer 388	75.3	10.6	10.2	4.0
PVP 50	79.0	7.9	9.7	3.4
Poloxamer 188	77.1	9.4	9.8	3.7

Table 4.2: Relative percentage elemental abundances for 5% solution coated samples

coating polymers could be due to different coating thicknesses or different coverage areas or a combination of the two. This method only gives an idea of the amount of coating a sample has received and it does not necessarily correspond to how effective the coating is.

4.6.3 Chlorine 2p

High resolution scans of the chlorine peaks confirm that it exists in only one chemical state in each sample (Figure 4.16). There are two peaks due to spin-orbit splitting and no shift in energy between samples relative to the C-C bond assigned to 285 eV. This tells us that the environment around the chlorine atom is not changing with each sample, and it suggests that coating is not chemically changing the drug, which if it were could have potentially hazardous consequences.

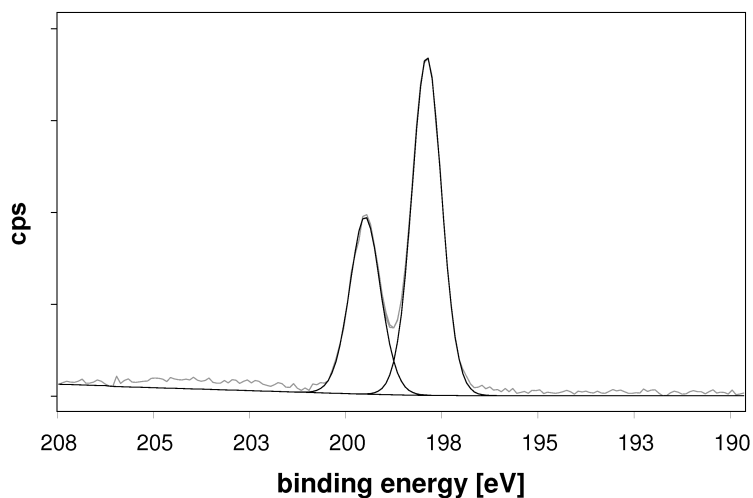


Fig. 4.16: SSR 180575 chlorine 2p spectra

4.6.4 Nitrogen 1s

The nitrogen atoms in the drug have essentially two very similar environments and this is reflected by assigning the spectra two very close peaks (Figure 4.17). A single broad peak could also be used but the peak width(Full Width Half Maximum) would be anomalously high.

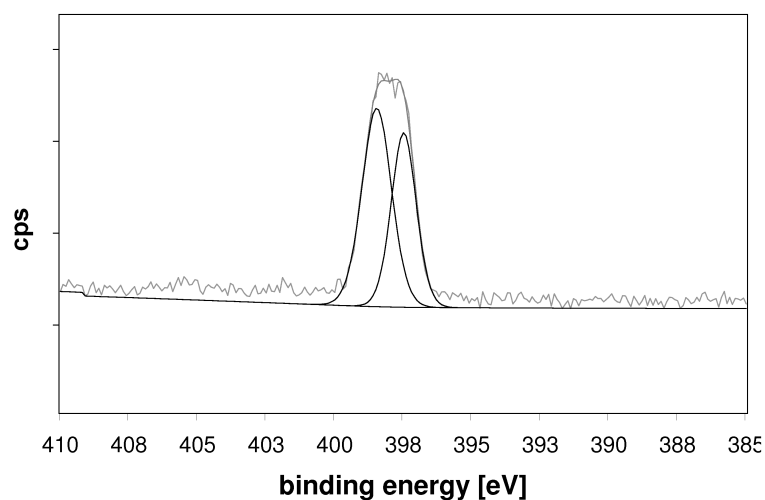


Fig. 4.17: SSR 180575 nitrogen 1s spectra

4.6.5 Carbon 1s

The analysis of carbon spectra is often problematic due to the ever present contamination. The C-C bonds are present in both drug and coating. Hydrocarbon contamination is also universally present as contamination even in inorganic samples. The C-C bond was assigned to 285 eV as is common practice^{3,4}, and used as the reference energy for the other spectra.

Chemical state assignments were based on comparing functional groups present in the samples. Increasing electronegativity showed up as higher binding energies than those present in the literature¹¹⁸ and appeared to agree with the ranges for similar functional groups present in polymers.

The peak next to the C-C peak (Figure 4.18) is quite broad and can be assigned to C-N or C-O or a combination of both which can not be deconvoluted with any confidence, both having a similar range of possible energies in the literature. If it was C-N then that would explain its presence in the pure drug, but the most likely case is that it is both C-N and C-O with very close energies, explaining its increased presence in the polymer coated samples. The ratio of C-O to C-C is much higher in the coating polymers than the C-N to C-C ratios in the drug. This peak then seems to correspond to the amount of physical material on the drug substrate. Table 4.3 shows the percentage values for the peak assignments of the different polymers.

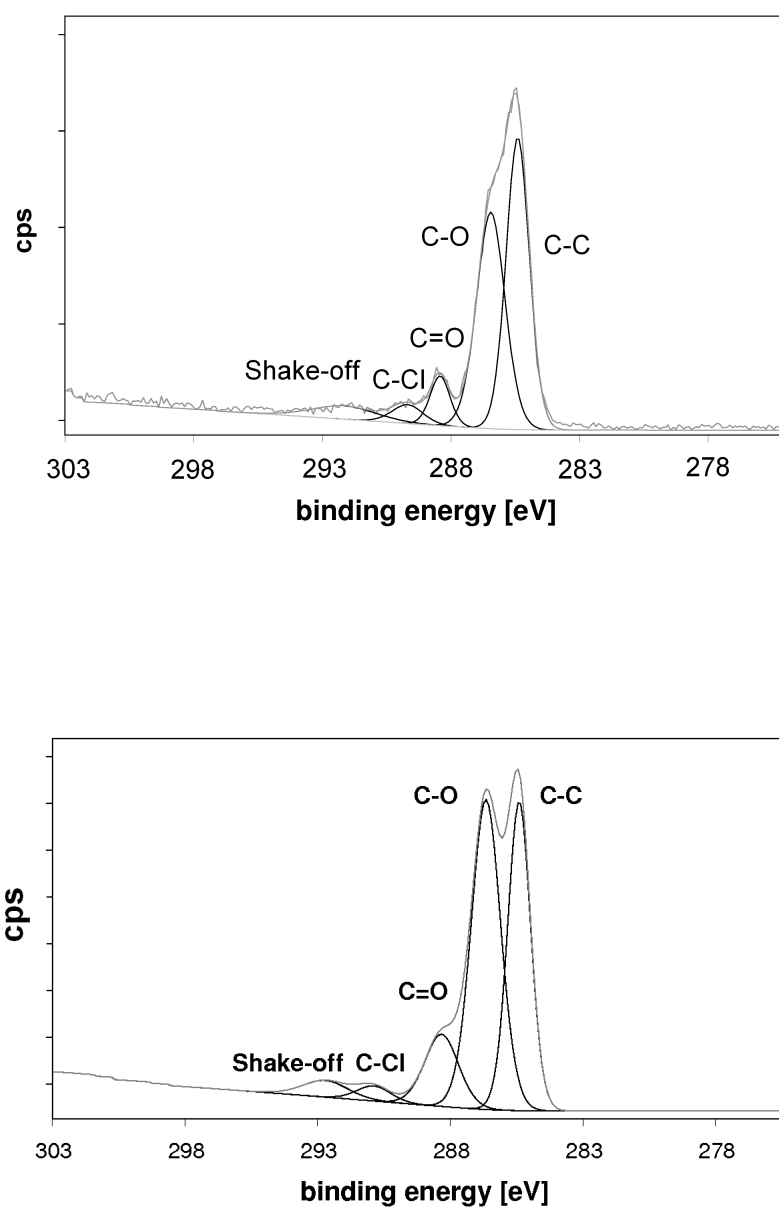


Fig. 4.18: SSR 180575 carbon 1s spectra of top: Pure drug, bottom: Poloxamer 388 coated drug. The coated sample shows a larger C-O peak from the Poloxamer 388, which could be used as an indicator for coating level.

Functional group	C-C	C-N/C-O	C=O	C-Cl	shake-off
PEG 3350	42	34	10	7	7
Poloxamer 388	36	47	12	3	4
PVP 50	51	34	8	1	6
Poloxamer 188	42	42	8	7	2
Polysorbate 80	60	30	6	4	1

Table 4.3: Carbon peak assignments for 5% solution coated samples

4.6.6 Oxygen 1s

The spectrum for the pure drug is far more complicated than would be expected for a molecule with two oxygen atoms, both with amide bonds (Figure 4.19). A possible reason for this would be differences in the local environment for oxygen on the surface, such as crystalline defects or even amorphous content, a possibility which is discussed in more depth for a different drug in Chapter 5. The pure excipient spectra all show a single O 1s peak except PVP which has an additional peak. Reference spectra from the polymer database¹¹⁸ assign this additional peak as adsorbed water due to the highly hygroscopic nature of the sample. The most likely reason that this only occurs with the PVP is because the PVP sample was a very fine powder and so had a much higher surface area to adsorb water onto (ESEM showed a typical particle size between 20-50 microns). The other samples were in the form of larger flakes or grains.

The coated samples show the four peaks from the drug (Figure 4.19), one of which is for the excipient C-O as expected and an additional peak. This additional peak is also in the right position for adsorbed water so it is possible that after the excipients have coated the sample they have a

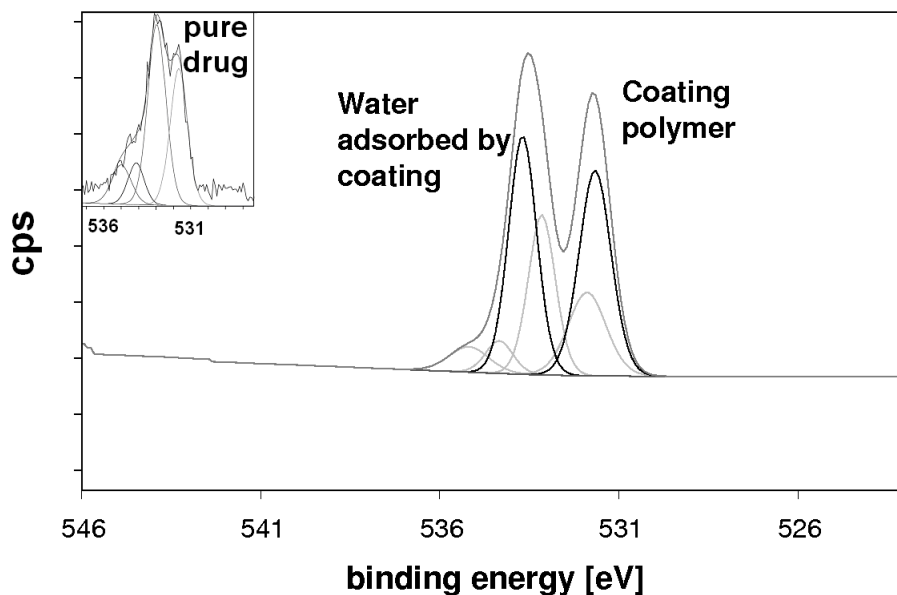


Fig. 4.19: SSR 180575 oxygen 1s spectra of PEG coated drug substance, inset: pure drug spectra. In the coated sample spectra there are two additional peaks, one from the coating polymer and the other is thought to be adsorbed water.

much higher surface area (The drug particles are small, long grains about 20 microns long and 2 microns wide).

The peak assigned to the coating polymer is similar to the idea of physical coverage indicated by the survey and carbon spectra. The adsorbed water, however, provides a better indicator of how effective the polymer is as a coating. This is similar to the X-ray absorption spectra of SR 142801 as shown previously, where surface water indicated a higher instantaneous dissolution rate and hence bioavailability. It seems to be the case that while

Component	Drug	Polymer	Water
PEG 3350	54	28	18
Poloxamer 388	41	29	30
PVP-K17	-	-	-
Poloxamer 188	42	29	29
Polysorbate 80	65	17	18

Table 4.4: Oxygen component assignments for 5% solution coated samples

the poloxamers and the PEG can get good coverage, the poloxamer 388 is the best at adsorbing water (Table 4.4).

4.7 Near Edge X-ray Absorption Fine Structure (NEXAFS)

Near Edge X-ray Absorption Fine Structure (NEXAFS) spectra were measured on the 6.1 multipole wiggler soft X-ray beamline using the Mark II cell. The set up was only capable of measuring total electron yield (surface) spectra at the carbon K-edge. Spectra were measured over the range 270 eV - 350 eV, with 0.1 eV energy steps and a measurement time of 0.5 s per point. Spectra were first measured in vacuum and then exposed to 100% relative humidity by simultaneously dosing water vapour into the system while cooling the sample holder via a nitrogen gas stream, and then measured in vacuum again. Repeated measurements were made of a single sample to check for radiation damage, no change of spectra over time was observed, so either damage did not occur or any damage occurred very quickly on the timescale of a single scan. Further spectra at the oxygen and nitrogen K edge were measured on the 5U.1 undulator soft X-ray beamline in vacuum. Data have been normalised to an I_0 mesh.

4.7.1 Carbon K-edge

At the carbon edge the pure drug shows a very pronounced π^* resonance at 285 eV, probably aromatic, and a smaller π^* resonance at 286 eV. There are a few inflections at 291 eV, 305 eV, and 315 eV which could be σ^* resonances. The dip in absorption coefficient just before the first π^*

resonance is an artifact from improper normalisation. As in the XPS data, the coated samples display features from the pure drug not present in the coating polymer. There appears to be little difference between the low and high concentration coatings for the PEG (Figure 4.20) but the Poloxamer tells a different story (Figure 4.21). The 5% coated material has almost completely obscured the 285 eV π^* resonance suggesting a good coating coverage and a significant difference between the 5% and 2.5% preparations.

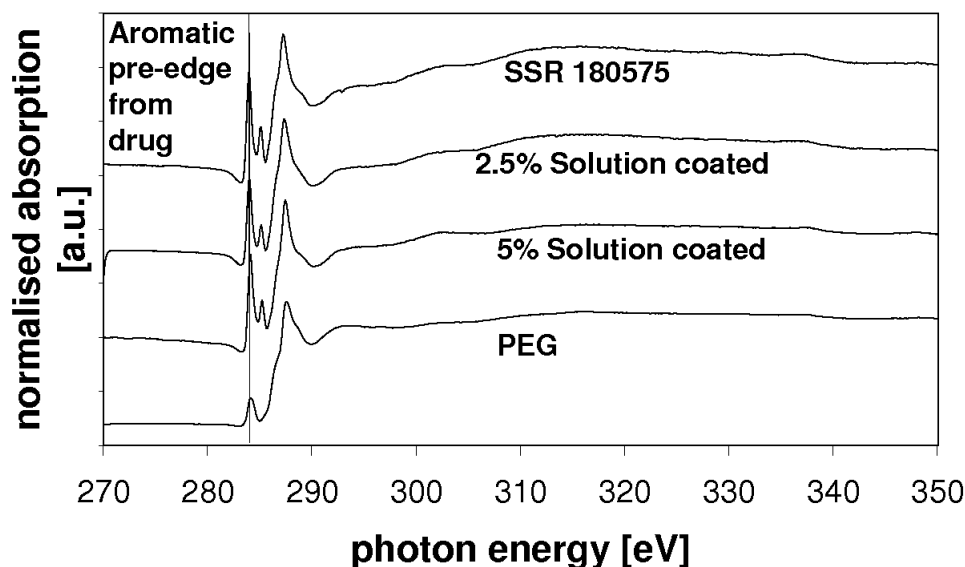


Fig. 4.20: SSR 180575 carbon K-edge total electron yield NEXAFS (PEG Coated). The distinct pre edge peak associated with the drug is present in the coated sample spectra.

After dosing water into the chamber, which took the relative humidity over 100%, spectra were retaken. The pure drug and polymer show no change

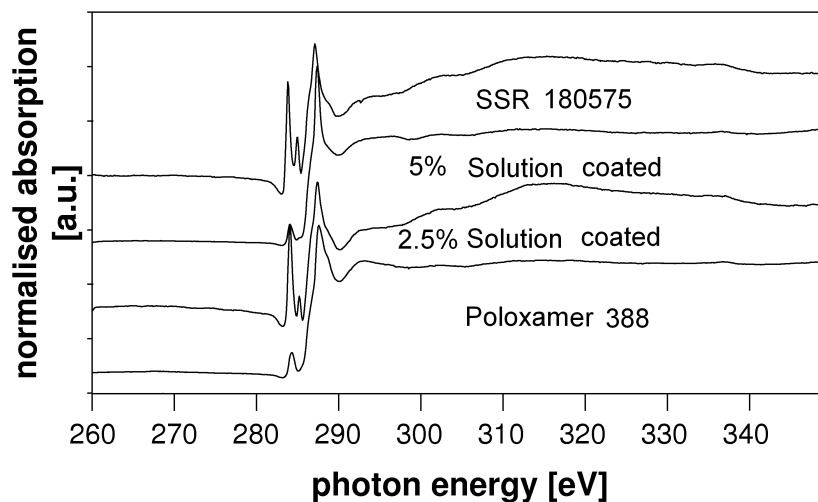


Fig. 4.21: SSR 180575 carbon K-edge total electron yield NEXAFS (Poloxamer Coated). The distinct pre edge peak associated with the drug is present in the 2.5% coated sample spectra.

after the treatment, the coated samples exhibit a big suppression of the two π^* resonances associated with the pure drug substance (Figure 4.22). This strongly suggests the high relative humidity does something to the polymer coating causing it to reduce the drug signal getting through. The strange pre-edge of the cooled pure drug is most likely caused by the warming up of the equipment after the gas dosing and opening of the beamline, disrupting the electron yield detection.

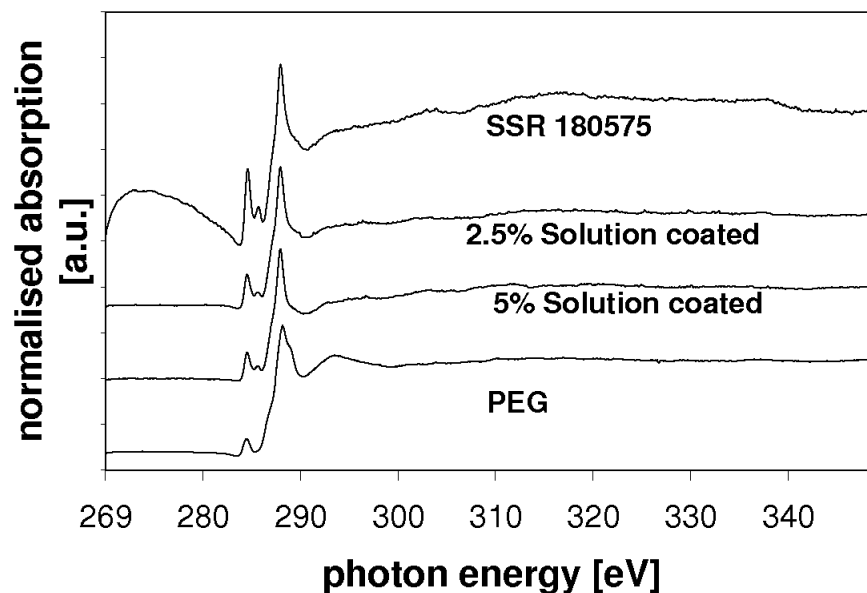


Fig. 4.22: SSR 180575 (humidity treatment, PEG) carbon K-edge total electron yield NEXAFS. The distinct pre edge peak associated with the drug is now heavily suppressed in the coated spectra after high humidity treatment.

4.7.2 Oxygen K-edge

Oxygen K-edge data (Figure 4.23) show the coated samples having intermediate spectra between the pure drug and the poloxamer. The π^* resonances for the pure drug and poloxamer are at different energies and have different relative heights between their π^* and σ^* , this giving the coated samples their extra structure. Also present is what looks like absorbed liquid-like water^{113–115} as opposed to adsorbed water more gas-like spectra in the previous drug.

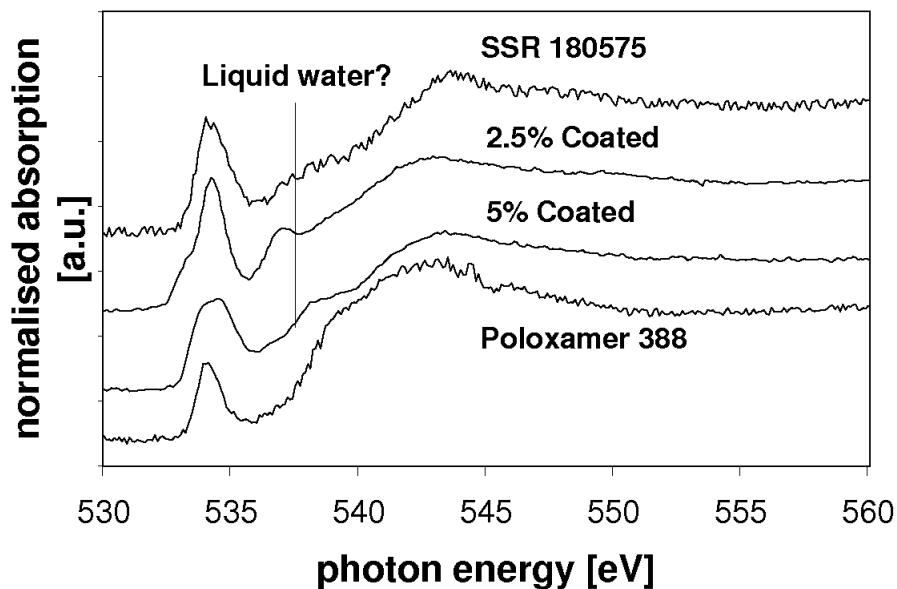


Fig. 4.23: SSR 180575 (Poloxamer 388) oxygen K-edge total electron yield NEXAFS. What looks like adsorbed liquid water is present on the coated sample spectra.

4.8 Environmental Scanning Electron Microscope (ESEM)

An Environmental Scanning Electron Microscope (ESEM) was used to look at what happened to the polymers and polymer coated drugs under the high humidity experienced during the water dosing in the NEXAFS experiment. The polymers start to dissolve when the relative humidity reaches approximately 85-90% (Figure 4.24). Repeating cycles of Dynamic Vapour Sorption (DVS), a technique which uses a microbalance to measure the uptake of water at varying relative humidity levels, shows no difference

suggesting that this is a completely reversible process. The images in Figure 4.24, which are taken over 1 cycle of rising and lowering humidity, show that it is not reversible. After humidity has returned to normal the material has formed a solid again but it has swelled and contracted, distorting the shape. It may be the case that during the coating process when in suspension the polymer completely covers the drug, but upon drying it shrinks and cracks, exposing the substrate. Micrographs of coated samples shows that after high humidity treatment the drug particles appear smoother (Figure 4.25). This could be due to either the coating polymer being washed off the drug completely or the polymer could be redistributed to a smoother more uniform coating. The latter is more likely considering the NEXAFS results.

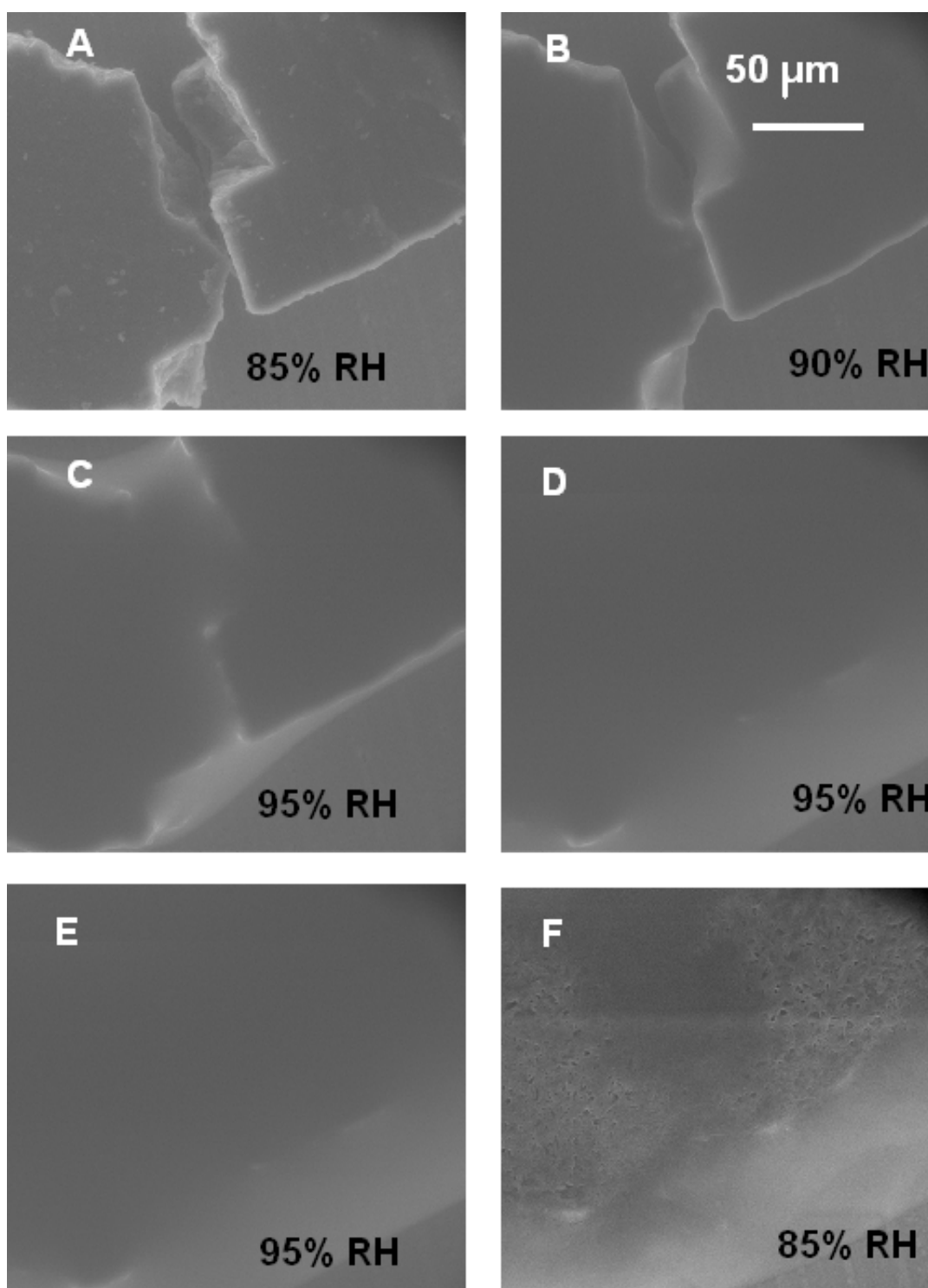


Fig. 4.24: ESEM images of PEG over one cycle of rising and lowering humidity from A to F. The polymer dissolves at high relative humidity, becoming smooth. As it dries it reforms into a different morphology.

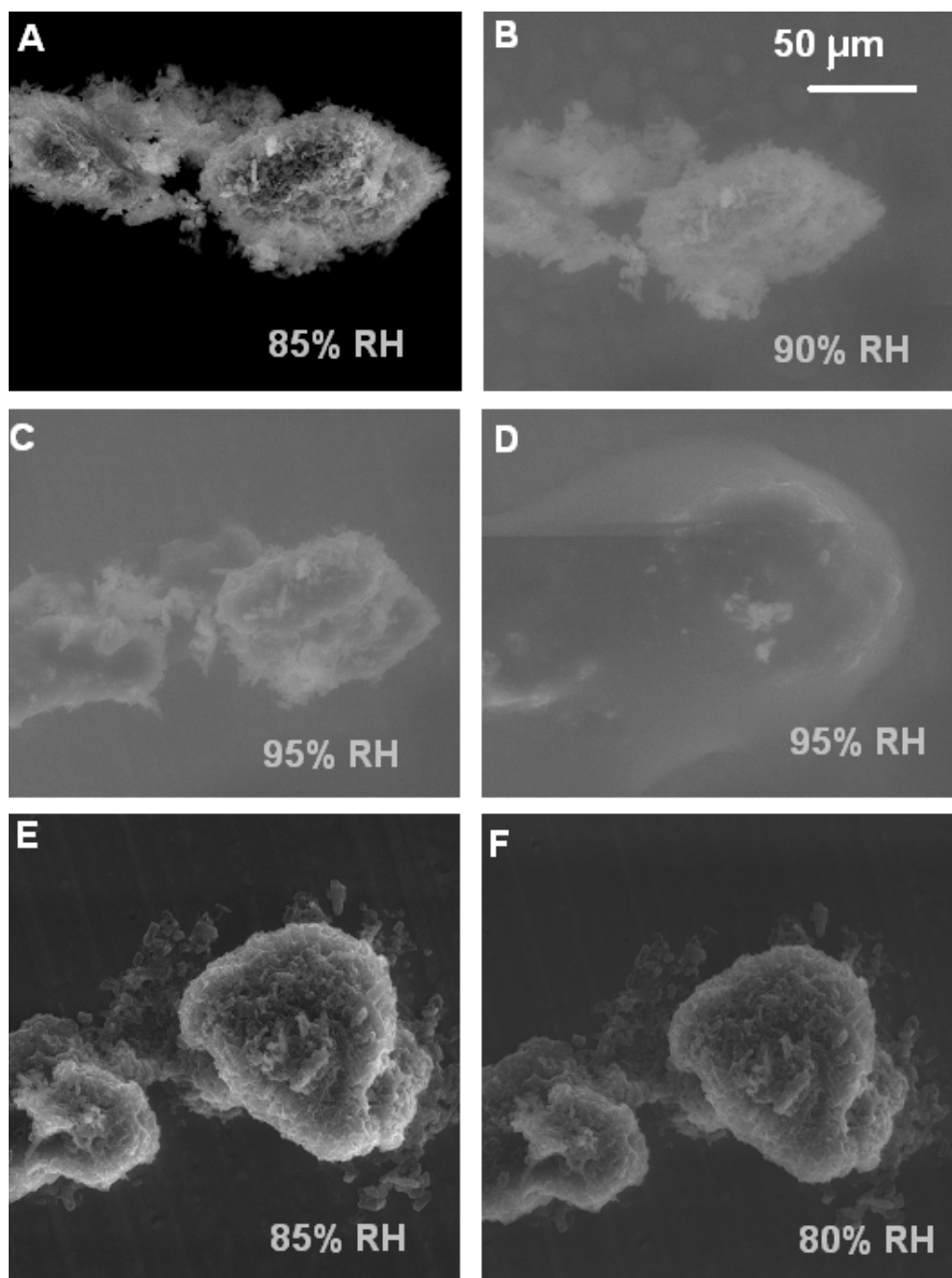


Fig. 4.25: ESEM images of PEG coated drug over one cycle of rising and lowering humidity from A to F. The crystals appear smoother after drying. Either the condensed water has washed off the polymer, or the polymer has been smoothed out on the drug surface.

4.9 Discussion

The presence of signal from the drug substrate in both XPS and NEXAFS, which are highly surface sensitive, suggests two possible models for how the polymer binds onto the surface of the drug particle. It could either be a homogeneous overlayer of polymer on the drug surface which is thin (\sim nm) enough to allow ejected electrons from the drug substrate to still reach the surface and the fraction of signal from the drug represents how thick the overlayer is. Alternatively, thicker ‘rafts’ of polymer deposited on the surface, may be present in patches with clear areas exposing the drug surface which explain the drug signal in the spectra, or a combination of these two models (Figure 4.26). In terms of how well each polymer performs, the carbon 1s suggests that the poloxamer 388 has the most polymer deposited on the surface and the oxygen 1s XPS suggest the poloxamer is better at adsorbing water. If the relationship between adsorbed water and improved performance in trials was to hold for this formulation then the poloxamer 388 would be the best formulation to start further trials on.

ESEM of the pure polymers shows that they contract and crack upon drying which could have happened to the polymer sitting on the drug surface as the material was first prepared. The NEXAFS supports the raft model with high humidity causing the polymer to rewet the drug surface to a more homogeneous overlayer which is still thick enough to obscure most of the drug signal (Figure 4.27). The use of synchrotron XPS would allow spectra to be measured at a series of different sampling depths and would confirm

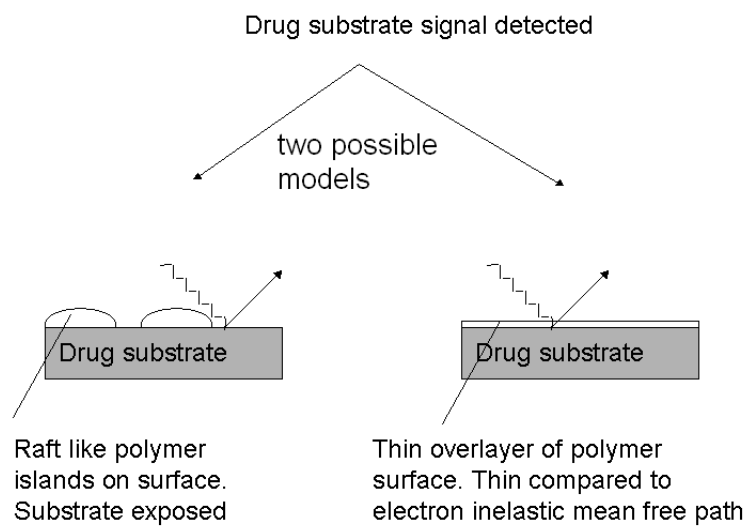


Fig. 4.26: Possible models for surface polymer present on drug. The presence of signal from the drug implies a partially exposed surface or a thin overlayer.

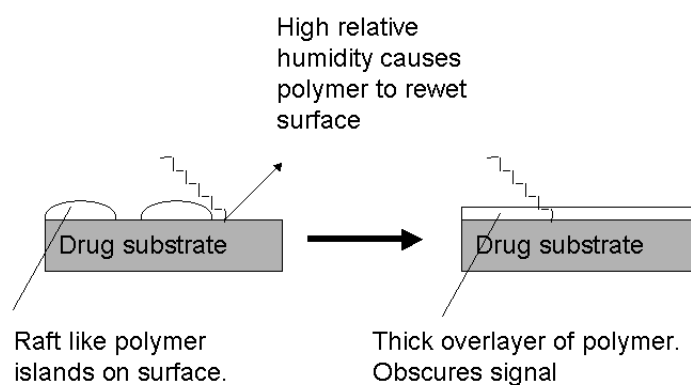


Fig. 4.27: Effects of high relative humidity on polymer coating. A suppression of the drug signal after dosing suggests a reforming or redistributing of the coating which obscures the substrate more in both coverage and thickness.

the raft model.

As with the previous drug, SR 142801, we can detect the coating material and water absorbed by the coating. While the amount of coating material might influence the dissolution rate of the formulation it is more likely that the amount of adsorbed water is a better and more direct indicator of improvements in dissolution rate. Interestingly the water signal in the first NEXAFS drug spectra (SR 142801) appears to be gas phase water absorbed on the surface but the additional features in the second drug oxygen NEXAFS spectrum (SSR 180575) appear to be closer to liquid water spectra^{113–115}. This is most likely from the greater surfactant levels used on the SSR 180575 which allow more H₂O to be adsorbed and perhaps to interact with neighbours to produce a more liquid-water like spectra.

It is planned that if the techniques used here are successful then they will be applied to a nanoparticle (particle size approximately 100 nm) formulation of the drug.

4.10 Conclusions

With the rising number of poorly water soluble drugs, formulation technology is getting more and more important. NEXAFS and XPS not only provide insight into how the polymer is sited on the drug substrate, but it may be possible that it could become a common screening tool for looking at large ranges of formulations. Many samples could be prepared and measured using laboratory XPS and the most promising could also be studied with the more expensive NEXAFS technique. This would allow the elimination of unsuitable compounds before proceeding to conventional trials where the pharmacokinetics and dissolution can be more directly studied. It is also of considerable use in obtaining a greater physical understanding of the drug formulation surface.

NEXAFS shows considerable promise as a method for investigating pharmaceutical formulations. The results show that the technique can be successfully applied to very complex systems to produce useful measurements without needing a complete understanding of the whole electronic structure. The ability to make surface measurements without having the samples under ultra-high vacuum is very beneficial for measuring pharmaceutical compounds which may dry out. The use of low vacuum also means samples can be changed far more quickly than if it were true UHV. In principle it would be possible to cool a sample down and dose water to take measurements of the effects of humidity on samples without needing near atmospheric pressures, which would open a further range of useful

experiments with NEXAFS.

There is also a reluctance to start using previously unused polymers as they require the same stringent testing as the active pharmaceutical ingredient. With this method it might be possible to discover an optimal formulation with a new material and have a reasonable expectation of success. As opposed to testing a new polymer without having any knowledge as to if it would be more useful than an already widely used and approved one.

Chapter 5

Crystalline and Amorphous Drug Surfaces

5.1 Introduction

The characterisation of crystallinity and crystalline defects in pharmaceutical compounds is of considerable importance due to the effects on bioavailability and possibly toxicity of the active pharmaceutical ingredient (API)¹¹⁹. It can also affect physical properties such as particle size, and mechanical strength which can have an effect on industrial processing such as forming into tablets^{120;121}. Intellectual property issues also necessitate a detailed study of the crystalline forms of any pharmaceutical product as it is desirable to have every crystal form of the drug patented.

Dynamic Vapour Sorption (DVS), Differential Scanning Calorimetry (DSC) and X-ray powder diffraction are well established for studying

crystallinity (XRPD or PXD)^{119;122} and solid-state nuclear magnetic resonance spectroscopy (SS-NMR) has been shown to be complementary to this¹²³. XRPD and SS-NMR are bulk techniques which make them unsuited for measuring changes in the surface region. The surface is of particular importance as it is the surface properties which will initially determine how the drug interacts with the media in the stomach. For example the high internal energy of the amorphous state can lead to higher instantaneous solubility making it better suited to producing a higher uptake^{119;122}, but it also means the substance is more susceptible to environmental variation. Particularly excess heat and/or humidity¹²² can cause undesired recrystallisation and polymorphism as the substance reaches a more thermodynamically stable state.

Mechanical processes such as micronisation¹²¹ can also cause also bulk and/or surface changes. It is important to know how much of the drug system is crystalline or amorphous because an excess of amorphous content where crystalline is expected could lead to overdosing and vice versa. Surface amorphous content is especially important as it is thought to lead bulk recrystallisation^{124;125}. Amorphous content can also affect other analytical testing by adsorbing unknown and variable amounts of moisture.

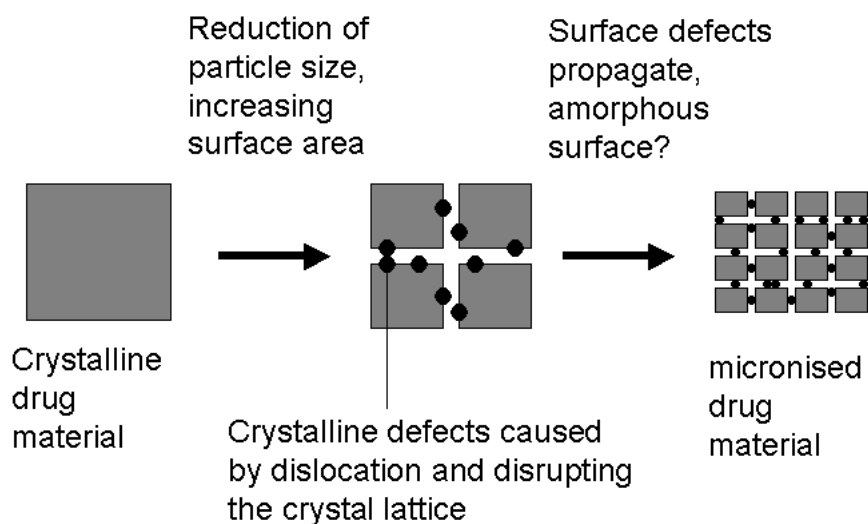


Fig. 5.1: Defects at a newly formed surface. During micronisation the surface area is increased by breaking up the material and hence the crystal lattice causing defects. The proportion of the surface with defects increases with the micronisation. It is thought this could lead to amorphous surfaces.

Surface changes associated with micronisation are introduced by the dislocation of the crystal structure caused by the breaking up of the particle and hence the crystal structure. Defects are introduced at the newly formed surface and any bulk changes can propagate defects to the surface (Figure 5.1). It is suggested by many workers that micronisation induces an amorphous or partially amorphous surface, which is a potential problem for many formulations and characterisation techniques. As such, characterisation of amorphous content is an active area of research^{121;123;126}. The level and distribution of amorphous content on the surface is also important and researchers have been successful in using phase contrast AFM to image differences between crystalline and amorphous areas and apply this

to monitoring differences between production batches¹²⁷⁻¹³⁰.

Sections of this work have been presented at XAFS XIII (X-ray Absorption Fine Structure) and have been published¹⁰⁹.

5.2 SR 49059

SR 49059 (Figure 5.2) is a vasopressin 1a receptor antagonist. Vasopressin is used by the body to regulate the excretion of water and salts from the blood stream by the kidneys. Vasopressin antagonists can be used to regulate blood pressure and they are potential treatments for a wide variety of blood pressure related complaints from heart disease¹³¹ to early onset labour related complications.

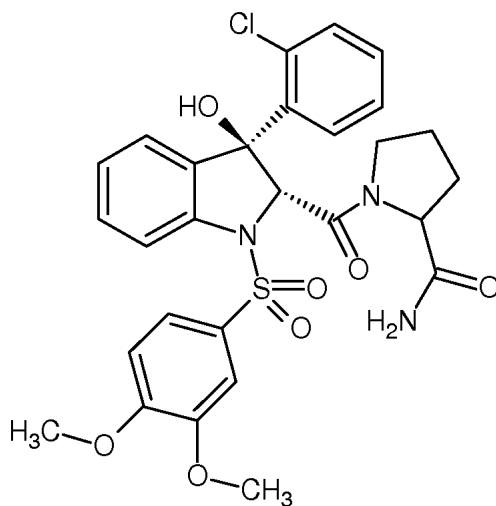


Fig. 5.2: SR 49059 molecular structure

While the drug is no longer in clinical development, problems that arose showed some of the potential for NEXAFS. The drug was supposed to be administered as micronised crystalline particles in an oral formulation but there were problems with the product relating to crystalline defects and amorphous content. The objective of this project was to try and determine

what was happening at the surface with respect to amorphous and crystalline content.

SR 49059 preparations have previously been studied with Solid-State Nuclear Magnetic Resonance (SS-NMR), Dynamic Vapour Sorption (DVS), Differential Scanning Calorimetry (DSC) and X-ray Powder Diffraction (XRPD) to try and characterise and quantify both the level of non-crystalline material in the compound and crystal defects¹²³. The crystalline defects are proposed to only have a small effect on crystal lattice parameters, meaning they will give a correspondingly small effect on XRPD patterns but combined with solid state NMR it has been shown it is possible to quantify the amorphous content and the defects. While XRPD and NMR are established techniques for bulk studies of crystallinity, they are unsuited for surface characterisation so other techniques such as X-ray Photoelectron Spectroscopy (XPS) and X-ray Absorption Fine Structure (XAS) were used to study the surface crystallinity. Three samples of the drug were provided, all produced by the same synthetic route; a crystalline batch, an amorphous batch and a micronised batch produced from the crystalline material.

5.3 X-ray Photoelectron Spectroscopy (XPS)

X-ray photoelectron spectra were measured using a Kratos Axis Ultra machine with a monochromated Al-K α source, hybrid (electrostatic and magnetic) lens system and charge neutralisation. A pass energy of 80 eV was used for surveys and 20 eV for high resolution scans. Survey scan was measured from 1100 to -5 eV with 0.5 eV steps and 200 ms dwell time. High resolution scans were taken around the peak of interest with 0.1 eV steps 300 ms dwell times and 3 (carbon and oxygen), 5 (nitrogen and valence band) or 10 (chlorine) repeats. Spectra were exported as VAMAS files. Analysis was carried out using the commercial CasaXPS software. Repeated measurements were made of a single sample to check for radiation damage. No change of spectra over time was observed, so either damage did not occur or any damage occurred very quickly on the timescale of a single scan.

5.3.1 Oxygen 1s

The oxygen 1s spectra (Figure 5.3) show little change between amorphous and crystalline samples. The fitting was attempted by assigning peaks to the different oxygen groups in the sample. The peak envelopes are the same and no peaks shift. The micronised batch shows a shifted peak envelope which could be from the shift of a single peak or shifts of all of them. One proposed reason for seeing a difference in the micronised batch but not the amorphous or crystalline is that the change arises from charging effects from the much smaller particle size of the micronised batch.

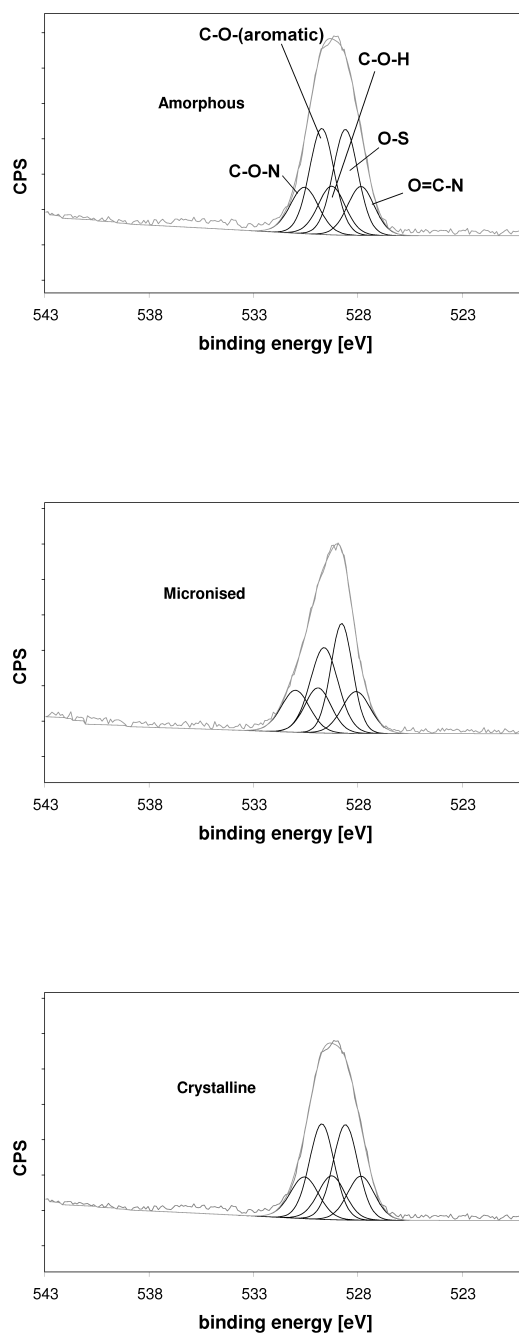


Fig. 5.3: Oxygen 1s XP Spectra for SR 49059.

5.3.2 Carbon 1s

The carbon spectra (Figure 5.4) show differences between the samples restricted to the peak at 286.2 eV assigned to C-O and the C-C peak (Table 5.1). The proposed reason for this is an orientation effect along the lines of Figure 5.9. The surface termination of the crystal structure could, in the crystalline form, result in relatively buried C-O bonds as there are 2 (of 3) C-O bonds close together at one end of the molecule. A random surface orientation such as in the amorphous batch causes more of the C-O bonds to be closer to the surface which results in observing an enrichment of the C-O peak.

Functional group	C-C	C-O	C=O	shake-off
Amorphous	41	41	10	8
Micronised	49	34	9	8
Crystalline	54	29	10	7

Table 5.1: Carbon peak assignments for SR 49059 samples

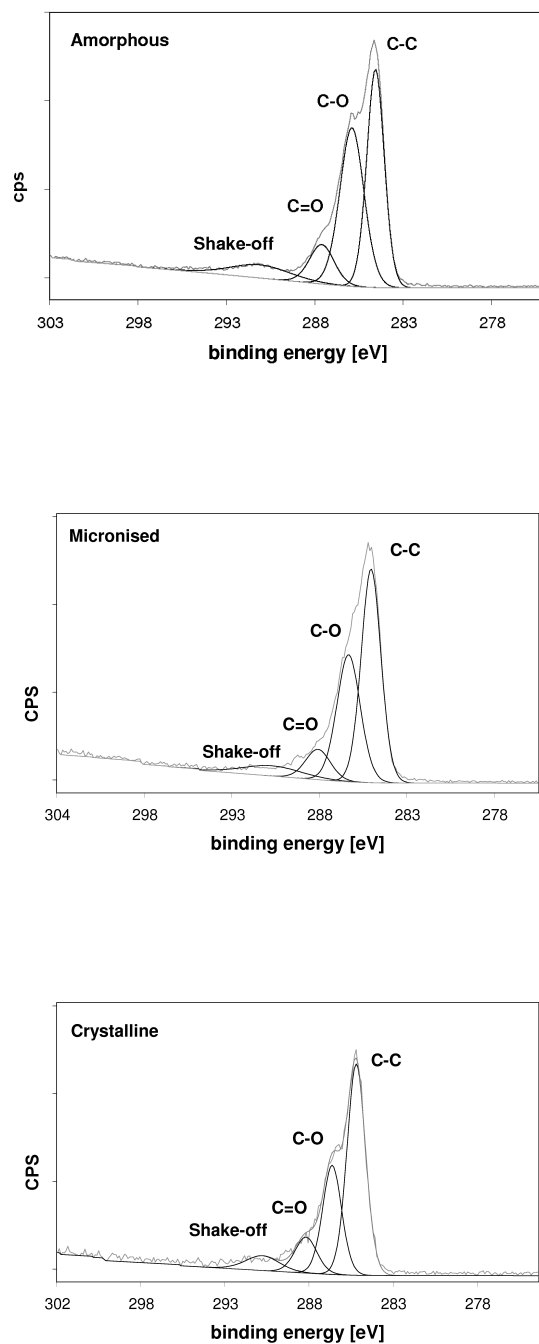


Fig. 5.4: Carbon 1s XP Spectra for SR 49059. Showing the differences between the C-O peaks for the amorphous, micronised and crystalline.

5.4 Near Edge X-ray Absorption Fine Structure (NEXAFS)

Near Edge X-ray Absorption Fine Structure (NEXAFS) spectra were measured on the 6.1 multipole wiggler soft X-ray beamline. The set up was only capable of measuring total electron yield (surface) spectra at the carbon K-edge. Spectra were measured over the range 270 eV - 350 eV, with 0.1 eV energy steps and a measurement time of 0.5 s per point. Spectra were first measured in vacuum and then exposed to 100% relative humidity by simultaneously dosing water vapour into the system while cooling the sample holder via a nitrogen gas stream, and then measured in vacuum again. Repeated measurements were made of a single sample to check for radiation damage, no change of spectra over time was observed, so either damage did not occur or any damage occurred very quickly on the timescale of a single scan. Further spectra at the oxygen and nitrogen K-edge were measured on the 5U.1 undulator soft X-ray beamline. Data have been normalised to an I_0 mesh.

5.4.1 Carbon K-edge

Carbon K-edge spectra (Figure 5.5) show clear differences between the amorphous and crystalline batches. The π^* resonance at 284 eV is much larger in the amorphous sample and allows amorphous content to be distinguished from crystalline. There is also a smaller resonance at 289 eV

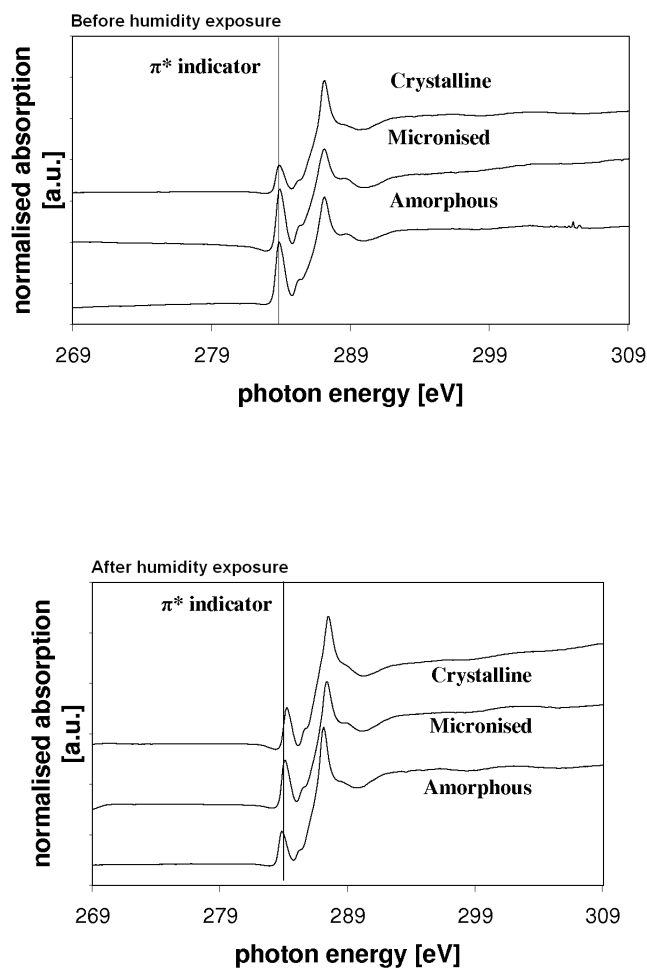


Fig. 5.5: Carbon K-edge NEXAFS spectra SR 49059 before and after exposure to 100% relative humidity. The pre edge feature is more prominent in the amorphous compared to the crystalline and this is also the case with the micronised spectra. This suggests that the micronised surface is completely amorphous. Exposure to high relative humidity causes a phase change which turns both the micronised and amorphous samples crystalline.

which appears to be more pronounced in the amorphous sample. The largest π^* resonance at 287 eV is the same in all the samples. Interestingly they also show that the micronised sample has what appears to be a completely amorphous surface layer. The resonances at 284 eV and 289 eV are the same as in the amorphous sample and difference spectra relative to the crystalline spectra confirm they are the same.

Previous studies of the drug¹²³ have shown that when exposed to high relative humidity the and in the presence of crystalline polymorph II material the amorphous drug compound gains sufficient mobility to reach a more thermodynamically stable state and recrystallise into polymorph II. After dosing water vapour into the chamber and cooling to take the relative humidity up to 100% both the amorphous and micronised spectra resembled the pure crystalline drug spectrum, indicating that they had undergone the predicted humidity induced phase transition. Difference spectra showed the recrystallised form was the same as the crystalline batch.

5.4.2 Oxygen K-edge

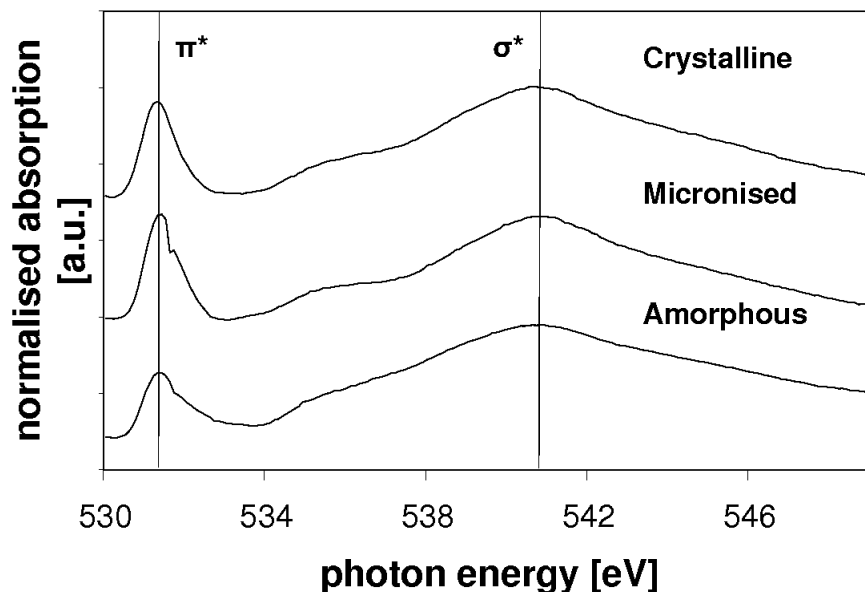


Fig. 5.6: Oxygen K-edge NEXAFS spectra SR 49059. At the oxygen edge the micronised batch is more of an intermediate between amorphous and crystalline suggesting it is partially amorphous. The discrepancy between this and the carbon edge can be explained by the difference in penetration depth.

Spectra at the oxygen K-edge (Figure 5.6) show less pronounced differences between the crystalline and amorphous samples than at the carbon edge. The amorphous sample π^* resonance shows a long tail or shoulder on the high energy side which is not present in the crystalline batch. This shoulder is partially present in the micronised batch. It appears to be the case that at the oxygen edge the micronised batch shows intermediate behavior between the crystalline and amorphous batches. Using the athena program in the IFFEFIT package it was possible to synthesise a micronised spectrum

from the crystalline and amorphous and the micronised batch appeared to be approximately 25% amorphous and 75% crystalline.

5.5 Transmission Electron Microscopy (TEM)

The environmental scanning electron microscope (ESEM) showed no differences between the amorphous and crystalline batches of the drug and even humidity changes to cause recrystallisation made no difference. The resolution was insufficient to resolve any detail in the micronised batch.

The TEM pictures in Figure 5.7 of the micronised batch at the highest magnification can easily resolve the micronised particles. Diffraction patterns of a thin section shown in Figure 5.8 however, show no evidence of crystallinity, meaning it is either too thick or it is surrounded by amorphous material.

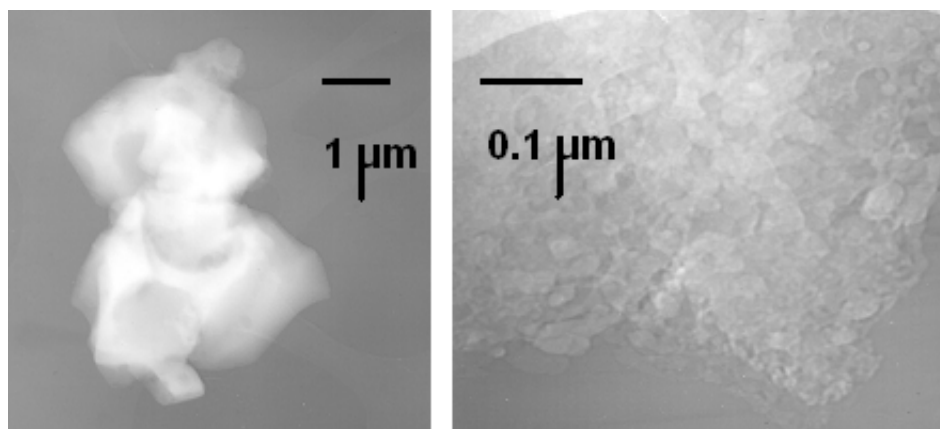


Fig. 5.7: Transmission electron micrograph of micronised drug at 20000x (left) and an edge section at 220000x magnification (right).

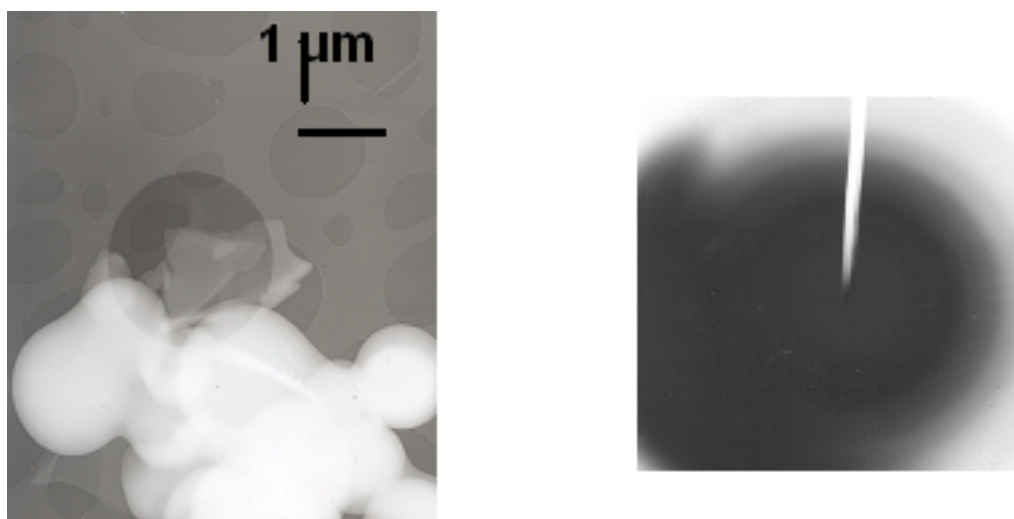


Fig. 5.8: A thin section of the micronised drug (left) and the diffraction pattern from the shaded area (right). The ring as opposed to spots in the diffraction pattern suggest that it is not crystalline.

5.6 Discussion

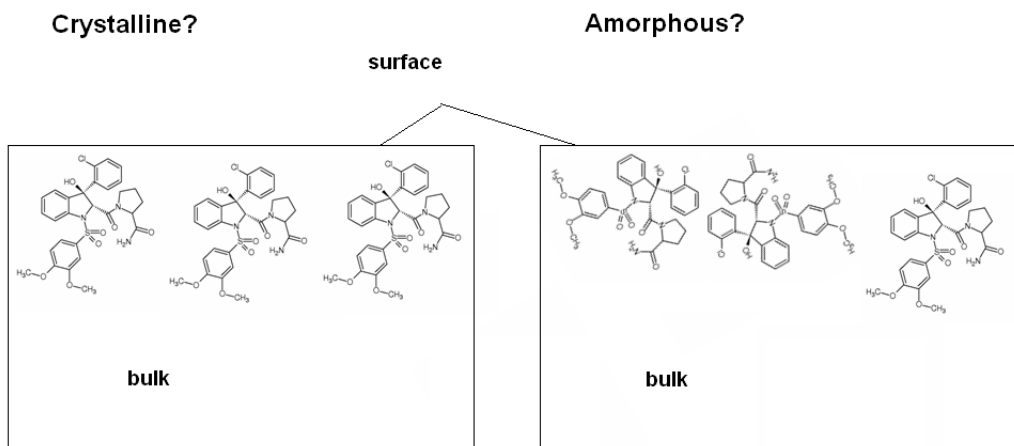


Fig. 5.9: Suggestion for surface orientation effects. The more dense collection of C-O bonds are buried relative to other species by the orientation of the crystal structure. Causing a suppression in the C-O peak for the crystalline material relative to the amorphous batch.

The results from XPS show a possible difference in the surface allowing us to distinguish between crystalline and amorphous surfaces. The relative abundances of the C-O and peaks seem to suggest something along the lines of Figure 5.9 where C-O are embedded below the surface in the crystalline form and randomised in the amorphous.

The NEXAFS results show a very clear distinction between the amorphous and crystalline batches at the carbon edge and it is still possible to distinguish between them at the oxygen edge. It also shows the micronised batch has an amorphous surface. The differences between the electron yield sampling depths of the oxygen and carbon edges (due to different electron energies) put an upper limit on the depth of the amorphous

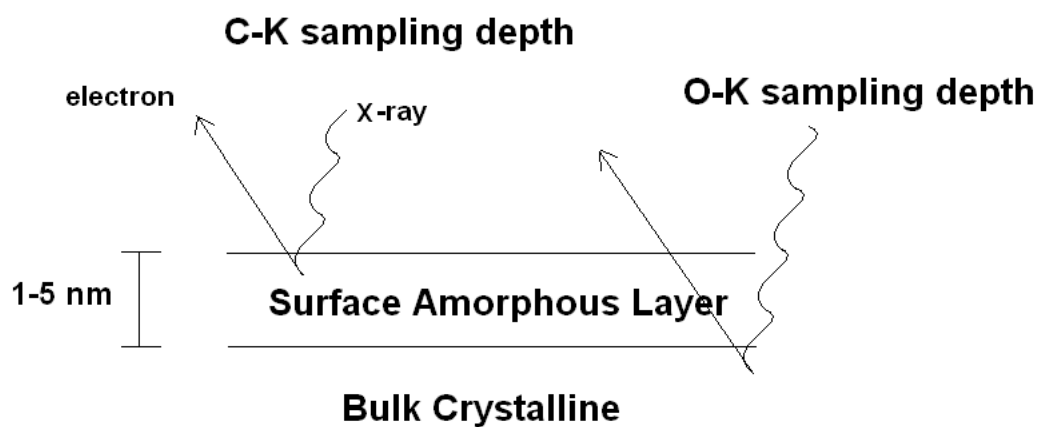


Fig. 5.10: Model for surface profile of micronised drug. Explaining why the carbon K-edge NEXAFS data makes the surface seem entirely amorphous but the oxygen K-edge shows a mixture. The difference in sampling depth means that this could be explained by an amorphous surface layer over a crystalline bulk no more than a few nm thick.

region of the order of 1-5 nm as shown in Figure 5.10.

5.7 Indomethacin

Indomethacin (Figure 5.11) is a non-steroidal anti-inflammatory drug (NSAID) used for treating fever, pain, stiffness and swelling. The drug is no longer under patent protection and is manufactured as a generic pharmaceutical. It has previously been studied in terms of crystalline vs amorphous behavior^{125;132} using Differential Scanning Calorimetry (DSC). Some workers have found an ultra thin nano-scale coating of gold can inhibit the recrystallisation of amorphous indomethacin¹²⁴ and a similar effect has been seen with polyvinylpyrrolidone (PVP)¹²⁵ suggesting surface amorphous content plays an important role.

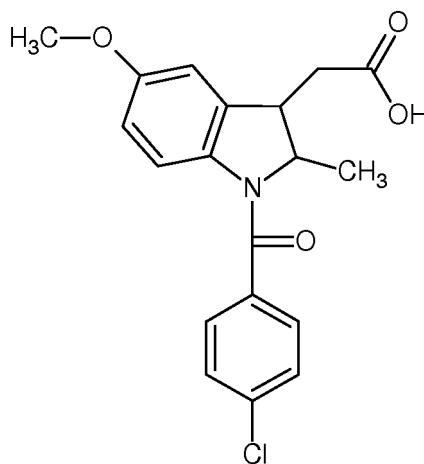


Fig. 5.11: Indomethacin molecular structure

Amorphous and crystalline batches of the drug were provided by Astra-Zeneca. Also included were two micronised batches one from (comparatively)

high pressure micronisation and one from low pressure micronisation. The aim was, as in the case of SR 49059, to determine if differences could be picked up between amorphous and crystalline batches and in what state was the surface of the micronised batches. The amorphous and micronised batches were sealed under an inert atmosphere (nitrogen), like SR 49059, excess humidity can caused a recrystallisation, but with indomethacin it can happen under ambient conditions.

5.8 Near Edge X-ray Absorption Fine Structure (NEXAFS)

Near Edge X-ray Absorption Fine Structure (NEXAFS) spectra were measured on the 1.1 bending magnet station of the SRS using total electron yield and a cell setup based on those in Chapter 3. Spectra were measured over the range 270 eV - 350 eV for the carbon K- edge, with 0.1 eV energy steps and a measurement time of 0.5 s per point, 395 eV - 425 eV for nitrogen and 515 eV - 550 eV for oxygen K-edges. Repeated measurements were made of a single sample to check for radiation damage, but no change of spectra over time was observed.

Due to the low flux, low concentration and beamline contamination nitrogen and oxygen K-edge spectra were of a very low quality. Measurements without a contamination barrier (boron window, see Chapter 3) showed no differences and sputter cleaning of the I_0 mesh and monochromator also made no noticeable improvement.

5.8.1 Carbon K-edge

Carbon K-edge spectra of the amorphous and crystalline indomethacin and the two different micronised batches were measured (Figure 5.12). Serendipitously additional spectra of the amorphous compound were also measured after it had been exposed to ambient humidity and temperature

(Figure 5.13).

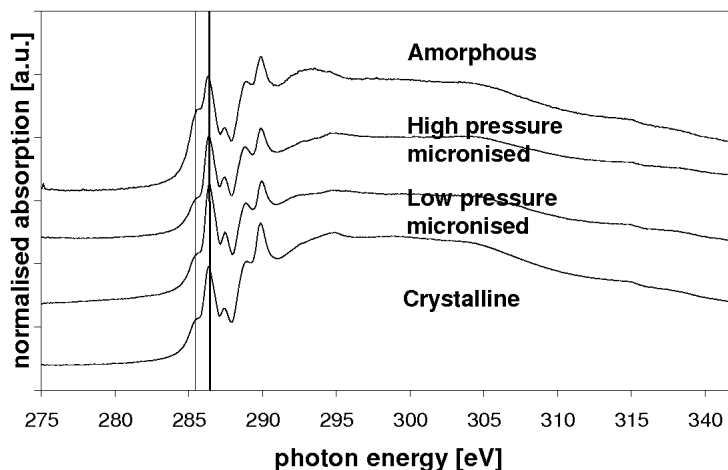


Fig. 5.12: Carbon K-edge NEXAFS spectra of indomethacin samples. Amorphous and crystalline spectra show some differences.

The spectra feature a strong pre-edge π^* resonance at 286 eV which has a shoulder on the low energy side. There is a minor pre-edge peak at 287 eV and another peak at 290 eV with an edge/shoulder at 289 eV. The amorphous sample has a much more pronounced shoulder to the 286 eV peak and the 286 eV peak is higher relative to the 290 eV peak when compared to the crystalline sample, confirmed with difference spectra. Interestingly the two micronised samples show no difference between them. They also show a small pre-edge shoulder at 286 eV similar to the crystalline sample but the 286 eV peak is high compared to the 290 eV peak like the amorphous sample. Because of the considerable contamination on the

beamline assigning spectral features is difficult and they can only be used comparatively in this case. Attempts to normalise the data to a sputter cleaned gold reference spectra did not show any improvement.

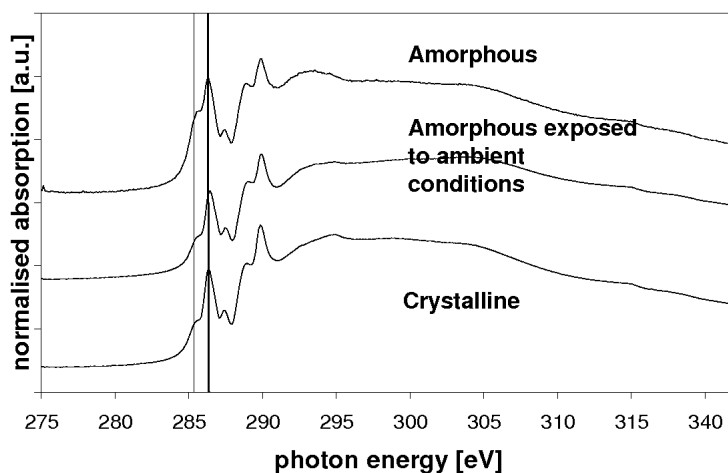


Fig. 5.13: Carbon K-edge NEXAFS spectra of indomethacin samples. After exposure to ambient conditions the amorphous batch started to look like a crystalline spectra, reminiscent of the water dosing experiment with the previous drug (SR 49059).

The amorphous batch of indomethacin was known to be very sensitive to humidity, much more so than SR 49059 so a batch was left open to ambient conditions at Daresbury Laboratory. As with the SR 49059 the amorphous sample has completely recrystallised and shows a crystalline surface.

5.9 Discussion

As with the SR 49059, NEXAFS is capable of distinguishing between amorphous and crystalline batches of indomethacin at the surface, and again it is a larger pre-edge associated with the amorphous sample. Again it was possible to observe a recrystallisation with the exposed amorphous drug becoming more like the crystalline batch. The micronised batches are a more complicated story for indomethacin as they appear to share features from both the amorphous and crystalline. The simple explanation for this would be that the micronised surface is part amorphous and part crystalline but in this case the spectrum should be intermediate rather than one bit from one spectra and one from another. It is possible that micronisation induces defects which allow the indomethacin to be in a different crystal form as the drug is known to exhibit polymorphism. Another possibility is that the micronised particles show different charging effects which may deform the spectra, similar to what can be seen compared whole and ground tablet forms of a drug (See Chapter 7).

5.10 Conclusions

These two examples show that it is possible to use NEXAFS electron yield to distinguish between different forms of a drug substance and that this can be applied to unknown (e.g. micronised) samples. We have also shown it is possible to recreate humidity induced phase transitions and record them. The most important aspect of this work is that it allows detection of amorphous content at very low levels, such as a few nm overlayer which would be beyond the capability of bulk techniques.

The presence of an amorphous surface layer makes controlling the dosage and release rate much harder. The amorphous overlayer would increase bioavailability but as shown by the NEXAFS, humid conditions could cause it to recrystallise lowering the bioavailability without warning, hence making it unsuitable for a product in its current state. While using this technique may not aid development of new drug compounds directly, it could be of use in determining which compounds should stop being developed due to micronisation problems. It could also be useful in determining if conditioning treatments, such as exposing an API to high relative humidity, are successful in producing uniform surface properties.

Chapter 6

Suspension Stability

6.1 Introduction

Generic compounds, those which no longer have patent protection, are often used in a wide variety of formulations; tablets, powders, and solutions. The commercial pressure for optimising processes and ingredients is even greater than for new drugs due to the lack of patent protection and the resultant higher level of competition in the generics market. Oral suspensions of a drug often require soluble additives to ensure the active pharmaceutical ingredient (API) remains in suspension. Oral suspensions are popular in pediatric medicine as they can be flavoured to provide a more pleasant delivery than a tablet formulation. This work has been conducted by the author and a masters student, Tom Lonsdale. The stability data, ESEM micrographs and XPS data have been submitted as part of a masters thesis and are included here for completeness. The 2-D correlation spectroscopy analysis is new.

6.2 Ibuprofen

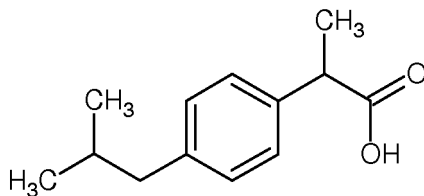


Fig. 6.1: Ibuprofen Molecular Structure

Ibuprofen (Figure 6.1) is a generic non-steroidal anti-inflammatory drug (NSAID) used for treating fever, pain, stiffness and swelling. The drug has been widely available for sufficient time to understand its side effects in the population at large: so called phase IV trials, and is currently available as an over-the-counter medicine. Its popularity has led to its inclusion in a number of products and formulations^{133;134}. The samples studied here are variations on the BASF standard formulation for an oral suspension of ibuprofen.

Samples of pharmaceutical grade ibuprofen were supplied by BASF and common pharmaceutical polymers by Sigma-Aldrich. Samples were prepared by making an aqueous solution by weight (5%, 10%, 15% and 20%) of a given polymer (PEG 3350, poloxamer 188, poloxamer 388, PVP-25 and PVP-50) and then placing 4%(wt) of Ibuprofen in the solution to create a suspension. Additionally for XPS, NEXAFS and ESEM, solid samples were produced by filtering this suspension to leave a powder.

6.3 Stability Tests

A stability test was used to determine how effective each formulation was at keeping the drug in suspension over a short period of time such as that from shaking a bottle to administering. Stability tests are also used in industry for long term testing to determine shelf lives for products, and it can take years for an experiment to be concluded.

A schematic of the test principle is included in Figure 6.2. It was chosen as it is as standard test in industry for determining stability. As the polymer solutions were transparent and the ibuprofen was opaque, a simple measure of how much of the drug was in suspension was obtained by how much light was transmitted; the higher the transmission, the worse the formulation was at keeping the drug in suspension. The data was measured using a probe which was inserted into the suspension and was measured at constant depths and path lengths. The data were presented in Tom Lonsdale's Master thesis¹³⁵.

The transmission data (Figure 6.3) are not normalised, but due to all the samples containing the same concentration of drug they all have the same maximum value. The data show that at low (5% (wt)) polymer concentrations the high chain length poloxamer 388 was the best at keeping the drug in suspension (45% after 70 min), followed by the shorter chain length poloxamer 188 (~55% after 70 min), then followed by the other polymers which were all roughly the same (~80% after 70 min).

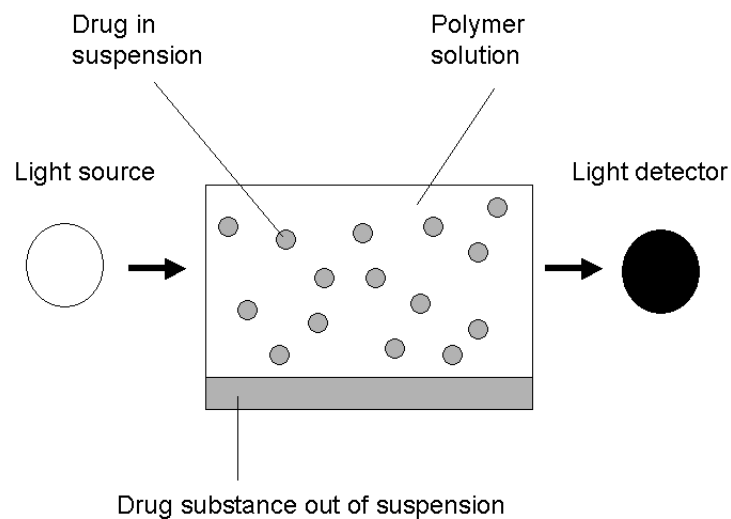


Fig. 6.2: Schematic showing the principal of transmission based suspension stability tests. The opacity of the suspension gives the fraction of drug still in suspension and measures which formulation performs the best.

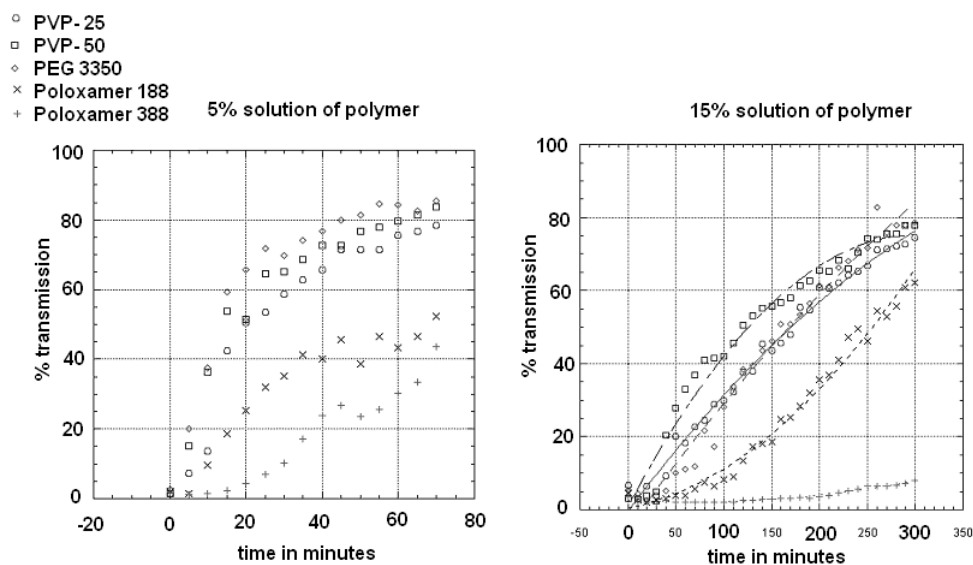


Fig. 6.3: Suspension stability data. All 15% polymer formulations are better than their respective 5% polymer formulations. They tend towards the same maximum as they have the same drug loading. As far as polymers go poloxamer 388 was the best, then poloxamer 188 then the rest.

At higher concentrations (15% (wt)) all the samples performed better than those at low concentration (5% (wt)) and the order of the different polymers was repeated, with poloxamer 388 ($\sim 10\%$ after 300 min) the best, followed by poloxamer 188 ($\sim 65\%$ after 300 min), followed by the rest ($\sim 80\%$ after 300 min). Sedimentation due to gravity is the most probable cause of the micron sized, insoluble ibuprofen coming out of suspension.

6.4 X-ray Photoelectron Spectroscopy (XPS)

X-ray photoelectron spectra were measured using a Kratos Axis Ultra machine with a monochromated Al-K α source, hybrid (electrostatic and magnetic) lens system and charge neutralisation. A pass energy of 80 eV was used for surveys and 20 eV for high resolution scans. Survey scans were measured from 1100 to -5 eV with 0.5 eV steps and 200 ms dwell time. High resolution scans were taken around the peak of interest with 0.1 eV steps 300 ms dwell times and 3 (carbon and oxygen) or 5 (nitrogen and valence band) repeats. Analysis was carried out using the commercial CasaXPS software. Due to the much higher levels of hygroscopic coating polymer used compared to those in Chapter 4 a much longer pumping time was required due to outgassing, in the order of weeks. While the samples were intended as suspensions it was hoped that the solid samples would still provide some insight into the formulations. It is possible that dehydration due to vacuum changes the samples but it is still possible to observe features which relate to how well they performed in the stability test.

6.4.1 Carbon 1s

The peaks present in the carbon spectra shown in Figure 6.4 (Table 6.1) are assigned as follows: The 285 eV peak is from C-C bonds present in all the coatings, the drug and present as contamination. The 286.5 eV peak is from C-O bonds in the coating polymers but not in the drug. Finally at 288.9 eV is the COOH functional group coming only from the drug.

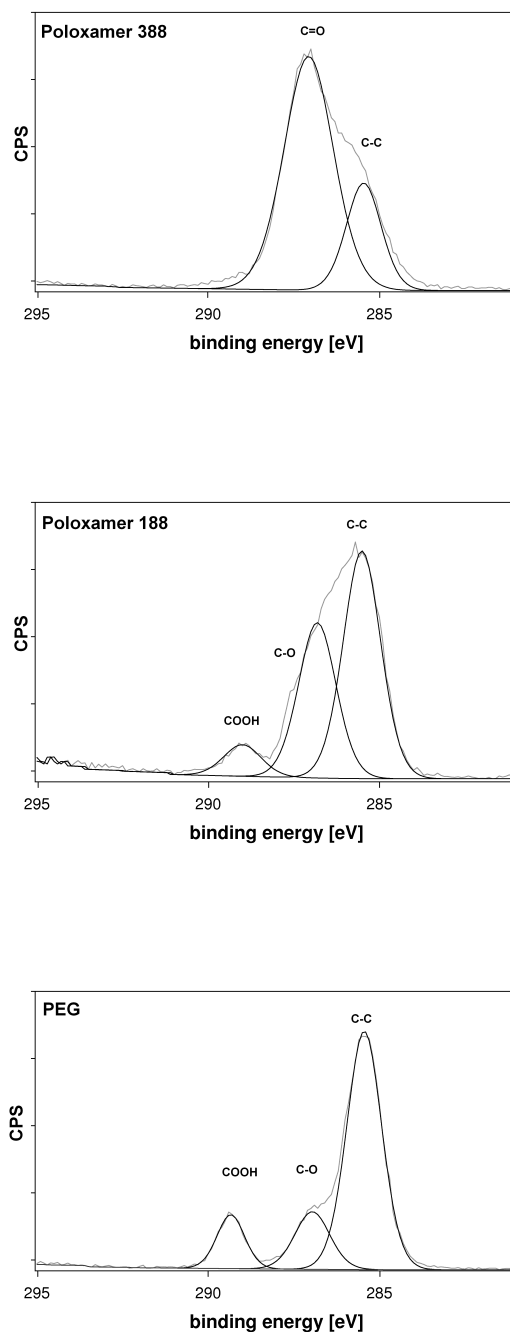


Fig. 6.4: Carbon 1s XP spectra for 15%(wt) poloxamer 388, 188 and PEG respectively. The much higher C-O peak in the poloxamer 388 and slightly higher peak in the poloxamer 188 match the order of how well each formulation performed in stability tests.

Functional group	C-C	C-O	COOH
Poloxamer 388	25	70	-
Poloxamer 188	57	36	7
PEG	70	17	13

Table 6.1: Carbon peak assignments for polymer coated ibuprofen

What appears to be happening is that the PEG, as the poorest performing polymer, has coated the ibuprofen the least effectively as evident by the larger COOH peak. As the coating polymer improves, the peak is less pronounced (poloxamer 188) and then gone altogether (poloxamer 388). The same occurs in reverse with the peak at 286.5 eV, which is from C-O bonds and is assumed to come from the coating. This suggests the reason for the better performance with the poloxamers is that there is physically more of it on the surface and it also obscures the less soluble drug material below more effectively.

6.4.2 Oxygen 1s

The oxygen spectra in Figure 6.5 (Table 6.2) show 2 peaks which are thought to be polymer on the low energy side and H₂O on the high energy side. With the PEG the contribution from the polymer is more dominant but as we move up through the polymers the poloxamer 188 shows the water peak to be higher than the coating peak. With the poloxamer 388 the water peak totally dominates the coating peak. This makes sense if the formulation which is more effective at keeping the drug in suspension is that way because it is more hydrophilic than the others. It would follow that this

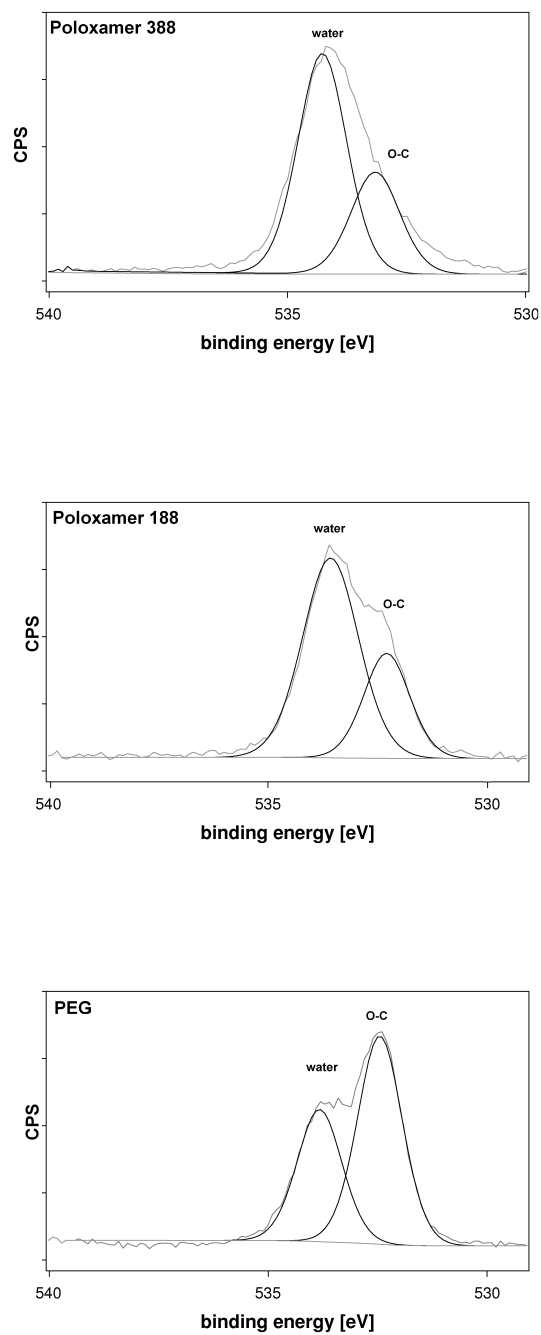


Fig. 6.5: Oxygen 1s XP spectra for 15%(wt) poloxamer 388, 188 and PEG respectively. The water peak is totally dominant for the poloxamer 388 and is still larger than the polymer peak for the poloxamer 188. This corresponds to the C-O peak in the carbon 1s data and the suspension data.

Functional group	Water	C-O
Poloxamer 388	70	30
Poloxamer 188	68	32
PEG	39	61

Table 6.2: Oxygen peak assignments for polymer coated ibuprofen

formulation should also be more effective at maintaining surface moisture under ultra-high vacuum conditions.

6.5 2-D correlation spectroscopy

High throughput methods first developed with biological and pharmaceutical screening and they have spread to many fields¹³⁶. With improvements in data collection, the time required for spectra measurements is reduced. This makes high throughput practical from an experimental point of view. This is not the sole requirement however, there is also a need to reduce and analyse the large amount of data which would be produced. This would allow high throughput type methodologies to be used to determine the optimum material type and quantity with further in-depth tests done as required. In the generics market it would provide a competitive advantage by allowing them to provide a better product. For new drug products it could be used to safely reduce the amount of formulation testing required by optimising the product before going to trials. The method which could be used here is to use small scale tests do determine which spectral features correspond to desired traits, such as a high C-O peak in C1 s spectra or high water peaks in O 1s. This would then be followed up with large datasets which can be studied to see which is the most suitable formulation for the desired spectral features.

2-D correlation spectroscopy is a powerful tool which allows easy identification of differences in large spectra groupings and is already well used in IR and NMR spectroscopy^{137;138}. A high throughput approach to something like formulation testing would find 2-D correlation spectroscopy invaluable. It allows simplification of complex spectra with overlapping peaks and also allows the order in which spectral features change to be

determined. 2-D correlation analysis allows us to project a stack of spectral data, varying with some perturbation, such as polymer concentration in our case, onto a grid from which additional information can be determined. The major drawback of correlation spectroscopy is the need for high quality spectra for the analysis.

Mathematically, the fundamentals of 2-D correlations spectroscopy are a 2-D spectrum, $X(\nu_1, \nu_2)$, which is the comparison of two spectra, ν_1 and ν_2 , with some external variable, t , between some period T_{min} and T_{max} ¹³⁷. They are related by:

$$X(\nu_1, \nu_2) = \langle \tilde{y}(\nu_1, t) \cdot \tilde{y}(\nu_2, t) \rangle, \quad (6.1)$$

Where $X(\nu_1, \nu_2)$ is the difference (or similarity) between the spectral variations $\tilde{y}(\nu, t)$ at ν_1 and ν_2 . $\langle \rangle$ is the cross correlation function which compares the dependence of the spectra with t ¹³⁷.

$X(\nu_1, \nu_2)$ is a complex number and is usually expressed with two orthogonal components as:

$$X(\nu_1, \nu_2) = \Phi(\nu_1, \nu_2) + i\Psi(\nu_1, \nu_2). \quad (6.2)$$

Φ and Ψ are known as the synchronous and asynchronous correlation intensities¹³⁷. In synchronous spectra along the diagonal line of $\nu_1 = \nu_2$ the intensity corresponds to differences between the spectra and is useful for determining at which frequencies changes occur. With asynchronous spectra

a positive correlation at a point (ν_1, ν_2) means that the change at ν_1 occurs (in t) before the change at ν_2 and vice versa.

Synchronous and asynchronous correlation spectra of XPS data for ibuprofen formulations were generated using the *2Dshige* software developed by Shigeaki Morita, Kwansei-Gakuin University, 2004-2005.

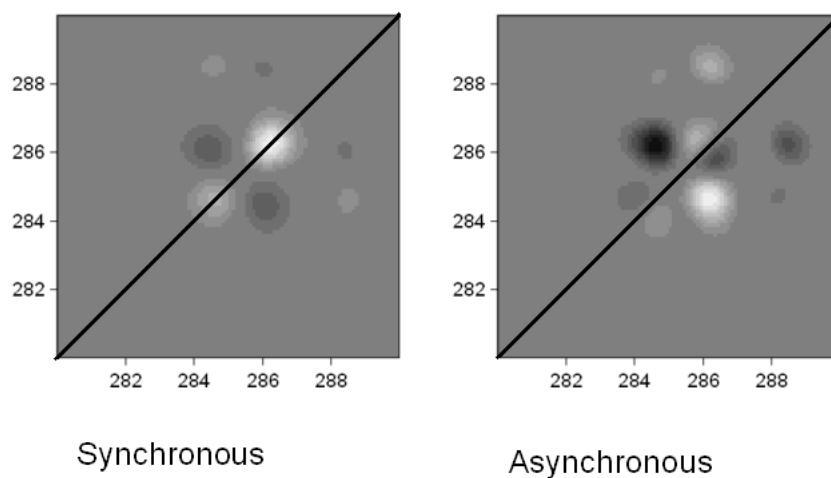


Fig. 6.6: 2-D correlation Spectra of poloxamer 188 formulations at (5%, 10%, 15% and 20%)

Figure 6.6 shows 2-D correlation plots from ibuprofen - poloxamer 188 formulations. The synchronous plot shows positive peaks at 285 and 286.5 eV which correspond to changes in the C-C and C-O peaks. The asynchronous plot show a positive correlation at (286.5 eV, 285 eV) which suggests that the C-O peak intensity changes before the C-C peak with respect to concentration of poloxamer 188. There are also smaller correlation peaks at (286 eV, 286.5 eV) and (286.5 eV, 290 eV) which are related to the COOH peak from the ibuprofen.

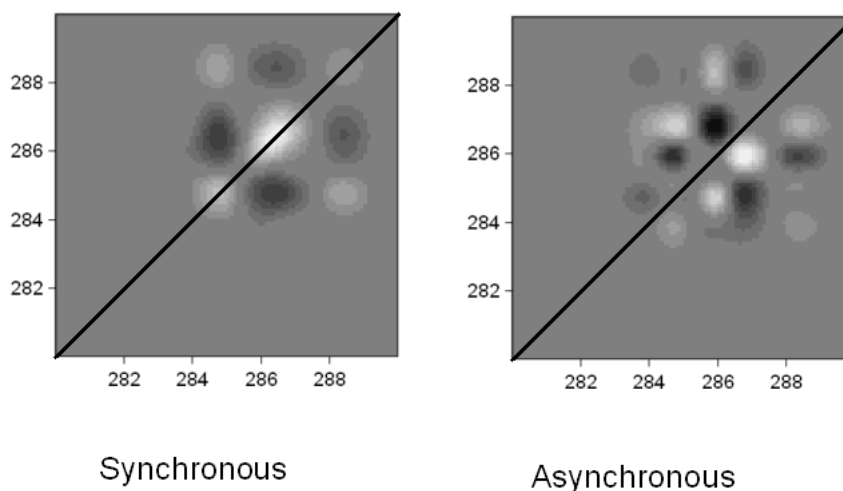


Fig. 6.7: 2-D correlation Spectra of poloxamer 388 formulations at (5%, 10%, 15% and 20%)

Figure 6.7 shows 2-D correlation plots from ibuprofen - poloxamer 388 formulations. The synchronous plot shows positive peaks at 285 eV and a long spread of correlation around 286-287 eV which corresponds to changes in the C-C and C-O peaks. As with the poloxamer 188 previously there is also a small change around 290 eV which corresponds to COOH from the drug being depleted. The asynchronous plot shows major positive correlation at (286 eV, 285 eV) from the C-O leading the C-C peak, (287 eV, 286 eV) from C-O shoulders and C-O (or possibly just a minor misalignment) and (285 eV, 287 eV) also from the C-C peak increase happening before the change in C-O. There are two smaller correlations at (286 eV, 290 eV) and (290 eV, 287 eV) which are from the C-O peak, from the coating diminishing the COOH peak from the drug. It seems likely that there may be a shift in the C-O peak explaining the big change in the synchronous spectrum and the presence of features at 286 eV and 287 eV in the asynchronous spectrum.

6.6 Discussion

The stability test was a relatively simple method of determining how well a formulation would work in terms of suspension stability. It provided a useful comparison and allowed us to determine the better formulations both in terms of coating level and polymer type.

The XPS data, interpreted in terms of suppression of the COOH peak from the drug and prominence of the C-O and water peaks from the coating, show a very strong agreement with the stability data. Having both carbon and oxygen data allows us to compare both the physical coating, in terms of how much of the drug surface is obscured, and the effectiveness of the coating, in terms of how much affinity it has for water. If we look at the poloxamer 388 it is a better coating both in terms of obscuring the drug and affinity for water.

The 2-D spectra confirm that for the poloxamer samples the data change at 285 eV and 286-287 eV which correspond to C-C and C-O respectively, and there is little change at 290 eV COOH. They suggest that the C-O peak tends to lead the reduction in COOH, the C-O peak also leads the C-C. This and the leading of the COOH could be explained by surfactant behaviour with the polymer preferentially adsorbing to the non-polar parts of the ibuprofen meaning some of the COOH is still exposed after the C-O

peak from the polymer has started to increase, explaining why the change in the C-O peak tends to occur first.

Care should be taken to not over interpret the 2-D spectra as there are only sets of only 4 spectra (5%, 10%, 15% and 20%) for each 2-D plot. 2-D correlation spectroscopy is of limited use for small datasets of simple spectra. It does, however, seem promising as a method of study for large data sets to try and determine the relevant changes. It would be of use in studying more complex drugs. Ibuprofen was chosen for ease of study because of having the COOH peaks as a drug only indicator.

6.7 Conclusions

XPS shows promise, although it is competing against the ease and cheapness of stability tests. XPS does provide supporting information to stability tests and with the adoption of high throughput methodologies such as 2-D correlation analysis it is possible in principle to use XPS to screen a large number of potential formulations.

Chapter 7

Additional Work

7.1 Introduction

The overall purpose of this work is to assess the value of soft X-ray surface science, X-ray Photoelectron Spectroscopy (XPS), Near Edge X-ray Absorption Fine Structure (NEXAFS) and X-ray PhotoElectron Emission Microscopy (XPEEM), to the pharmaceutical industry. In addition to the largely successful techniques and drug compounds shown previously there is also a body of less successful experimental techniques and unsuitable compounds which are included here for the sake of completeness, to illustrate some of the limitations and pitfalls encountered and as a potential basis for future work.

This section includes work on:

- Ink and pigments as a similar class of systems which preceded the drug work, both consisting of an active crystalline component (pigment or API) in an inactive polymer matrix.
- XPEEM data for SSR 180575 as shown in Chapter 4 to try and observe the rafts of polymer materials thought to be present, as well as work on some additional drugs.
- Two further drug compounds; a nanoparticle formulation and a melt extruded tablet studied with NEXAFS.
- Preliminary work with other techniques; *in situ* XPS and X-ray Excited Optical Luminescence (XEOL) an alternative method for X-ray Absorption Spectroscopy data acquisition.

7.2 Ink Films

Ink adhesion to polyefin films is an important industrial problem and polymer films have a long history of study by surface scientists^{5–9;139–141}. Ink formulation is considered by many to be more of an art than a science, with some formulations working on a particular customer's printing press but not on another, or working on only a particular grade of polypropylene¹⁴².

Various pretreatments are used to improve the printability of substrates including chemical (acid), flames and electric (corona) discharge. Corona treating is the most widespread for films as it the most practical for treating a vast amount of film right off the production line. Corona treatment works by adding chemical functionality in the form of -OH, -NH₂ and -COOH groups to the surface to improve wettability. It also binds low molecular weight materials, such as additives left over from the production process, to the surface which otherwise could cause a cohesive failure.

The ink itself can be considered an analogue of drug formulations. They both consist of an active crystalline component (pigment in the of case inks) in a polymer matrix. Ink formulations are very complex and consist of a pigment to provide the colour, a binder (usually a polymer) which supports the pigment and adheres to the substrate, a solvent to allow the binding to wet the surface and frequently other additives such as adhesion promoters or wax, to act as a protective coating.

Samples of three different inks on two different substrates were provided by SunChemicals and are listed in Table 7.1, which gave us examples of good and bad adhesion with the same ink. Samples 1,2 and 6 showed good adhesion and samples 3,4 and 5 showed poor adhesion as determined by the industry standard ‘tape test’ whereby adhesion quality is determined by how much ink is removed when a piece of adhesive tape is attached to the sample then peeled off.

Ink	Triton	Sigma	SunEster
Polypropylene substrate	Sample 1	Sample 2	Sample 3
Polyester substrate	Sample 4	Sample 5	Sample 6

Table 7.1: Ink samples

The ink has several components: the vehicle which is made up of solvent and binder which forms a matrix in which the ‘active ingredient’ copper phthalocyanine pigment is sited. Also present are additives. ‘Triton’ consists (in order of amounts present) of nitrocellulose, polyurethane, plasticiser and wax. ‘Sigma’ has nitrocellulose, polyurethane, plasticiser and wax and an adhesion promoter. ‘SunEster’ has nitrocellulose, plasticiser and polyurethane.

7.2.1 X-ray Photoelectron Spectroscopy (XPS)

X-ray photoelectron spectra were measured using a Kratos Axis Ultra machine with a monochromated Al-K α source, hybrid (electrostatic and magnetic) lens system and charge neutralisation. A pass energy of 80 eV

was used for surveys and 20 eV for high resolution scans. Survey scans were measured from 1100 to -5 eV with 0.5 eV steps and 200 ms dwell time. High resolution scans were taken around the peak of interest with 0.1 eV steps 300 ms dwell times and 3 (carbon and oxygen), 5 (nitrogen and valence band) or 10 (chlorine) repeats. Analysis was carried out using the commercial CasaXPS software. Sputtering was performed using an Ar⁺ ion gun with a filament current of ≤ 10 mA and a beam energy of ≤ 1 kV for cumulative periods of 10, 15, 30 and 45 seconds. Angle resolved XPS was measured at angles of 0°, 15°, 30°, 45°, 55°, 65°, 70° and 75° degrees relative to the electron analyser. Samples were also washed in acetone to remove most of the ink layers to study the substrate.

The carbon 1s envelope can be deconvolved but due to the large number of components present in the ink it is difficult to determine which part of the spectrum is from which component. The nitrogen 1s spectrum can be broken down into two areas: a large single peak at 406 eV, which is from the NO₂ groups in the nitrocellulose and two peaks around 400 eV from the pigment (copper phthalocyanine). Both are present at the surface. For these reasons the nitrogen 1s was considered the most interesting. Further measurements were made after the samples were washed with acetone to remove most of the ink layers. Samples showing 'good' adhesion also showed nitrocellulose still adhering to the substrate after solvent washing. Those samples with adhesion promoters also showed traces of the (titanium based) promoter at the substrate surface after washing.

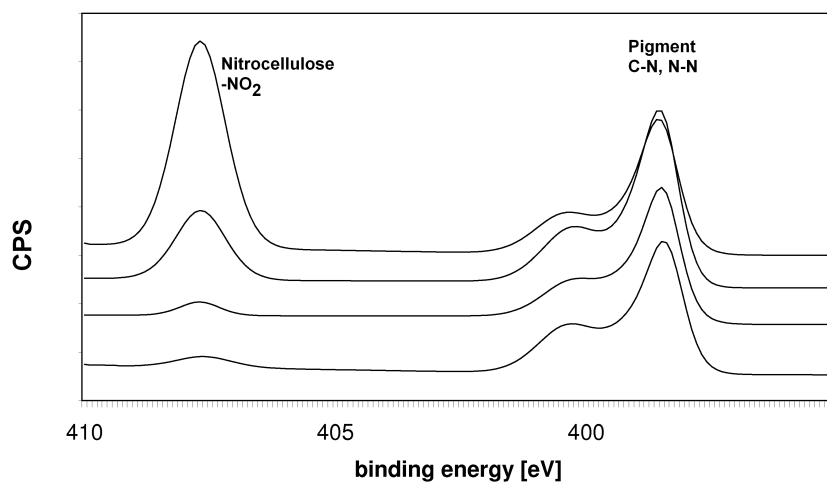


Fig. 7.1: XPS spectra of Ar^+ sputtered ink coating. The nitrocellulose peak on the left is depleted with sputtering time suggesting an overlayer of nitrocellulose being blasted away.

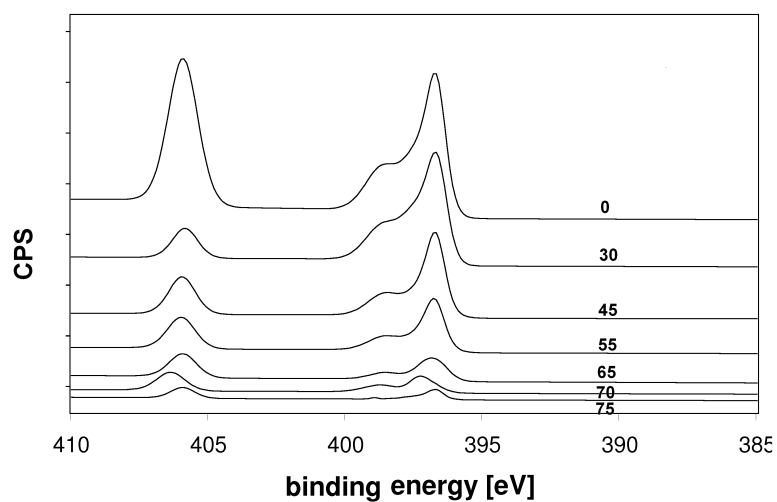


Fig. 7.2: ARXPS ink coating.

Ar^+ Sputtering is widely used for cleaning and depth profiling inorganic samples but it not generally considered to be suitable for organic samples. Sputtering was attempted with very low sputtering times and the nitrocellulose peak slowly disappeared with increased sputtering times suggesting, if the sputtering process was reliable, that there was a surface layer of nitrocellulose (Figure 7.1). Ar^+ beams can be reducing so it could be due to a chemical change being induced. Angle-resolved XPS showed a change in nitrocellulose in angle but it proved difficult to model (Figure 7.2). At a low angle (normal to the surface) the nitrocellulose peak was quite prominent and it decreased as the angle increased. However, at the most surface sensitive (largest) angle the nitrocellulose peak had returned. This could suggest a lot of nitrocellulose in the bulk followed by a depletion then a very thin overlayer right at the surface.

7.2.2 Atomic Force Microscopy (AFM)

Atomic Force Microscopy (AFM) was carried out using a Nanoprobe IIIa operated in tapping mode.

The image shown in Figure 7.3 is of the adhesive failure on a tape tested sample (Sigma on corona treated polypropylene). It shows the boundary between the substrate (exposed during the test) and the ink layer (along the top right). It also illustrates that failure in the ink is due to adhesive failure, the ink layer coming off from the substrate, rather than cohesive

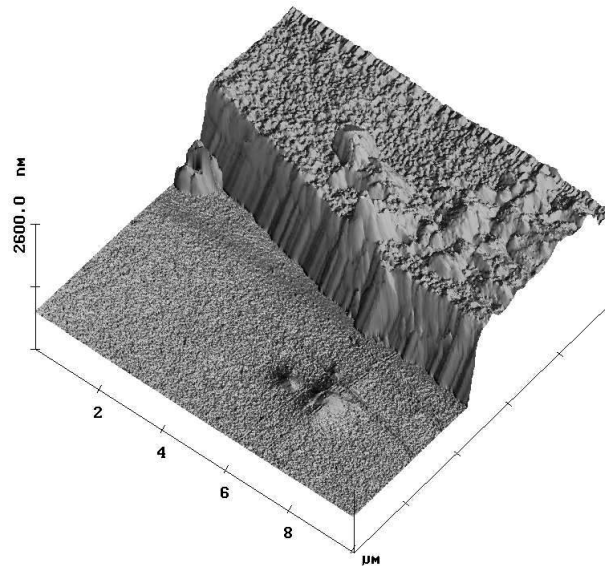


Fig. 7.3: AFM image showing partially removed ink layer on polymer substrate (Sigma on corona treated polypropylene). The raised area is the ink film still attached after a tape test. The other section shown is the smooth polypropylene substrate where the ink has failed to adhere. Two wear tracks are visible next to the adhered section which may have contributed to the failure.

failure where the ink layer cannot hold itself together and some of the ink layer still adheres to the substrate.

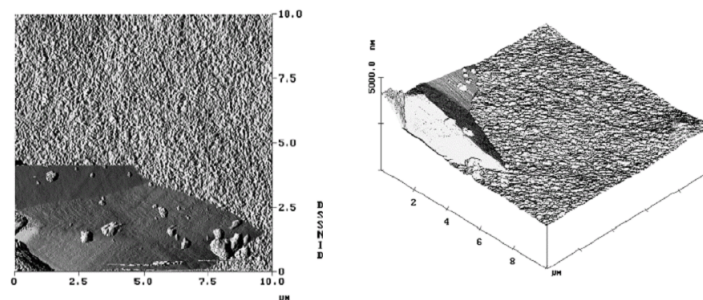


Fig. 7.4: AFM image showing wax particle protruding through polymer melt (Sigma on corona treated polypropylene). The wax is added to improve the feel and wear properties of the ink so it is desirable that it is present at the surface.

The image in Figure 7.4 (Sigma on corona treated polypropylene) shows two types of material, from phase contrast, one of which appears to be a

crystalline area protruding through, or being covered by another material. This is thought to be a crystalline wax particle, which are added to improve surface wear texture ('feel'), embedded in the primary polymer matrix of nitrocellulose. For the wax to have an effect on the surface properties it needs to be present at the surface and this together with XPEEM confirms that is the case. It is possible that some phase separation occurs in the mixture during drying and that the wax migrates to the surface during this process.

7.2.3 X-ray PhotoElectron Emission Microscopy (XPEEM)

X-ray PhotoEmission Microscopy was carried out on the 041 VLS-PGM beamline at the Synchrotron Radiation Center (SRC) using a medium energy grating. Samples were prepared by sputter coating with platinum (50 Å in the region of interest, $\geq 1000\text{\AA}$ for the rest of the sample) to reduce the severe charging effects. The beam intensity was also much higher than any previously used because better focusing optics are a requirement for imaging. In an attempt to reduce radiation damage, the electron optics were focused using an edge which did not change with damage, and once focused the sample was moved in a plane so that the beamspot was in focus on a previously unexposed section of sample and images were recorded for the new spot. Images were recorded at the nitrogen, carbon, oxygen K-edges and copper L-edge.

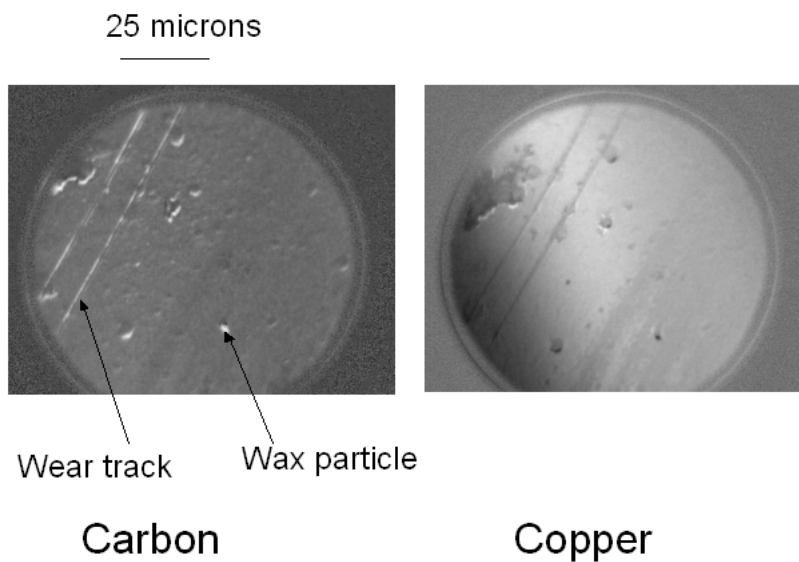


Fig. 7.5: XPEEM image of a ink coating. Visible in both carbon (polymer and wax) and copper (pigment) are wear tracks and wax particles. They show up as enrichment in carbon and depletion in copper.

The 100 micron field of view image in Figure 7.5 (Sigma on corona treated polypropylene) shows an over view of an ink film imaged at the most prominent carbon (left) and copper (right) peaks. Features to note are the wear tracks, which are also seen in optical and scanning electron microscopy and are caused by a microscopic nick or contaminant in the printing press, and wax particles, also identified in the AFM images.

A close up image of a wax particle at 25 micron field of view is shown in Figure 7.6. The carbon image looks quite uniform with only a slight contrast, which maybe be more to do with surface features than chemical

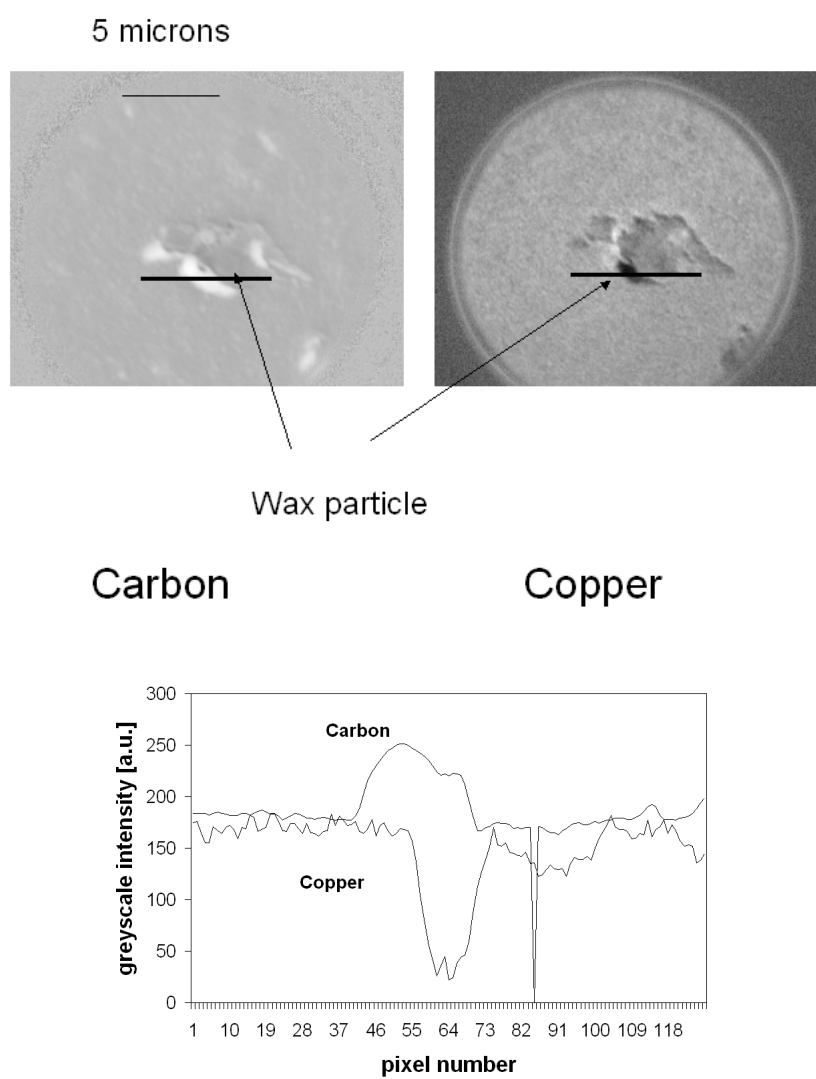


Fig. 7.6: Close up XPEEM image of a wax particle on the ink surface. The copper pigment is depleted around the wax particle and enriched in the carbon. The AFM wax particle is of a comparable size. A greyscale line profile from the black line shows the copper/carbon differences match.

differences, allowing us to pick out the wax particle. The copper data maps copper phthalocyanine pigment concentrations and the darkest patch at the copper edge corresponds to the lightest in the carbon showing that an abundance of pigment means less binder at a given area. A line profile taken across the black line shows the decrease in the copper corresponding to the increase in the carbon.

7.2.4 Conclusion

This ink study formed the basis of the later work on pharmaceuticals and lessons learned were important for the rest of the work presented in this thesis. The work, failed however to make a major contribution to understanding how and why different inks work under some conditions and fail under others. It did give an improved understanding of the surface structure of the finished ink product, which may prove of help in determining wear and texture characteristics. A tentative model for what we see in the ink layer is shown in Figure 7.7 with some migration of components like wax and nitrocellulose to the surface and the interface.

The most important aspects of this work with respect to the rest of the work shown in this thesis were the lessons learned in how to deal with complex and unsuitable materials. Beam damage was a consideration with the nitro groups in the nitrocellulose; the method adopted to deal with this was to repeat measurements of the sample to look for changes with

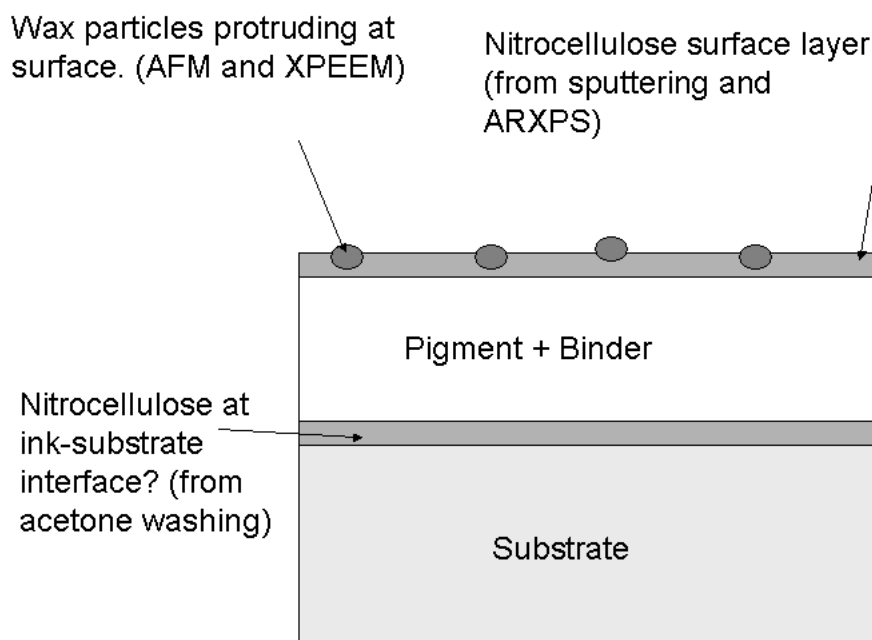


Fig. 7.7: Tentative model for ink layer on (polymer) substrate. Additives (wax and adhesion promoter) migrate from the bulk to the surface.

radiation exposure which was adopted throughout this thesis. The complex nature of the samples required an approach which did not necessarily require understanding or explanation of the whole spectra but still obtained useful information. With the inks this was exemplified by the nitrogen edge where the pigment and binder (nitrocellulose) components could be clearly and meaningfully distinguished. This was useful when dealing with the drug formulations; the oxygen edge could be used to pick out bound water and coatings and differences in carbon spectra could be used to assess crystallinity.

7.3 SSR 180575 - X-ray PhotoElectron Emission Microscopy (XPEEM)

X-ray PhotoEmission Microscopy was carried out on the 041 VLS-PGM beamline at the Synchrotron Radiation Center (SRC) using a medium energy grating. A number of sample preparations were attempted in order to reduce sample charging. Firstly, drug and drug formulation powder were mixed with indium powder in the ratio of 1:3 respectively, then the resulting mix was pressed onto indium foil for mounting. Despite the presence of a large amount of metal powder in the sample and a conducting support, imaging was still very problematic, so in addition to the indium treatment the samples were sputter coated with 50 Å of platinum.

Figure 7.8 shows XPEEM images of pure SSR 180575 micronised crystals, the inset shows a scanning electron micrograph of the same. The images are formed from the two peaks highlighted and normalised with the empty pre-edge region. The crystals as shown in the XPEEM appear to be the same size as in the SEM. This does not necessarily mean, however, that we are seeing the particles as a result of chemical mapping and contrast with the indium powder. The particles can protrude several microns from the surface (this also makes focusing problematic) and surface topography can dominate the deflection of the outgoing photoelectrons. This is mitigated somewhat by comparing the map of the peaks to a map of the pre edge region, but it does not necessarily eliminate it.

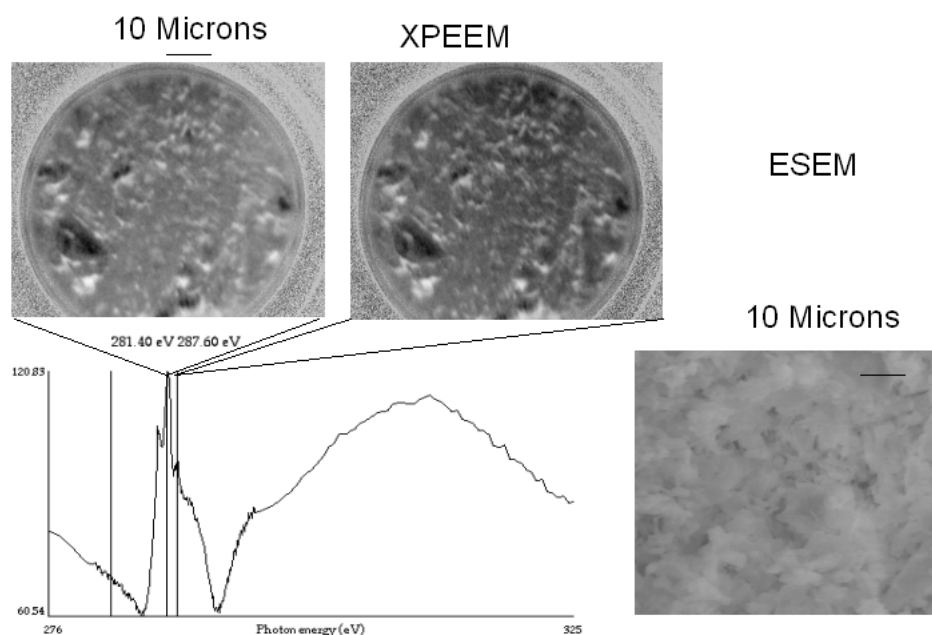


Fig. 7.8: XPEEM images of pure SSR 180575 crystals. The images are of the two peaks highlighted in the spectra normalised to the flat pre edge region. They are of a comparable size to those observed using Scanning Electron Microscopy (SEM).

Figure 7.9 shows XPEEM images of PVP coated SSR 180575 from Chapter 4. A flatter region of the sample was found for study and it was initially hoped to be able to image the PVP rafts of polymers thought to be present on the surface. While we can see something it is again thought to be dominated by surface topography. The oxygen K-edge data failed to map at all, but carbon and nitrogen (present in the drug and PVP) could both be mapped. The nitrogen map appears to match, albeit with less detail, than the carbon map, which suggests that the image produced is real (not an instrument artifact). No evidence was seen of polymer rafts, which could be explained by the relative low resolution we could achieve due to the non-ideal nature of the samples.

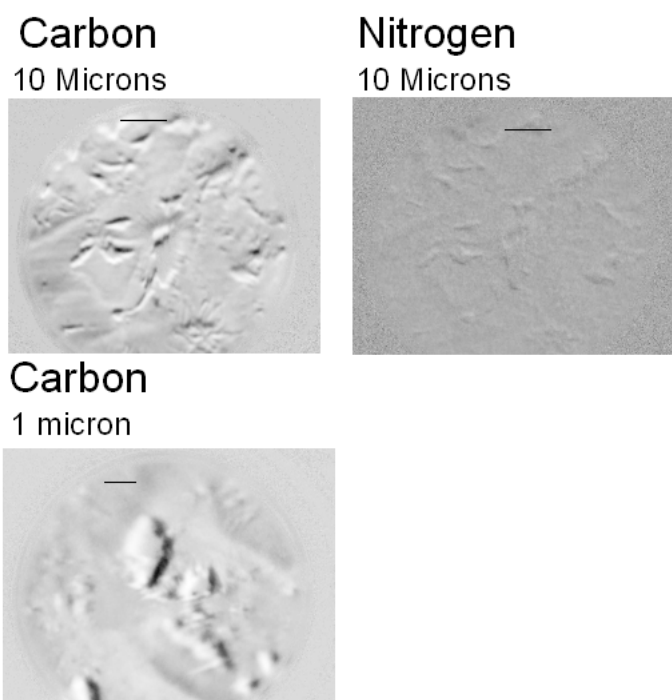


Fig. 7.9: XPEEM images of PVP coated SSR 180575. The resolution is too poor to resolve any detail on the surface of the coated drug particles.

7.4 Drug Nanoparticle Formulations - XPEEM

Nanoparticles, in this context those with a particle size around 100 nm, show promise as a new method of formulating drug products with increased bioavailability. The main hurdle to their wide spread adoption is the issue of stability. The nanoparticles have a very high surface energy and show a tendency to agglomerate, so care needs to be taken when choosing excipients. With spectromicroscopy we hoped to open up the possibility of observing the active ingredient, AVE 9488, within the formulation and determining distribution and chemical state.

Samples were prepared for XPEEM by mixing with indium powder in a 1:3 ratio of drug to indium. This was then pressed into indium foil and then sputter coated with 50 Å of platinum. Measurements were made of the pure active ingredient and a ground up formulated tablet.

Figure 7.10 shows particles of the pure AVE 9488 which has a particle size of around 100 nm. Images were made using slices at the two peaks shown and normalised to the pre-edge slice shown. The two images are very similar, suggesting that what is shown is real and due to the small particle size. Surface topology effects were greatly reduced. What is shown are clumps of material inside the indium powder matrix. It is possible that what is observed is the agglomeration of the nanoparticle material as a result of its high surface energy.

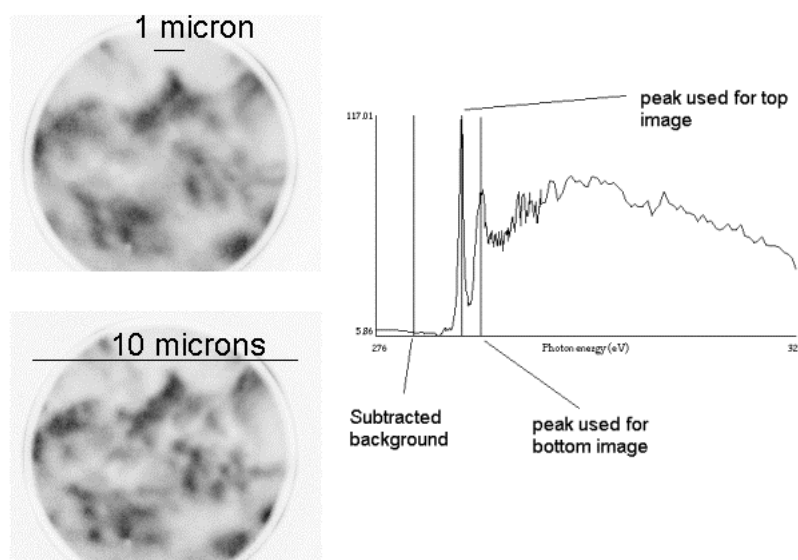


Fig. 7.10: Carbon K-edge XPEEM of drug nanoparticles. It appears to be agglomerated particles of the particles dispersed in the indium powder.

Figure 7.11 shows a ground up tablet of the formulation in which AVE 9488 is the active ingredient. It was impossible to use a whole tablet because of the surface roughness and outgassing caused by using a whole fragment of the tablet. There is a large dark patch in the bottom left which is presumably agglomerated drug material. There are also small patches which are around a few hundred nm in size scattered over the image. These could be either artifacts caused by the image slice not being properly aligned with the normalising slice, or particles/clumps of the active material which have not agglomerated due to the tablet being correctly formulated to keep them apart.

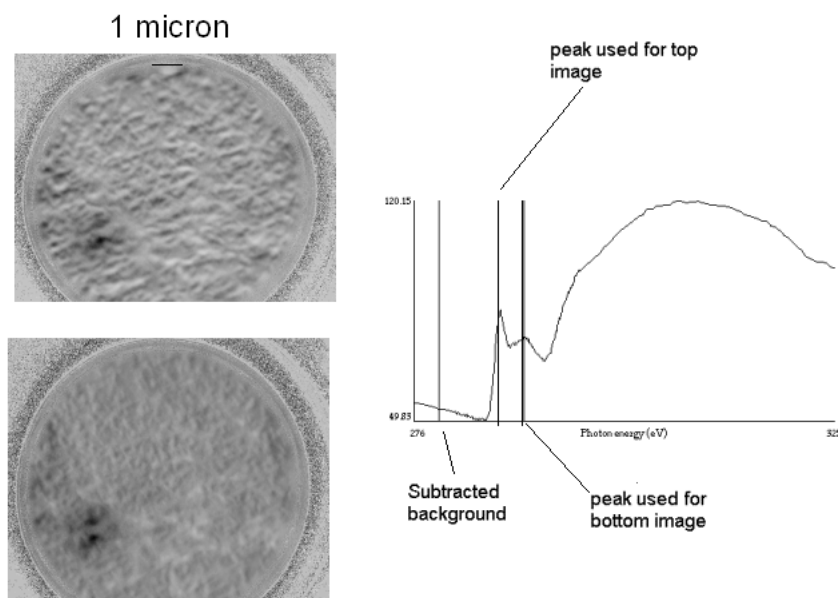


Fig. 7.11: Carbon K-edge XPEEM of ground tablet containing drug nanoparticles. The dark patches could be particles of the formulation and the bottom left area a large patch of the intact material.

The main problems of using XPEEM on pharmaceutical samples are the surface roughness and charging effects. Surface topology frequently dominates the image plane and charging effects make it necessary to use sample treatments which may significantly damage or change the material. Even with the use of indium metal powder as a bulking agent, severe charging effects were still observed including sparking. The use of a 50 Å layer of platinum eliminated some of the effects but it was still an issue and more platinum sputtering simply obscured any detail.

7.5 Further NEXAFS

NEXAFS spectra were measured on the 1.1 bending magnet station of the SRS using total electron yield and a cell setup based on the ones in Chapter 3. Spectra were measured over the range 270 eV - 350 eV for the carbon K- edge, with 0.1 eV energy steps and a measurement time of 0.5 s per point. 395 eV - 425 eV for nitrogen and 515 eV - 550 eV for oxygen K-edges. Several comparison spectra were made to illustrate some of the things which may be important for future researchers to consider.

Bending magnet vs undulator spectra were made for SR 49059, the drug studied in chapter 5. There was not a major change in the quality of the spectra but this may be due to extra windows and gold mesh being present when measuring on the undulator (Mark II cell vs. Mark III). Other work, specifically *in situ* catalysis, suggests that using an undulator beamline produces significantly better spectra¹¹. Normally contamination barriers (boron or magnesium windows) are a requirement for operating on UHV beamlines, but due to circumstances (the beamline was closing down) we were allowed to measure without a window to try and improve the spectra. This allowed a valuable opportunity to compare spectra with and without a contamination barrier, but no difference was observed.

The ultimate aim of many formulations is to produce a substance suitable for tablet production which includes the active pharmaceutical ingredient, additives, bulking agents and so forth. Most of the work in this thesis has

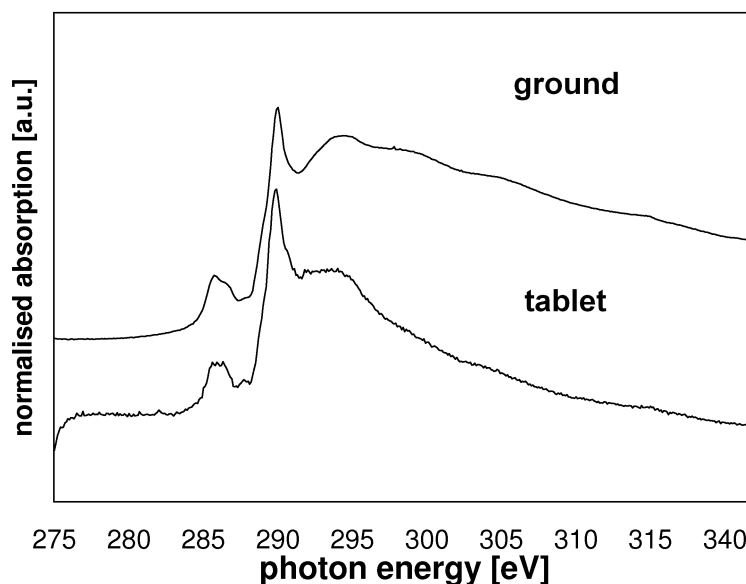


Fig. 7.12: Carbon K-edge NEXAFS comparing intact and ground samples of the same melt extruded tablet.

been on active ingredients or the beginning of the formulation process, but future work may be directed towards tablet forms. The XPEEM of drug nanoparticles showed that sample preparation, grinding, mixing and coating can significantly modify what is being studied and it is important to have an idea of what this can do. Figure 7.12 shows NEXAFS spectra of a simple two component tablet both whole and ground up to illustrate differences in spectra of the same sample under different preparation conditions. The ground up tablet shows a much clearer spectra than the whole tablet but retains the same spectral features. The whole tablet suffers from the besetting problems of pharmaceutical soft X-ray studied, charging and outgassing. The spectra of the whole tablet is significantly worse than that of the ground tablet. The noise is much worse and there are several spectral

features which are suppressed due to the rapid tail off after about 295 eV. The reason the tablet spectrum is worse is due to charging and outgassing. While charging is not as much of a problem with NEXAFS as it is with XPEEM it still has an effect with such large insulating samples. Grinding does not appear to add any new spectral features and just serves to improve spectral quality.

7.6 Hemispherical Ambient Pressure Photoelectron Yield (HAPPY) Analyser

In addition to *in situ* X-ray Absorption Spectroscopy (XAS) it is possible, using a synchrotron source, to perform *in situ* X-ray Photoelectron Spectroscopy (XPS). It is made more difficult by the fact that the kinetic energies of the electrons need to be measured. This means the gas environment attenuates on the electron signal rather than improving it, but it does still help neutralise a build up of charge. The electron energy analyser needs to be connected to the chamber and kept at a sufficiently low pressure to function due to the high electric field in the analyser. The HAPPY (Hemispherical Ambient Pressure Photoelectron Yield) analyser (Figure 7.13) was developed for *in situ* XPS using a differential pumping scheme similar to that of an ESEM where the sample section is kept at the highest pressure and small apertures are used to connect it to the next section (electron optics) which is a few orders of magnitude lower in pressure, then to the electron analyser section which is kept close to UHV pressure.

The analyser was tested on a stainless steel plate (sample holder) in air and a well understood model system²⁴, TiO₂ in an O₂ atmosphere. The measurements were made on the 1.1 bending magnet station of the SRS. The TiO₂ was prepared by sputtering with Ar⁺ ions at a 500 V potential for 30 mins then flash heating to 700°C.

Figure 7.14 shows test data from TiO₂ in O₂ at UHV and in 10⁻² mbar

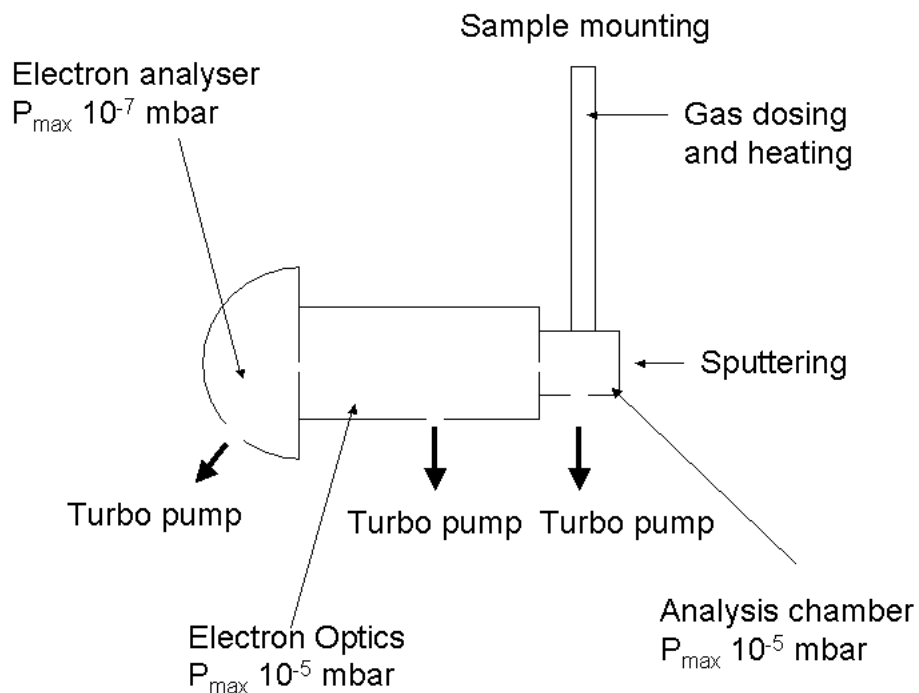


Fig. 7.13: Schematic of the 'HAPPY' *in situ* XPS analyser. The pressure in the analysis chamber is limited to 10^{-2} mbar, any higher and the pressure in the electron analyser cannot be kept at 10^{-7} mbar, the threshold for operating the channeltron.

of O_2 . The peak intensity is reduced while operating at high pressure it is still possible to measure useful data. The peaks in both spectra show a slight shift of about 0.5 eV to higher kinetic energy (lower binding energy). It is conjectured¹⁴³ that this could be a change in the work function due to adsorbed O_2 .

The data illustrate that it is possible to measure XPS at pressures up to at least 10^{-2} mbar, which could prove valuable to the drug work both in terms of negating the outgassing problems of many samples and, in principal, measuring XPS spectra under the influence of relative humidity which would be a powerful complementary tool to the NEXAFS data in Chapters 4 and

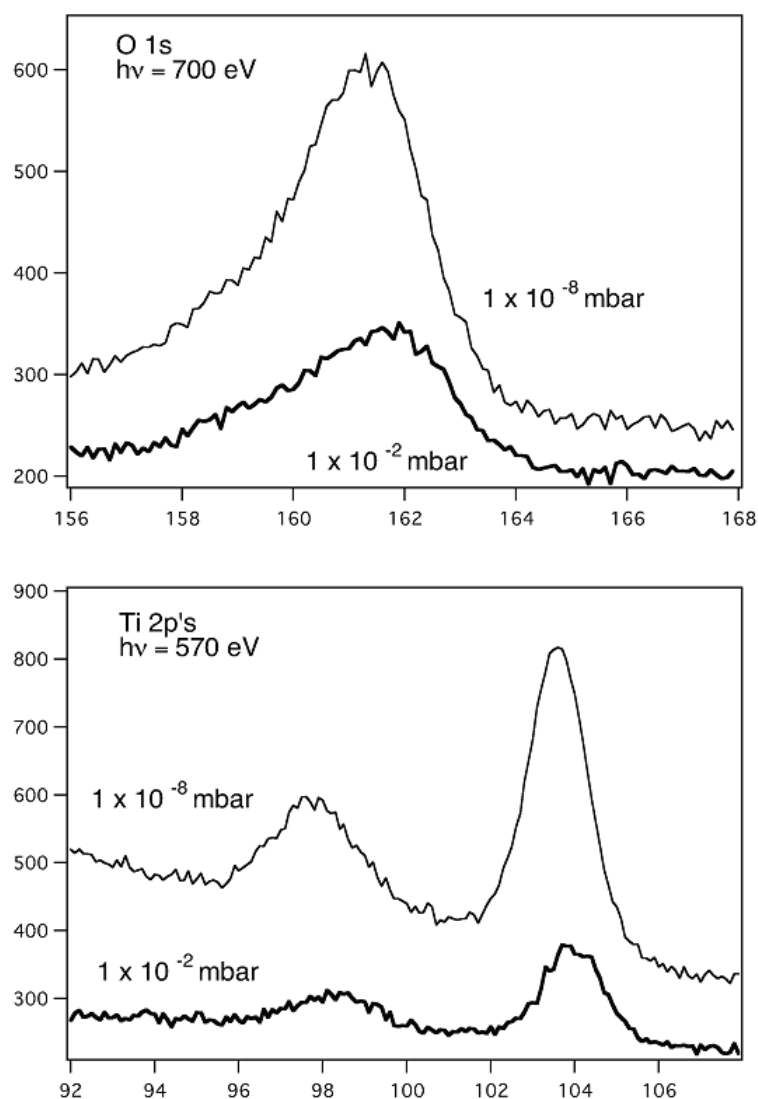


Fig. 7.14: Preliminary data with HAPPY on a test system, Oxygen Absorption on TiO_2 . Top oxygen 1s, bottom titanium 2p. There is a small shift in peak energy when measured in oxygen, which may be due to a change in the work function caused by adsorbed oxygen.

5. Additionally, the ability to gain a measure of non-destructive depth profiling by varying the photon energy could prove invaluable, allowing further confirmation of the model of polymer rafts and the model of a thin nm over layer of amorphous material on a crystalline bulk.

7.7 X-ray Excited Optical Luminescence (XEOL) detection

There is a constant problem with this work of not being able to operate at normal atmospheric pressure. Although it would eliminate the surface sensitivity it currently appears as if it will be possible to measure bulk XAS of the carbon, nitrogen and oxygen K-edges at atmospheric pressures. While the purpose of this thesis was the study of surface properties it may still be of value to be able to obtain bulk XAS.

The method used is X-ray Excited Optical Luminescence (XEOL). XEOL measures the optical luminescence produced by soft X-rays exciting the target element as a function of monochromator energy, which appears to correlate with $\mu(E)$. The advantages of this method of detection are two-fold. Firstly, as optical photons have a much greater mean free path in air than either electrons or soft X-ray photons it is possible to keep the pressure in the chamber much higher than would otherwise be the case. The only potential problem would be getting enough X-ray photons onto the sample initially, and the window design in Chapter 3 would provide an effective way of limiting the path distance for the X-ray photons. Secondly, the energy of the optical emission is dependent on the electronic structure and chemical environment of the target atom. This means that by selecting only one

optical emission to study, via the use of filters, it is possible to measure site specific XAS and obtain spectra for a single atom in a molecule. XEOL is already established as a reliable technique in various areas of semiconductor science and nanotechnology.

Figure 7.15 shows a preliminary test of some of the drug samples, that were excited with photons from a laser and the fluorescence was measured. All of the samples showed some fluorescence which makes them suitable for study with XEOL.

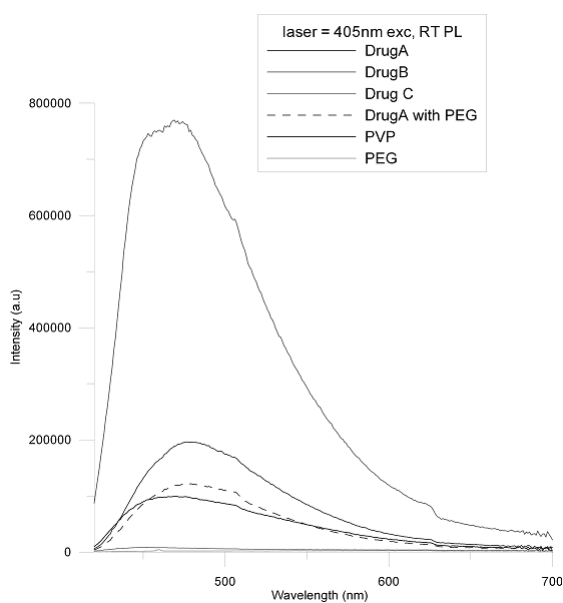


Fig. 7.15: Preliminary Test data for X-ray Excited Optical Luminescence (XEOL). A laser was used to excite the sample and check for optical fluorescence. Three of the active ingredients were tried and all showed sufficient fluorescence for measuring with XEOL.

Chapter 8

Conclusions

8.1 Importance

The two primary areas in which the project has made progress are the determination of surface water content (Chapters 4 and 6) in polymer-drug formulations, and the determination of surface amorphous content (Chapter 5).

The ability to determine surface water content was demonstrated using X-ray Photoelectron Spectroscopy (XPS) and Near Edge X-ray Absorption Fine Structure (NEXAFS). This is potentially of great importance with respect to poorly water soluble compounds which make up an increasing number of lead compounds. SR 142801 showed that the appearance of water peaks in the surface spectra corresponded to improved bioavailability. This opens up the possibility of using NEXAFS to screen formulations and turn lead compounds into products which might otherwise have to be abandoned

due to poor solubility. At the time of writing SSR 18075, the second drug in Chapter 4 has not undergone clinical trials but it is hoped that the principal of using water peaks to predict bioavailability will be applicable. While this idea of using NEXAFS/XPS screening of formulations is new and relatively untested, considering the highly regulated nature of the industry, if it is shown to be reliable and reproducible it could save millions in reducing and targeting the amount of testing which needs to be done when formulating a new drug.

Chapter 6 uses the same techniques as Chapter 4 but the application here is suspension stability. Again it is the presence of surface water and spectral features from the coating polymers which correspond to the desired property. It is not unexpected as the reason for the poor bioavailability in the previous example was a lack of solubility in water, also a desired property for a suspension.

The other area where the project has made a contribution is in using NEXAFS to probe amorphous content at surfaces. Amorphous vs crystalline content is an area of great interest in the pharmaceutical industry and there is a big drive to develop and improve techniques, especially to try and detect amounts below that which is observable in powder X-ray diffraction, the workhorse of crystallinity studies. The limits of X-ray diffraction are about 5-10% and other techniques, such as dynamic vapour sorption are also in this range. While the XPS may be interesting it is NEXAFS which allowed the unambiguous determination of surface crystallinity, although admittedly

limited to the surface layers. As a fraction of the total volume it allows the detection of amorphous content well below that which can be observed with other techniques. This is especially useful in dealing with micronisation induced amorphous content.

8.2 Practicality

While what has been shown is scientifically interesting and important, the purpose of the project and this thesis is to look at the value of these techniques to the pharmaceutical industry. How useful these techniques are and what they can tell us is the most important part, but another consideration which has to be included here is how practical these techniques are.

NEXAFS and XPEEM (X-ray PhotoElectron Emission Microscopy) both require the use of synchrotrons. The cost of proprietary experiment time at a synchrotron, in the order of £10,000 a day, would make it prohibitively expensive for routine testing of generic formulations such as ibuprofen. With the massive cost of clinical trials, however, it might be justifiable to buy synchrotron time to pick out the optimum formulations and only proceed to trials with those that are thought to be hopeful. If it could be used to save a promising compound from being discontinued then the price would be justified.

The use of NEXAFS to study amorphous content could be useful as a one-off approach to study the surface crystallinity of lead compounds in the early stages of testing. This could be to identify compounds which may need conditioning or even which compounds should be abandoned. Being able to abandon development at an early stage due to crystallinity problems thus saving on additional unnecessary testing would be as much of a boon

as being able to continue development with poorly soluble compounds and would justify the cost of synchrotron time.

XPS does not necessarily need to be performed at a synchrotron and there are several manufacturers who produce laboratory XPS instruments and many universities and research laboratories operate their own. The cost of an XPS machine is in the order £100,000-300,000. If it were to be used for screening formulations, perhaps prior to a synchrotron NEXAFS experiment, then it might be worth the investment, especially for a large company which would have many compounds in development at the same time. It is also worth noting that several companies already exist offering specialised surface analysis techniques such as XPS and ToF-SIMS (Time of Flight-Secondary Ion Mass Spectrometry) so further exploitation of XPS for pharmaceuticals would not necessarily require acquiring an instrument.

8.3 Future Developments

The future progress of surface soft X-ray spectroscopy for pharmaceuticals, especially given the exploratory nature of this thesis, is an area open to a wide amount of speculation. In the short term there are suggestions of possible systems to study and techniques and methodologies which seem promising. In the long term we can conjecture about the impact of these techniques and to what extent they may be adopted.

As far as drugs and formulations go it would be useful to have results from a wider range of drug compounds to ensure that any generalisations made, such as more surface water corresponds to higher bioavailability, are valid. It would be of particular interest, as will hopefully be the case with SSR 180575, to use these techniques to predict which would be the best formulation then proceed to trials for confirmation, rather than the case with SR 142801 where it was already known which was the better formulation. It would also be of interest to apply high throughput methodologies to the formulation screening, which would help make the most efficient use of expensive experimental time.

As far as new techniques go, the work in Chapter 7 is illustrative of what the future may hold. XPEEM, if the problems with charging and beam damage can be mitigated, would be an incredibly powerful tool for obtaining chemical and spatially sensitive information from a sample. There are many formulation problems, such as phase separation of components

where XPEEM could prove useful. *In situ* synchrotron XPS is a perfectly viable technique and will doubtless prove of use to pharmaceutical research in the future, indeed the only reason it has not been used so far was a lack of beamtime. X-ray Excited Optical Luminescence (XEOL) looks like a promising new method of data collection for XAS. Preliminary tests show that the compounds we had are suitable for study and the potential to perform site specific EXAFS would be of great scientific interest. The technique has already proved popular with semi-conductor studies and with increasing interest in amorphous state pharmaceuticals EXAFS would be a useful crystallographic tool requiring no long range order and allowing the determination of structure around a specific atom.

While it is unlikely that a pharmaceutical company would be prepared to build their own synchrotron it is not unheard of for them to fund beamlines for protein crystallography, as one of the primary beneficiaries of the discovery of new protein targets. While it is an optimistic view of the future of this work it would be the ultimate accolade if, in 20 years, pharmaceutical companies have funded soft X-ray beamlines in the same way as protein crystallography.

References

- [1] *Association of The British Pharmaceutical Industry*.
<http://www.abpi.org.uk>, (2006).
- [2] Feast, W., Munro, H., and Richards, R. *Polymer Surfaces and Interfaces 2*, volume 2 of *Polymer Surfaces*. John Wiley & Sons, Chichester, 1st edition, (1993).
- [3] Briggs, D. and Seah, M. P. *Practical Surface Analysis*. John Wiley & Sons, Chichester, 2nd edition, (1990).
- [4] Watts, J. and Wolstenholme, J. *Surface Analysis by XPS and AES*. John Wiley & Sons, Chichester, 1st edition, (2003).
- [5] Briggs, D., Brewis, D. M., and Konieczko, M. B. *Journal of Materials Science* **11**(7), 1270–7 (1976).
- [6] Briggs, D. and Kendall, C. R. *Polymer* **20**, 1053–1054 (1979).
- [7] Briggs, D., Zichy, V. J. I., Brewis, D. M., Comyn, J., Dahm, R. H., Green, M. A., and Konieczko, M. B. *Surface and Interface Analysis* **2**(3), 107–14 (1980).
- [8] Briggs, D., Brewis, D. M., and Konieczko, M. B. *Journal of Materials Science* **14**(6), 1344–8 (1979).
- [9] Briggs, D., Brewis, D. M., and Konieczko, M. B. *Journal of Materials Science* **12**(3), 429–33 (1977).
- [10] Castner, D. G. and Ratner, B. D. *Surface Science* **500**, 28–60 (2002).

-
- [11] Braum, S. *PhD Thesis*. University of Manchester, (2008).
- [12] Kipp, J. *International Journal of Pharmaceutics* **284**, 109–122 (2004).
- [13] Hippocrates. *Hippocratic Corpus*. Cos, (300 B.C.).
- [14] M.H.R.A., *Medicines and Healthcare products Regulatory Agency*.
<http://www.mhra.gov.uk>, (2006).
- [15] Abbot. *Chemistry world* **4**(7), 7 (2007).
- [16] Brewis, D. M. and Briggs, D. *Industrial Adhesion Problems*. (1985).
- [17] Fulghum, J. E. *Journal of Electron Spectroscopy and Related Phenomena* **100**, 331–355.
- [18] Krueger, R. and Potente, H. *Journal of Adhesion* **11**(2), 113–24 (1980).
- [19] Kammer, H. and Piglowski, J. In *Polymer Blends*, Kryszewski, M. and Galeski, A., editors, volume 2, 19–34. Plenum Press, New York 1st edition (1979).
- [20] Brewis, D. M. and Briggs, D. *Polymer* **22**(1), 7–16 (1981).
- [21] Briggs, D., Kendall, C. R., Blythe, A. R., and Wootton, A. B. *Polymer* **24**, 47–52 (1982).
- [22] Sutherland, I., Popat, R. P., Brewis, D. M., and Calder, R. *Journal of Adhesion* **46**(1-4), 79–88 (1994).
- [23] Sharples, L. *Plastics and Polymers* **37**(128), 135–145.
- [24] Diebold, U. *Surface Science Reports* **48**, 53–229.

-
- [25] Castner, D. G., Ratner, B. D., and Hoffman, A. S. *Journal of Biomaterials Science, Polymer Edition* **1**, 191–206.
- [26] Ratner, B. D. *Journal of Vacuum Science & Technology, A: Vacuum, Surfaces, and Films* **8**, 2306–17.
- [27] Castner, D. *Journal of Biomaterials Science, Polymer Edition* **3**, 463–80.
- [28] Ratner, B. D. and Castner, D. G. *Colloids and Surfaces, B: Biointerfaces* **2**, 333–46.
- [29] Tyler, B. J., Ratner, B. D., Castner, D. G., and Briggs, D. *Journal of Biomedical Materials Research* **26**, 273–89.
- [30] Hitchcock, A. P., Morin, C., Heng, Y. M., Cornelius, R. M., and Brash, J. L. *Journal of Biomaterials Science, Polymer Edition* **13**(8), 919–937 (2002).
- [31] Hitchcock, A. P. *Journal of Synchrotron Radiation* **8**(2), 66–71 (2001).
- [32] Urquhart, S. G., Hitchcock, A. P., Smith, A. P., Ade, H. W., Lidy, W., Rightor, E. G., and Mitchell, G. E. *Journal of Electron Spectroscopy and Related Phenomena* **100**, 119–135 (1999).
- [33] Carli, F. and Garbassi, F. *Journal of Pharmaceutical Sciences* **74**(9), 963–7 (1985).
- [34] Carli, F., Colombo, I., Magarotto, L., Motta, A., and Torricelli, C. *International Journal of Pharmaceutics* **33**(1-3), 115–24.

- [35] Carli, F., Colombo, I., Lovrecich, M., Rubessa, F., and Torricelli, C. *Polymer Science and Technology (Plenum)* **34**(Polym. Med. 2), 397–407.
- [36] Garbassi, F. and Carli, F. *Surface and Interface Analysis* **8**(6), 229–33 (1986).
- [37] Canal, T., Lovrecich, M., De Nardo, M., and Rubessa, F. *Pharmaceutica Acta Helvetiae* **63**(9-10), 271–7 (1988).
- [38] Layre, A., Couvreur, P., Chacun, H., Richard, J., Passirani, C., Requier, D., Benoit, J. P., and Gref, R. *Journal of controlled release* **111**(3), 271–80 (2006).
- [39] Feng, S.-S., Li, M., Chen, B.-H., and Pack, D. *Materials Science & Engineering, C: Biomimetic and Supramolecular Systems* **C20**(1-2), 85–92 (2002).
- [40] Mu, L., Seow, P.-H., Ang, S.-N., and Feng, S.-S. *Colloid and Polymer Science* **283**(1), 58–65 (2004).
- [41] Zhang, Z. and Feng, S.-S. *Biomacromolecules* **7**(4), 1139–1146.
- [42] Scholes, P. D., Coombes, A. G. A., Illum, L., Davis, S. S., Watts, J. F., Ustariz, C., Vert, M., and Davies, M. C. *Journal of Controlled Release* **59**(3), 261–278 (1999).
- [43] Davies, M. C., Wilding, I. R., Short, R. D., Khan, M. A., Watts, J. F., and Melia, C. D. *International Journal of Pharmaceutics* **57**(3), 183–7 (1989).

-
- [44] Davies, M. C., Short, R. D., Khan, M. A., Watts, J. F., Brown, A., Eccles, A. J., Humphrey, P., Vickerman, J. C., and Vert, M. *Surface and Interface Analysis* **14**(3), 115–20 (1989).
- [45] Davies, M. C., Khan, M. A., Short, R. D., Akhtar, S., Pouton, C., and Watts, J. F. *Biomaterials* **11**(4), 228–34 (1990).
- [46] Davies, M. C., Khan, M. A., Lynn, R. A. P., Heller, J., and Watts, J. F. *Biomaterials* **12**(3), 305–8 (1991).
- [47] Brindley, A., Davis, S. S., Davies, M. C., and Watts, J. F. *Journal of Colloid and Interface Science* **171**(1), 150–61 (1995).
- [48] Leadley, S. R., Davies, M. C., Vert, M., Braud, C., Paul, A. J., Shard, A. G., and Watts, J. F. *Macromolecules* **30**(22), 6920–6928 (1997).
- [49] Buckton, G., Bulpett, R., and Verma, N. *International Journal of Pharmaceutics* **72**(2), 157–62 (1991).
- [50] John, C. M., Odom, R. W., Salvati, L., Annapragada, A., and Fu Lu, M. Y. *Analytical chemistry* **67**(21), 3871–8.
- [51] Westwood, A. D., Leder, D. J., and Donabedian, D. H. *Polymeric Materials Science and Engineering* **76**, 130–131 (1997).
- [52] Kronig, R. d. L. *Zeitschrift fuer Physik* **70**, 317–23.
- [53] Sayers, D. E., Stern, E. A., and Lytle, F. W. *Physical review Letters* **27**(18), 1204–7 (1971).

- [54] Nicolis, I., Curis, E., Deschamps, P., and Benazeth, S. *Journal of Synchrotron Radiation* **10**(1), 96–102 (2003).
- [55] Elder, R. C., Eidsness, M. K., Heeg, M. J., Tepperman, K. G., Shaw, C. F., I., and Schaeffer, N. *ACS Symposium Series* **209**(Platinum, Gold, Other Met. Chemother. Agents: Chem. Biochem.), 385–400.
- [56] Elder, R. C., Ludwig, K., Cooper, J. N., and Eidsness, M. K. *Journal of the American Chemical Society* **107**(17), 5024–5.
- [57] Curis, E., Provost, K., Bouvet, D., Nicolis, I., Crauste-Manciet, S., Brossard, D., and Benazeth, S. *Journal of Synchrotron Radiation* **8**(2), 716–718 (2001).
- [58] Curis, E., Provost, K., Nicolis, I., Bouvet, D., Benazeth, S., Crauste-Manciet, S., Brion, F., and Brossard, D. *New Journal of Chemistry* **24**(12), 1003–1008 (2000).
- [59] Mazid, M. *Journal of the Chemical Society, Chemical Communications* **1**, 1261–3 (1980).
- [60] Bouvet, D., Michalowicz, A., Crauste-Manciet, S., Brossard, D., and Provost, K. *Inorganic Chemistry* **45**(8), 3393–3398 (2006).
- [61] Nicolis, I., Deschamps, P., Curis, E., Corriol, O., Acar, V., Zerrouk, N., Chaumeil, J. C., Guyone, F., and Benazeth, S. *Journal of Synchrotron Radiation* **8**(2), 984–986 (2001).
- [62] Stohr, J. *NEXAFS Spectroscopy*. Springer-Verlag, Berlin, 2nd edition, (1992).

-
- [63] Dhez, O., Ade, H., and Urquhart, S. *Journal of electron spectroscopy and related Phenomena* **128**, 85–96 (2003).
- [64] Knop-Gericke, A., Havecker, M., Neisius, T., and Schedel-Niedrig, T. *Nuclear Instruments & Methods in Physics Research Section a- Accelerators Spectrometers Detectors and Associated Equipment* **406**(2), 311–322 (1998).
- [65] Havecker, M., Knop-Gericke, A., and Schedel-Niedrig, T. *Applied Surface Science* **142**(1-4), 438–442 (1999).
- [66] Senaratne, W., Andruzzi, L., Sheets, E. D., Holowka, D., Ilic, B., Hexemer, A., Baird, B., Kramer, E. J., and Ober, C. K. *PMSE Preprints* **88**, 337–338 (2003).
- [67] Ade, H. and Urquhart, S. *Advanced Series in Physical Chemistry* **12A**(Chemical Applications of Synchrotron Radiation, Pt. 1), 285–355 (2002).
- [68] Seki, K. *Vac. Ultraviolet Radiat. Phys., Proc. VUV Conf., 10th* , 385–94 (1993).
- [69] Zubavicus, Y. and Grunze, M. *Science* **304**, 974–976 (2004).
- [70] Wernet, P., Nordlund, D., Bergmann, U., Cavalleri, M., Odelius, M., Ogasawara, H., Naslund, L., Hirsch, T., Ojamae, L., Glatzel, P., Pettersson, L., and A.Nilsson. *Science* **304**, 995–999 (2004).
- [71] Raymond, E. A. and Richmond, G. L. *Journal of Physical Chemistry B* **108**, 5051–5059 (2004).

- [72] Soderstrom, J. *Journal of Electron Spectroscopy and Related Phenomena* **144**, 283–285 (2005).
- [73] Chao, W., Harteneck, B. D., Liddle, J. A., Anderson, E. H., and Attwood, D. T. *Nature* **435**, 1210–1213 (2005).
- [74] Yasufuku, H., Yoshikawa, H., Kimura, M., Ito, K., Tani, K., and Fukushima, S. *Surface and Interface Analysis* **36**(8), 892–895 (2004).
- [75] Heun, S. *Hyomen Kagaku* **26**(12), 721–728 (2005).
- [76] Usov, D., Sheparovych, R., Scholl, A., Doran, A., Stamm, M., and Minko, S. *Abstracts of Papers, 227th ACS National Meeting, Anaheim, CA, United States, March 28-April 1, 2004*, PMSE-366 (2004).
- [77] Bertsch, P. M. and Hunter, D. B. *Chemical Reviews* **101**, 1809–1842 (2001).
- [78] Hitchcock, A. P., Stoever, H. D. H., Croll, L. M., and Childs, R. F. *Australian Journal of Chemistry* **58**, 423–432 (2005).
- [79] Tokarev, I., Krenek, R., Burkov, Y., Schmeisser, D., Sidorenko, A., Minko, S., and Stamm, M. *Macromolecules* **38**(2), 507–516 (2005).
- [80] Hitchcock, A. P., Morin, C., Zhang, X., Araki, T., Dynes, J., Stoever, H., Brash, J., Lawrence, J. R., and Leppard, G. G. *Journal of Electron Spectroscopy and Related Phenomena* **144-147**, 259–269 (2005).
- [81] Hitchcock, A. P., Morin, C., Tyliczszak, T., Koprinarov, I. N., Ikeura-Sekiguchi, H., Lawrence, J. R., and Leppard, G. G. *Surface Review and Letters* **9**(1), 193–201 (2002).

-
- [82] Hartman, P. *Synchrotron Radiation News* **1**, 28 (1988).
- [83] *Bending Magnet Radiation Power Calculator*.
<http://www.aps.anl.gov/>, (2007).
- [84] Thompson, A. C. and Vaughan, D. *X-ray Data Booklet*. Center for X-ray Optics and Advanced Light Source, Lawrence Berkeley National Laboratory, 1st edition, (2001).
- [85] Baldwin, A. *Design your own undulator*. Daresbury synchrotron radiation summer school, 1st edition, (2004).
- [86] Esfahanian, H. *Masters Thesis*. University of Cantabury, (2003).
- [87] Rehr, J. and Albers, R. *Reviews of Modern Physics* **72**(3), 621–654 (2000).
- [88] Schroeder, S. *Solid State Communications* **98**(5), 405–409 (1996).
- [89] Jablonski, A. and Powell, C. *Surface Science Reports* **47**, 33–91 (2002).
- [90] Seah, M. and Dench, W. *Surface and Interface Analysis* **1**(1), 2 (1979).
- [91] Cumpson, P. J., Seah, M. P., and Spencer, S. J. *Spectroscopy Europe* **10**, 2 (1989).
- [92] Tougaard, S. *Physics Review B* **34**(10), 6779 – 6783 (1986).
- [93] Sugimoto, Y., Pou, P., Abe, M., Jelinek, P., Perez, R., Morita, S., and Custance, O. *Nature* **446**, 64 (2007).

-
- [94] Lipp, J., Bateman, J., Derbyshire, G., Kirkman, I., van der Laan, G., Stephenson, R., and Teodorescu, C. *Journal of Synchrotron Radiation* **19**, 455–460 (2003).
- [95] Harland, R. S., Gazzaniga, A., Sangalli, M. E., Colombo, P., and Peppas, N. A. *Pharmaceutical research* **5**(8), 488–94 (1988).
- [96] Schroeder, S. *Personal Communication*. (2004).
- [97] *PSP Vacuum*. <http://www.pspvacuum.com/>, (2007).
- [98] *Hositrad Vacuum Products*. <http://www.hositrad.nl/>, (2007).
- [99] *Caburn-MDC*. <http://www.caburn.co.uk/>, (2007).
- [100] Lipinski, C., Lombardo, F., Dominy, B., and Feeney, P. *Advanced Drug Delivery Reviews* **23**, 3–25 (1997).
- [101] Hargel, L. and Yu, A. *Applied Biopharmaceutics & Pharmacokinetics*. McGraw-Hill, New York, 4th edition, (1999).
- [102] Loftsson, T., Fridriksdottir, H., and Gudmundsdottir, T. K. *International Journal of Pharmaceutics* **127**(2), 293–6 (1996).
- [103] *F.D.A., American Food and Drug Administration*. <http://www.fda.gov>, (2006).
- [104] Saettone, M. F., Giannaccini, B., Boldrini, E., and Bianchini, P. *Process for solubilizing pharmaceutically active ingredients in water and in aqueous vehicles*. (Farmigea S.P.A., Italy), (1999).

- [105] Ambuehl, M., Haeberlin, B., Lueckel, B., Meinzer, A., Lambert, O., and Marchal, L. *Solid pharmaceutical compositions containing surfactants and solubilizers*. (Novartis A.-G., Switz.; Novartis-Erfindungen Verwaltungsgesellschaft m.b.H.), (2001).
- [106] Jao, F., Edgren, D., Skluzacek, R., and Yam, N. *Methods and dosage forms for increasing solubility of drug compositions for controlled delivery by using a solubilizing surfactant*. (Alza Corporation, USA), (2005).
- [107] Smithey, D. T., Miller, W. K., Friesen, D. T., and Babcock, W. C. *Solid compositions of low-solubility drugs and Poloxamer*. (Pfizer Products Inc., USA), (2005).
- [108] Chokshi Rina, J., Zia, H., Sandhu Harpreet, K., Shah Navnit, H., and Malick Waseem, A. :*Drug delivery* **14**(1), 33–45 (2007).
- [109] Booth, A. M., Braun, S., Lonsbourough, T., Purton, J., Patel, S., and Schroeder, S. L. M. *American Institute of Physics, Conference Proceedings* **882**(X-Ray Absorption Fine Structure (XAFS13)), 325–327 (2007).
- [110] Booth, A. M., Braun, S., Lonsbourough, T., and Schroeder, S. L. M. *Conference Proceedings* **5**(Synchrotron Radiation in Material Science), 248 (2007).
- [111] Emonds-Alt, X., Bichon, D., Ducoux, J., Heaulme, M., Miloux, B., Poncelet, M., Proietto, V., Broeck, D. V., Vilain, P., Neliat, G.,

- Soubrie, P., Fur, G. L., and Brele'ere, J. *Life Science* **56**(10), PL27–PL32 (1994).
- [112] England, D. D. and Byard, D. S. *Personal Communication*. (2004).
- [113] Myneni, S., Luo, Y., Naslund, L., Cavalleri, M., Ojamae, L., Ogasawara, H., Pelmenchikov, A., Wernet, P., Vaterlein, P., Heske, C., Hussain, Z., Pettersson, L., and Nilsson, A. *Journal of Physics: Condensed Matter* **14**, L213 (2002).
- [114] Wernet, P., Nordlund, D., Bergman, U., Cavalleri, M., Odelius, M., Ogasawara, H., Naslund, L., Hirsch, T., Ojamae, L., Glatzel, P., Pettersson, L., and Nilsson, A. *Science* **304**, 995 (2004).
- [115] Cavalleri, M., Naslund, L., Edwards, D., Wernet, P., Ogasawara, H., Myneni, S., Ojamae, L., Odelius, M., Nilsson, A., and Nilsson, A. *Journal of Chemical Physics* **124**, 194508 (2006).
- [116] Ferzaz, B., Brault, E., Bourliaud, G., Robert, J.-P., Poughon, G., Claustre, Y., Marguet, F., Liere, P., Schumacher, M., Nowicki, J.-P., Fournier, J., Marabout, B., Sevrin, M., George, P., Soubrie, P., Benavides, J., and Scatton, B. *Pharmacology and Experimental Therapeutics* **301**(3), 1067–1078 (2002).
- [117] Bureau, C., Chong, D. P., Endo, K., Delhalle, J., Leycayon, G., and Moel, A. L. *Nuclear Instruments & Methods in Physics Research Section b- Beam Interactions with Materials & Atoms* **131**(1-4), 1–12 (1997).

-
- [118] Beamson, G. and Briggs, D. *The XPS of Polymers Database*.
- [119] Saleki-Gerhardt, A., Ahlneck, C., and Zografi, G. *International Journal of Pharmaceutics* **101**, 237–247 (1994).
- [120] Hancock, B. C., Carlson, G. T., Ladipo, D. D., Langdon, B. A., and Mullarney, M. P. *International Journal of Pharmaceutics* **241**(1), 73–85 (2002).
- [121] Mackin, L., Sartnurak, S., Thomas, I., and Moore, S. *International Journal of Pharmaceutics* **231**(2), 213–226 (2002).
- [122] Lechuga-Ballesteros, D., Bakri, A., and Miller, D. P. *Pharmaceutical Research* **20**(2), 308–318 (2003).
- [123] Byard, S. J., Jackson, S. L., Smail, A., Bauer, M., and Apperley, D. C. *Journal of Pharmaceutical Sciences* **94**(6), 1321 (2005).
- [124] Wu, T., Sun, Y., Li, N., de Villiers, M. M., and Yu, L. *Langmuir* **23**, 5148 (2007).
- [125] Crowley, K. J. and Zografi, G. *Pharmaceutical Research* **20**(9), 1417–1422 (2003).
- [126] Royall, P. G., ya Huang, C., wah Jai Tang, S., Duncan, J., de Velde, G. V., and Brown, M. B. *International Journal of Pharmaceutics* **301**(14), 181–191 (2005).
- [127] Price, R. and Young, P. M. *Journal of Pharmaceutical Sciences* **93**(1), 155–164 (2004).

- [128] Price, R. and Young, P. M. *Micron* **36**(6), 519–524 (2005).
- [129] Begat, P., Young, P. M., Edge, S., Kaerger, J. S., and Price, R. *Journal of Pharmaceutical Sciences* **92**(3), 611–620 (2003).
- [130] Ward, S., Perkins, M., Zhang, J., Roberts Clive, J., Madden Claire, E., Luk Shen, Y., Patel, N., and Ebbens Stephen, J. *Pharmaceutical research* **22**(7), 1195–202 (2005).
- [131] Gal, C. S.-L., Wagnon, J., Garcia, C., Lacour, C., Guiraudou, P., Christophe, B., Villanova, G., Nisato, D., Maffrand, J. P., and Fur, G. L. *Journal of Clinical Investigation* **92**(1), 224–231 (2005).
- [132] Royall, P. G., Kett, V. L., Andrews, C. S., and Craig, D. Q. M. *Journal of Physical Chemistry B* **105**(29), 7021–7026 (2001).
- [133] Williams Adrian, C., Timmins, P., Lu, M., and Forbes Robert, T. *European journal of pharmaceutical sciences* **26**(3-4), 288–94 (2005).
- [134] Gavrilin, M. V., Lukashova, L. A., Fat'yanova, E. A., Van Ziep, C., and Kompantseva, E. V. *Pharmaceutical Chemistry Journal* **33**(11), 604–606 (2000).
- [135] Lonsdale, T. *MChem Thesis*. University of Manchester, (2006).
- [136] Beesley, A., Tsapatsaris, N., Weiher, N., Tromp, M., Evans, J., Dent, A., Harvey, I., and Schroeder, S. L. M. *American Institute of Physics Conference Proceedings* **CP 879**, 1735 (2006).
- [137] Noda, I. and Ozaki, Y. *Two-Dimensional Correlation Spectroscopy*. John Wiley & Sons, Chichester, (2004).

- [138] Noda, I. *Vibrational Spectroscopy* **36**(2), 143 (2004).
- [139] Blythe, A. R., Briggs, D., Kendall, C. R., Rance, D. G., and Zichy, V. J. I. *Polymer* **19**, 1273–1278 (1978).
- [140] Carrino, L., Moroni, G., and Polini, W. *Journal of materials and processing technology* **121**, 373–382 (2002).
- [141] Cui, N.-Y. and Brown, N. M. *Applied Surface Science* **189**, 31–38 (2002).
- [142] Walker, A. *Personal Communication*. (2004).
- [143] Lindsay, R. *Personal Communication*. (2004).